ARMY RESEARCH LABORATORY

Analysis of the Static and Dynamic Response of a T-38 Wing and Comparison With Experimental Data

Jong-Ho Woo

ARL-TR-99

March 1993

APPROVED FOR PUBLIC RELEASE; DISTRIBUTION IS UNLIMITED.

NOTICES

REPORT DOCUMENTATION PAGE

Form Approved
OMB No. 0704-0188

1. AGENCY USE ONLY *(Leave blank)*	2. REPORT DATE	3. REPORT TYPE AND DATES COVERED
	March 1993	Final, Aug 90–Nov 91

4. TITLE AND SUBTITLE

Analysis of the Static and Dynamic Response of a T-38 Wing and Comparison With Experimental Data

5. FUNDING NUMBERS

PR: 1L162618AH80

6. AUTHOR(S)

Jong-Ho Woo

7. PERFORMING ORGANIZATION NAME(S) AND ADDRESS(ES)

U.S. Army Research Laboratory
ATTN: AMSRL-SL-BA
Aberdeen Proving Ground, MD 21005-5068

8. PERFORMING ORGANIZATION REPORT NUMBER

9. SPONSORING/MONITORING AGENCY NAME(S) AND ADDRESS(ES)

U.S. Army Research Laboratory
ATTN: AMSRL-OP-CI-B (Tech Lib)
Aberdeen Proving Ground, MD 21005-5066

10. SPONSORING/MONITORING AGENCY REPORT NUMBER

ARL-TR-99

11. SUPPLEMENTARY NOTES

12a. DISTRIBUTION/AVAILABILITY STATEMENT

Approved for public release; distribution is unlimited.

12b. DISTRIBUTION CODE

13. ABSTRACT *(Maximum 200 words)*

This report documents the investigation of a three-dimensional finite element model for calculating the static displacement and dynamic structural response of a T-38 wing and comparison of the analytical results with T-38 wing experimental data from Northrop Aircraft, Inc.

The wing structure is modeled by rod and bar (beam), quadrilateral plate, triangular plate, and shear panel finite elements. The general structural analysis programs MSC/NASTRAN and MSC/PAL2 are used to calculate deflections, natural frequencies, and mode shapes.

The wing finite element model yielded excellent agreement between calculated and experimental results for the eight loading conditions studied. The methodology developed in this study is expected to provide a valuable tool for the static aeroelastic response and dynamic analysis of wing structures in conjunction with aircraft ballistic vulnerability assessments.

14. SUBJECT TERMS

T-38 wing; deflection; natural frequency; finite element methods; shear panel; MSC/NASTRAN; MSC/PAL 2; resonant frequency

15. NUMBER OF PAGES 102

16. PRICE CODE

17. SECURITY CLASSIFICATION OF REPORT	18. SECURITY CLASSIFICATION OF THIS PAGE	19. SECURITY CLASSIFICATION OF ABSTRACT	20. LIMITATION OF ABSTRACT
UNCLASSIFIED	UNCLASSIFIED	UNCLASSIFIED	SAR

NSN 7540-01-280-5500

Standard Form 298 (Rev 2-89)
Prescribed by ANSI Std Z39-18
298-102

INTENTIONALLY LEFT BLANK

TABLE OF CONTENTS

INTENTIONALLY LEFT BLANK

LIST OF FIGURES

LIST OF TABLES

INTENTIONALLY LEFT BLANK

1. INTRODUCTION

This study represents the first step in the development of a methodology to analyze the structural response of aircraft wings with combat damage. An attempt is made to find an adequate structural model that could subsequently be used to accurately calculate static and dynamic aeroelastic characteristics.

The first step in this effort involved the following tasks:

a) Develop modeling techniques for efficiency and accuracy
b) Compare calculated deflections with experimental data
c) Calculate natural frequencies and mode shapes

The overall objectives of this work are to:

a) Select a finite element model and predict failure loads for a damaged wing structure

b) Develop an aerodynamic model based on the finite element model (item a.) for static aeroelasticity, flutter analysis, and dynamic aeroelasticity.

c) Idealize a box-beam type finite element model as a plate-beam type to save computing time and reduce the effort required to model a damaged wing.

T-38 wing deflection data from tests conducted in 1960 were obtained from the Northrop Corporation, Norair Division, See Reference [1]. During these tests, the aircraft was supported at the forward and aft fuselage by two steel jigs tied to a steel erectile structure. Wing loading was accomplished by means of hydraulic hand pumps and pressure gages, Northrop electrically-operated load maintainers, and Edison hydraulic proportioning units.

1.1 General Approach to the Problem

The MSC/NASTRAN and MSC/PAL2 finite element analysis programs were used initially to analyze the wing structure. They have special tools for the analysis of thin-skinned aircraft structures. Following this effort, the MSC/NASTRAN Aeroelastic code was used for static aeroelastic response, flutter, and dynamic aeroelastic analyses.

The finite element model designated as Model 1, shown on pages 7 and 8, is the baseline for the study and is used in each of the analyses. These analyses and the associated MSC/NASTRAN and MSC/PAL2 solutions are approached as follows:

1. Finite element models of the structure are developed to obtain static displacements for comparison with experimental data. A static solution option is used.

2. Natural frequencies and mode shapes, involving an eigenvalue problem solution, are determined using a dynamic option.

Four finite element model variations were developed and compared with test results. Different types of wing skin elements are used for each of the models. Shear panel elements are used for the spar and rib webs. Two different finite element models are applied for the spar and rib chords, one is modeled with the beam element and the other is modeled with the rod element. To verify these finite element models, Rattinger's wing, Reference[2], is modeled and shown to have very good agreement with the test results. See Appendix C. The best structural finite element model was then used to calculate the wing static displacement, and to develop the influence coefficients needed for the aeroelastic analysis.

2. WING FINITE ELEMENT MODEL ANALYSIS

2.1 Wing Description

The T-38 wing structure is composed of aluminum panels (upper and lower surfaces) that are riveted to the root rib, main spar, auxiliary spar, and tip rib. Data necessary to describe the physical characteristics of the wing for MSC/NASTRAN and/or MSC/PAL2 were generated from engineering drawings. The numbers shown in Figure 1 represent the wing assembly parts. There are two missing parts on the drawing: the leading edge spar chord and web and the minor rib chord and web. These two webs were reconstructed by knowledge of the dimensions of connecting rib webs and edge views of these parts. More detail is shown in Figure 2.

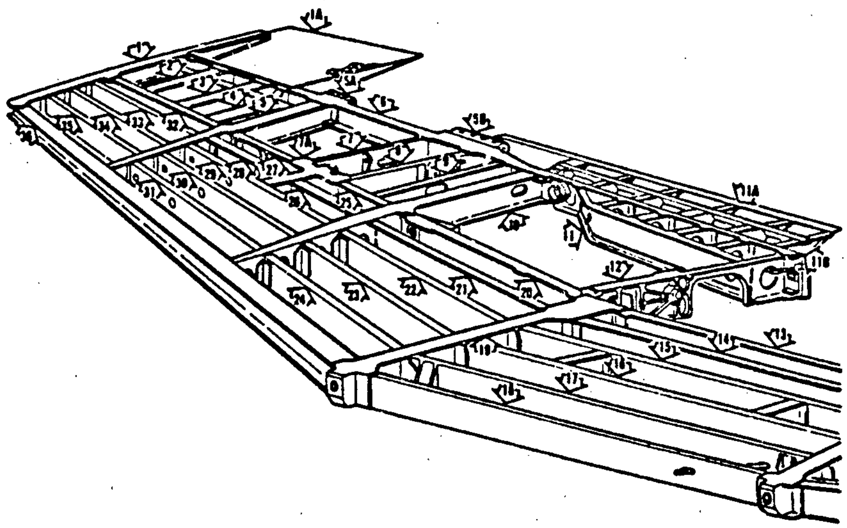

Figure 1. T-38 Real Wing Structure.

2.2 Development of the Finite Element Model

The first, and simplest, finite element model developed to describe the wing geometry shown in Figure 2 is illustrated by Figures 3a and 3b. This baseline model is labeled Model 1. The nodes in this model are located on the top and bottom surfaces of the wing at the intersection of two or more of the spar caps, rib flanges, or stringers. This model(Model 1) has a large aspect ratio quadrilateral plate. See Figures 3a and 3b. To reduce the aspect ratio, three other finite element models were created. The second model has an increased number of elements between two major ribs. For example, as seen in Figure 2, the area between ws 125.0 and ws 101.0 has an increased number of elements. The same applies between ws 101.0 and ws 64.8. See Figures 4a and 4b. The third model has an even greater number of the elements defined between the wing tip and wing root as shown in Figures 5a and 5b. The fourth model is further modified to include triangular plates and quadrilateral plates, See Figure 6. All the models used rod (beam), membrane plate, and shear panel finite elements. The element substructures that are used to model the wing skins are triangular membrane and bending elements and quadrilateral membranes and bending elements. As shown in Figure 6 and Table 1, models QTSR4.DAT and QTSB4.DAT are composed of triang'.'lar and quadrilateral plate elements for the wing skins. Several quadrilateral elements are divided into triangular elements for geometrical reasons or to change mesh spacing between assemblies of quadrilateral plates. For models 1, 2, and 3 only triangular or quadrilateral plates are used for the wing skins. Model 1 has plate elements with large aspect ratios. To avoid large aspect ratios, model 2 and 3 have been utilized. MSC/NASTRAN and MSC/PAL2 have special rod(truss element) and shear panel model tools for the analysis of thin-skinned curved structures such as aircraft. The shear panel element does not represent bending stiffnesses. The quadrilateral SHEAR element(PSHEAR property card) supports an extensional force at grid points and a shear stress within the element. Reinforcing ROD elements are used to carry the extensional load. Consequently, SSR1.DAT is used for this treatment and represents the shear panel elements that are used for the wing skins and the spar and rib webs, while rod elements are used for the spar and rib chords.

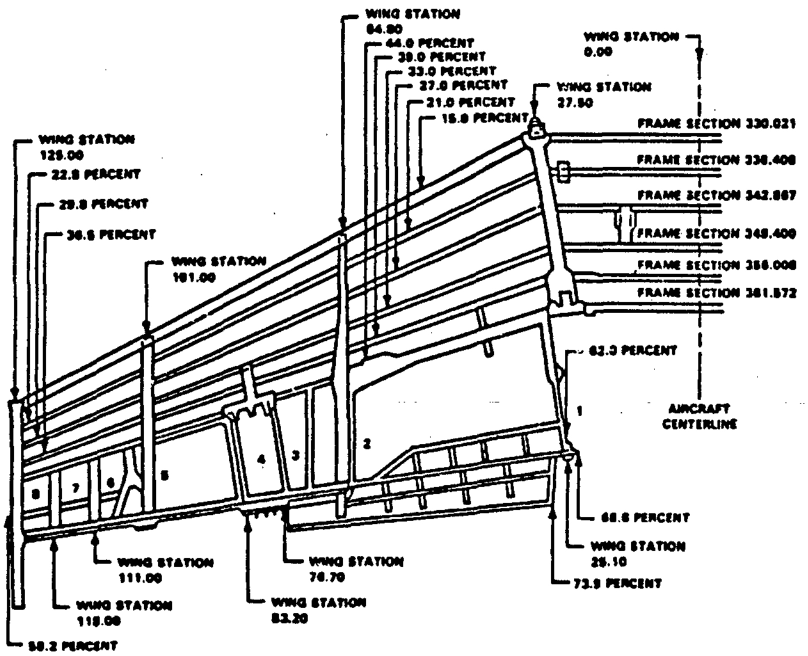

Figure 2. T-38 Wing Internal Structure.

The physical and material properties used in describing the substructure elements are defined as follows:

a) Property cards(PSHELL, PSHEAR) identify the physical characteristics of the elements, such as thickness, material identify, inertia, and mass of the wing skin and web.

b) Property cards(PBEAM, PROD) identify the physical characteristics of the spar and rib caps.

c) Material card(MAT1) describes the material characteristics, such as Young's modulus, shear modulus, Poisson's ratio: MAT1 is used for isotropic material.

d) Grid points(GRID) are assigned unique geometric locations in terms of fuselage station(FS), wing station(WS), and water line(WL). GRID identifies the appropriate coordinate system and unique constraints for the grid point.

e) Quadrilateral plate cards(CQUAD4) identify the connection definition for an isoparametric quadrilateral with bending and membrane stiffness.

f) Triangular plate cards(CTRIA3) identify the connection definition for an isoparametric triangle with bending and membrane stiffness.

g) Quadrilateral plate cards(CSHEAR) identify the connection definition for shear panel.

h) Elastic line element cards(CBEAM) identify the connection definition for general beam element.

i) Elastic line element cards(CONROD) identify the connection and property definition for rod with axial and torsional stiffness.

j) Load cards(FORCE) define concentrated loads at grid points.

k) Constraint cards(SPC) define single-point constraints and enforced displacements.

The finite element models of the T-38 wing structure were used to calculate static displacements for comparison with the Northrop test results. Of these four models, the one that compares best to test results will be used in future analyses of the damaged T-38 wing and used in the MSC/NASTRAN static and dynamic aeroelasticity and flutter solutions.

2.3 Designation of Finite Element Model

The file names for the wing models follow the format XYZi.DAT, where X represents the wing skin elements, Y the spar and rib web elements, Z the truss elements, i represents the wing model number, and DAT represents the file extention. X denotes Q for quadrilateral plate elements and T for triangular plate elements. Y denotes S for shear panel elements Z denotes R for rod elements and B for beam elements. For instance, TSR1.DAT means the triangular plate element is used for the wing skins, shear panel elements are used for the spar and rib webs, and rod elements are used for spar and rib caps for Model 1. All webs in all models are represented by shear elements. See Tables 1a and 1b.

Table 1a. Designation of Finite Element Model 1

MODEL 1					
FILE NAME	QSB1.DAT	QSR1.DAT	TSB1.DAT	TSR1.DAT	SSR1.DAT
WING SKIN	CQUAD4	CQUAD4	CTRIA3	CTRIA3	CSHEAR
SPAR & RIB WEB	CSHEAR	CSHEAR	CSHEAR	CSHEAR	CSHEAR
SPAR & RIB CHORD	CBEAM	CONROD	CBEAM	CONROD	CONROD

Table 1b. Designation of Finite Element Model 2

MODEL 2				
FILE NAME	QSB2.DAT	QSR2.DAT	TSB2.DAT	TSR2.DAT
WING SKIN	CQUAD4	CQUAD4	CTRIA3	CTRIA3
SPAR & RIB WEB	CSHEAR	CSHEAR	CSHEAR	CSHEAR
SPAR & RIB CHORD	CBEAM	CONROD	CBEAM	CONROD

Table 1c. Designation of Finite Element Model 3

MODEL 3				
FILE NAME	QSB3.DAT	QSR3.DAT	TSB3.DAT	TSR3.DAT
WING SKIN	CQUAD4	CQUAD4	CTRIA3	CTRIA3
SPAR & RIB WEB	CSHEAR	CSHEAR	CSHEAR	CSHEAR
SPAR & RIB CHORD	CBEAM	CONROD	CBEAM	CONROD

Table 1d. Designation of Finite Element Model 4

MODEL 4		
FILE NAME	QTSB4.DAT	QTSR4.DAT
WING SKIN	CQUAD4 & CTRIA3	CQUAD4 & CTRIA3
SPAR & RIB WEB	CSHEAR	CSHEAR
SPAR & RIB CHORD	CBEAM	CONROD

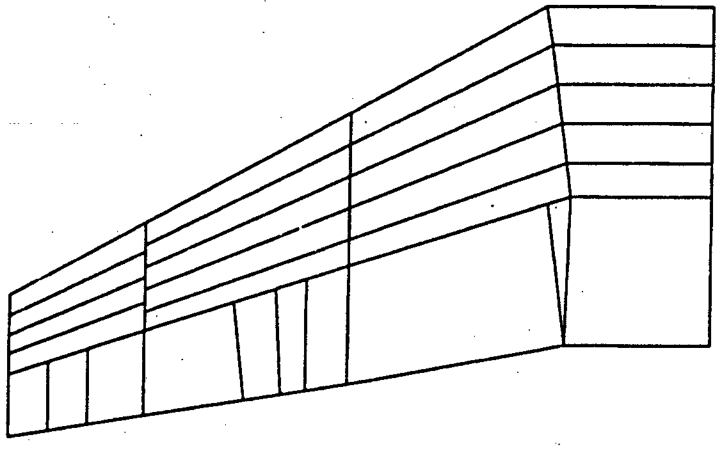

Figure 3a. Topview of Finite Element Model 1, QSB1.DAT and QSR1.DAT.

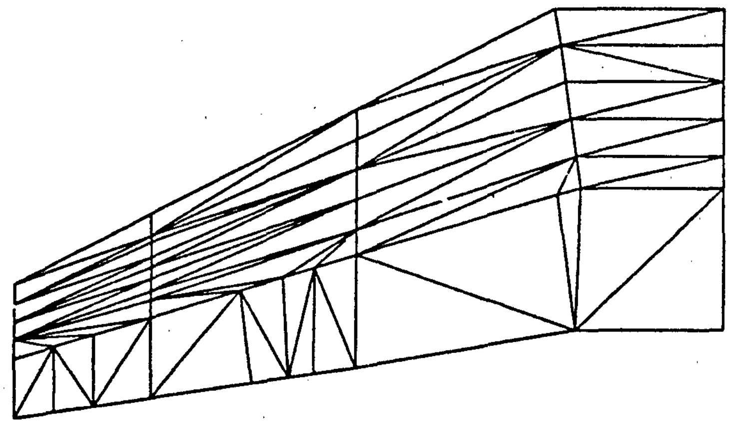

Figure 3b. Topview of Finite Element Model 1, TSB1.DAT and TSR1.DAT.

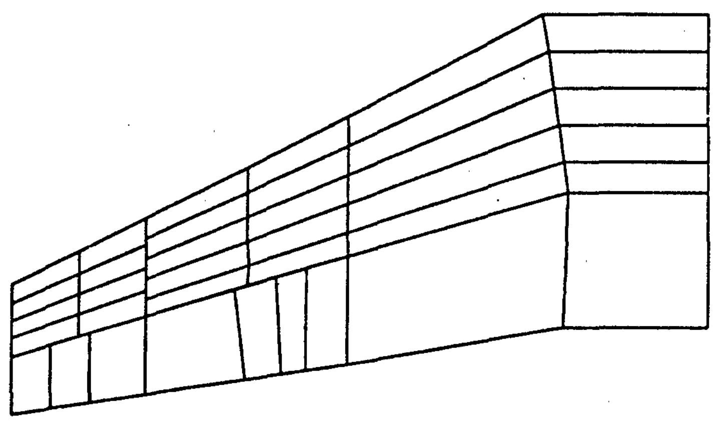

Figure 4a. Topview of Finite Element Model 2, QSB2.DAT and QSR2.DAT.

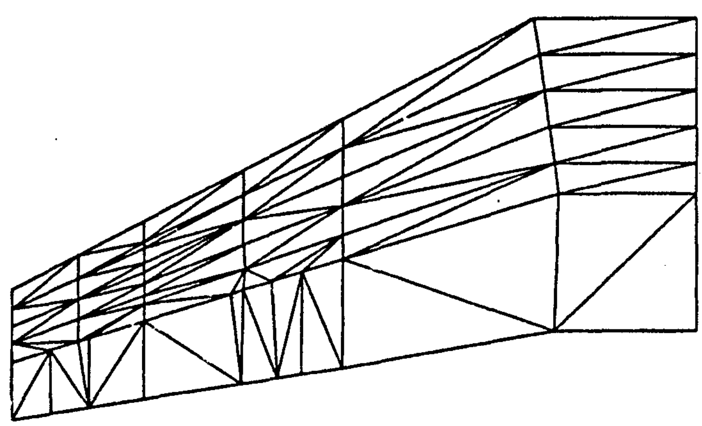

Figure 4b. Topview of Finite Element Model 2, TSB2.DAT and TSR2.DAT.

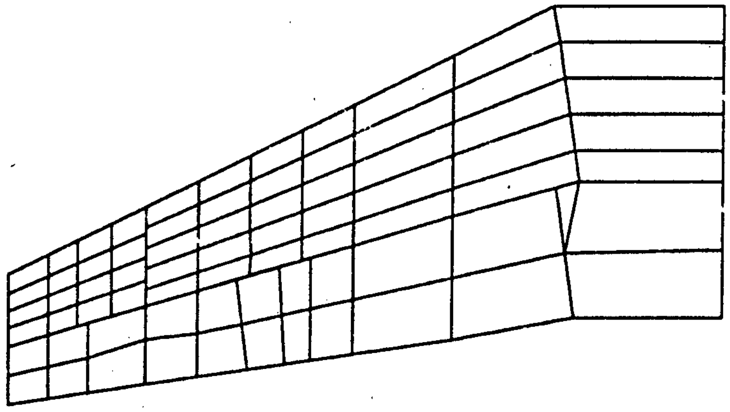

Figure 5a. Topview of Finite Element Model 3. QSB3.DAT and QSR3.DAT.

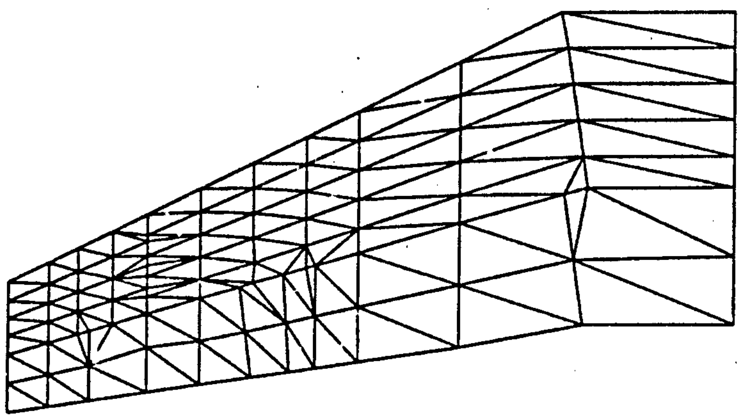

Figure 5b. Topview of Finite Element Model 3. TSB3.DAT and TSR3.DAT.

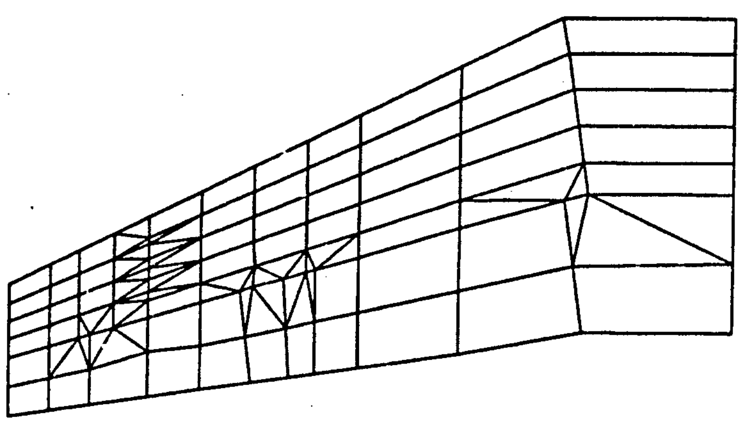

Figure 6. Topview of Finite Element Model 4. QTSB4.DAT and QTSR4.DAT.

2.4 Sizing of Rod Elements

In this study, rod and beam elements, activated through use of two optional cards(CONROD and CBEAM), are used for spar and rib caps. As shown in Figures 7 and 8, the Channel-beam and I-beam have top and bottom caps. The top and bottom caps are represented as a cross section of a rectangular beam. Areas of the cross sections, I_{xx}, and I_{yy} are input for the CBEAM option. The two caps (top and bottom) are resized as rod elements for the CONROD option. The rationale for sizing rod elements representing spar caps or rib caps is presented by Reference [3] and [4]. Property relationships are first determined for a structural member's cross section. The distance from the top surface of the section to the centroidal axis is identified as h_t. Similarly, the distance from the centroidal axis to the bottom surface of the section is h_b. Maximum bending stress at top and bottom surfaces, respectively, are:

$$\sigma_T = \frac{Mh_t}{I} \tag{1.a}$$

and

$$\sigma_B = \frac{Mh_b}{I} \tag{1.b}$$

where M is the applied bending moment, and I is the section moment of inertia about the centroidal axis.

In the four finite element models, the rod elements are assumed to be point areas and are positioned at the top and bottom surfaces of a cross section of wing skins. The rod areas are sized to maintain the location of the centroidal axis and the value of I for the section. Such a relationship yielded

$$A_t h_t = A_b h_b \tag{2}$$

with A_t and A_b being the areas of the top and bottom rods. The bending moment, M, in the model then becomes

$$M = \sigma_T A_T h_t + \sigma_B A_B h_b \tag{3}$$

Next, using actual section properties and desired model properties, the relationships of Equations (1), (2), and (3) are combined to produce

$$A_t = \frac{I}{h_t(h_t + h_b)} \tag{4.a}$$

and

$$A_b = \frac{I}{h_b(h_t + h_b)} \tag{4.b}$$

which are the rod element areas.

The actual T-38 wing has two major types of beams: C-beam and I-beam. The two different types of beams were sized as rod elements to take a CONROD option for spar and rib chords. See Figures 7 and 8. All calculated input data for rod/beam elements are presented in Appendix D.

a) C-Beam case: ws 125.0, between 15% chord and 22.75% chord

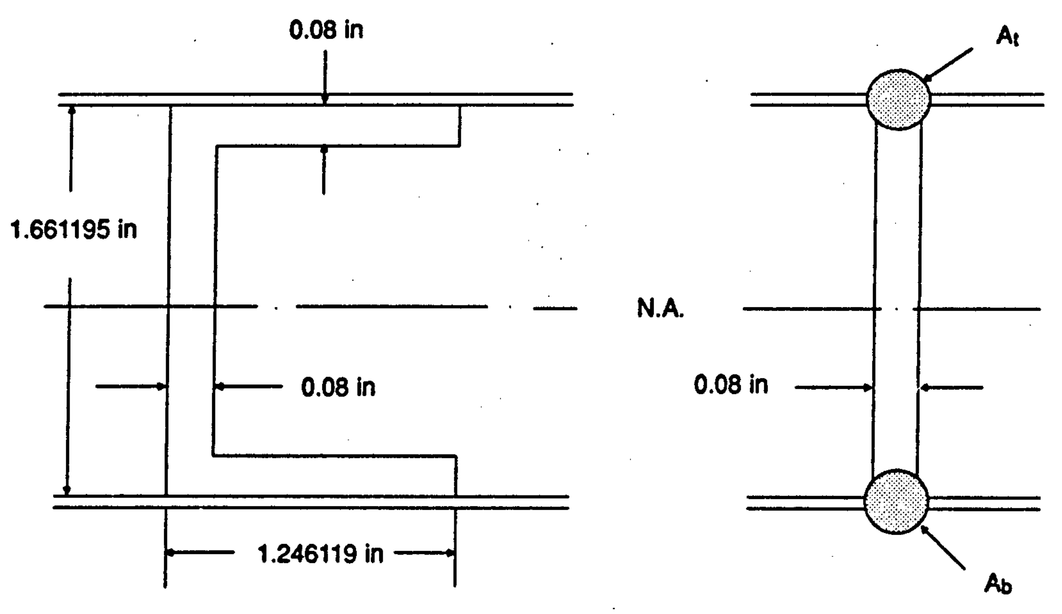

Figure 7. C-Beam Case.

$$I_{xx} = \frac{(1.246119)(1.661195)^3 - (1.246119)(1.661195 - 2 \times 0.08)^3}{12} = 0.1472808$$

$$I_{yy} = 0.04938$$

From equations (4.a) and (4.b), the rod cross-section area for top and bottom is

$$A_{t,b} = \frac{0.1472808}{0.8305975 \times 1.661195} = 0.1067419$$

and the cross-section area of beam is

$$A_{c,b} = 0.08 \times 1.2461188 = 0.09969$$

In the case of the CONROD option, 0.10674 in^2 is used for the rod area and CBEAM option 0.09969 in^2 is used for the beam cross area.

b) I-Beam case: ws 101.0, between 15% chord and 22.75 % chord

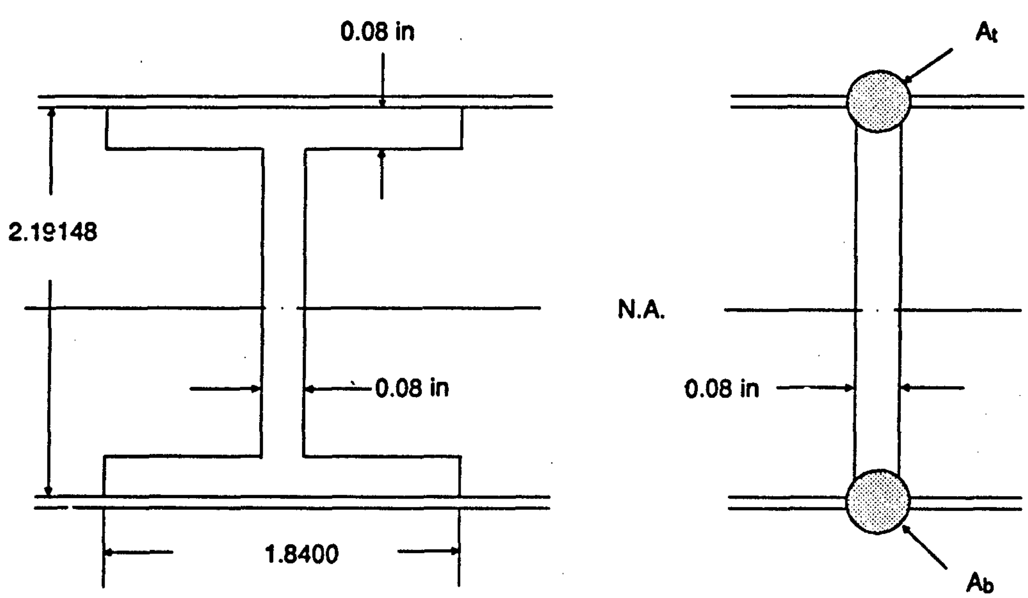

Figure 8. I-Beam Case.

$$I_{xx} = \frac{(1.84)(2.19148)^3 - (1.84 - 0.08)(2.19148 - 2\times 0.08)^3}{12} = 0.384183$$

$$I_{yy} = \frac{2(0.08)(1.84)^3 + (2.19148 - 2\times 0.08)(0.08)^3}{12} = 0.0831467$$

From Equations (4.a) and (4.b), the rod and beam cross-section area for top and bottom is obtained.

$$A_{t,b} = \frac{0.384183}{1.09574 \times 2.19148} = 0.159778$$

$$A_{c,b} = 0.08 \times 1.84 = 0.1472$$

In the above equations, the neutral axis(NA) is taken half the distance between the top and the bottom because of the symmetric beam shape.

2.5 Boundary Conditions

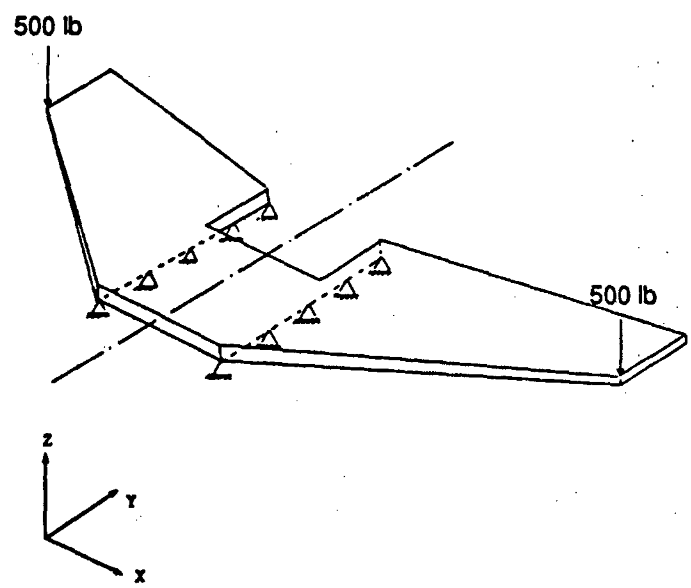

Figure 9. Loading Condition for T-38 Wing from Boundary Condition at Node A(500 lb).

The finite element model boundary conditions are based on the experimental conditions. As shown in Figure 9, the y-z plane is a plane of symmetry and therefore x-displacements in this plane are assigned zero values. The finite element models used in this report are constrained in the x-directions at the aircraft centerline and in the z-direction at the wing roots. Point loading is applied symmetrically at each of the loading points. See Figure 9.

3. GENERAL STRUCTURAL ANALYSIS EQUATION

Finite element structural analysis is a mathematical procedure to determine displacements, velocity, acceleration, stress, and support reaction forces due to applied mechanical and/or thermal loads that may or may not vary with time. The wing structures described in this study have several hundred multiple degrees of freedom(MDOF).

Equations of equilibrium may be derived for each DOF in the structure and expressed as a general structural analysis equation in matrix form:

$$[M]\{\ddot{u}\} + [B]\{\dot{u}\} + [K]\{u\} = \{P\} + \{N\} \qquad (5)$$

where [M], [B], and [K] are mass, damping, and stiffness matrices of the structure, respectively. The symbols $\{\ddot{u}\}$, $\{\dot{u}\}$, and $\{u\}$ represent acceleration, velocity, and displacement vectors, respectively, for the N degrees of freedom (N DOF) in the structure. Right hand side terms {P} and {N} refer to static and/or time-varying applied linear and nonlinear mechanical and/or thermal loads in Eq. 5. Constraint forces from the structure supports are obtained in the data recovery.

3.1 Linear Static Analysis

For static analysis of the T-38 wing, the solutions(SOL 24 or 101) in MSC/NASTRAN and (STAT2) in MSC/PAL2 are used. The mathematical formulation of the solution process is based on the linear theory of elasticity. The stiffness matrix is formulated and then partitioned with respect to the constrained and unconstrained degrees of freedom to be solved.

The finite element model developed allows the load(force) to be concentrated at a grid point for the static analysis. The set of forces is reduced to 1-set for the nodal forces from the constraint partitioning resulting from satisfying the equilibrium equations for stiffness versus force. In the static load case Eq. 5 reduces to

$$[K]\{u\} = \{P\} \tag{6}$$

The vectors {P} and {u} represent the nodal forces and displacements, respectively, and the matrix [K] represents the Finite Element Model stiffness matrix. For solution of the equations, MSC/PAL2 and MSC/NASTRAN reduces the stiffness matrix into its upper and lower triangular factors. Then forward-backward substitution is performed for all the lower cases having the same constraints, which is the case here. In this study, eight different loads are applied at each different grid point as shown in Table 2. The displacement solution for each load case contains three translational values for each grid point(except those displacements which are constrained). In this manner, transverse displacements are calculated for nine grid points(A-I) shown in Figure 10. These displacements are plotted and compared with experimental data. Figures 11 through 18 present these comparisons for load applications from 200 lb to 5000 lb. Each loading has 6 plots a, b, c, d, e, and f. Plots a and b represent comparisons of displacements from models TSBi.DAT and TSRi.DAT and test data. Plots c and d represent comparisons of displacements from models QSRi.DAT and QSBi.DAT and test data. Plots e represent comparisons of displacements from models SSR1.DAT and test data and plot f represents a comparison of displacements from QTSR4.DAT and QTSB4.DAT and test data. Each plot has three stations. The top station shows deflections of grid points A, B, and C(See Figure 10), the middle station shows grid points D, E, and F, and the lower station shows the deflections of grid points G, H, and I. In other words, the top station represents three grid points on the wing station 125.0, the middle station represents three grid points on the wing station 101.0 and the lower station represents three grid points on the wing station 64.8 The three grid points at each station correspond to chord positions of 15.0 %, 44.0 %, and 66.6 % chord, respectively.

3.2 Dynamic Analysis

The modal analysis of the finite element model of T-38 wing is important to performing flutter analysis. Theoretically, this is because the response of a structure to forced vibration (i.e., flutter) is taken to be the infinite sum of the structure's free vibration mode shapes. Therefore, it is important that verified mode shapes for the proper boundary conditions be obtained. In this report, the dynamic analysis solution DYNA2 in MSC/PAL2 is used to calculate normal mode shapes and natural frequencies.

For this analysis, applied loads, geometric stiffnesses, and structural damping are set to zero. Further assume that displacements at all locations on the structure have sinusoidal time variations with the same frequency and phase relationship:

$$\{u\} = \{\varphi\} \cos \omega t \qquad (7)$$

where $\{\varphi\}$ is a vector of real numbers called an eigenvector. The general structural analysis Eq. 5 becomes

$$[k - \omega^2 M]\{\varphi\} = 0 \qquad (\ )$$

where ω is the circular frequency, and k is stiffness matrix.

Roots of the matrix in Eq. 8 yield structural natural frequencies. Many numerical eigenvalue extraction techniques are available [Ref. 5] to determine the discrete set of eigen-frequencies(or natural frequencies). Substitution of a discrete frequency into Eq. 8 allows evaluation of $\{\varphi\}$ if one degree of freedom is assigned an arbitrary magnitude. The column vector $\{\varphi\}$ is thus a normalized eigenvector.

Individual terms in $\{\varphi\}$ may be visualized as vibration displacement extremes along the structure as it vibrates sinusoidally at a specific natural frequency. Structural natural frequencies are useful to know so that applied time-varying loads do not result in resonance with the structural natural frequencies. Also, the eigenvalues and eigenvectors are useful in applying an arbitrary time history to a structure.

Mass distribution is important in a dynamic vibration analysis. The default in most finite element programs is to lump element mass into adjoining grid points. This is called a lumped mass approach and results in a diagonal mass matrix. An alternative consistent mass approach uses the same element shape functions used for element stiffness. A consistent mass matrix will have off-diagonal terms as does the stiffness matrix.

Table 2. Load Distribution at Each Node

Node	Wing Station	Chord Percent	Load, lb
A	125.0	15.0	500
B	125.0	44.0	1,000
C	125.0	66.6	200
D	101.0	15.0	1,500
E	101.0	44.0	2,500
F	101.0	66.6	500
G	64.8	15.0	3,000
H	64.8	44.0	5,000
I	64.8	66.6	NONE

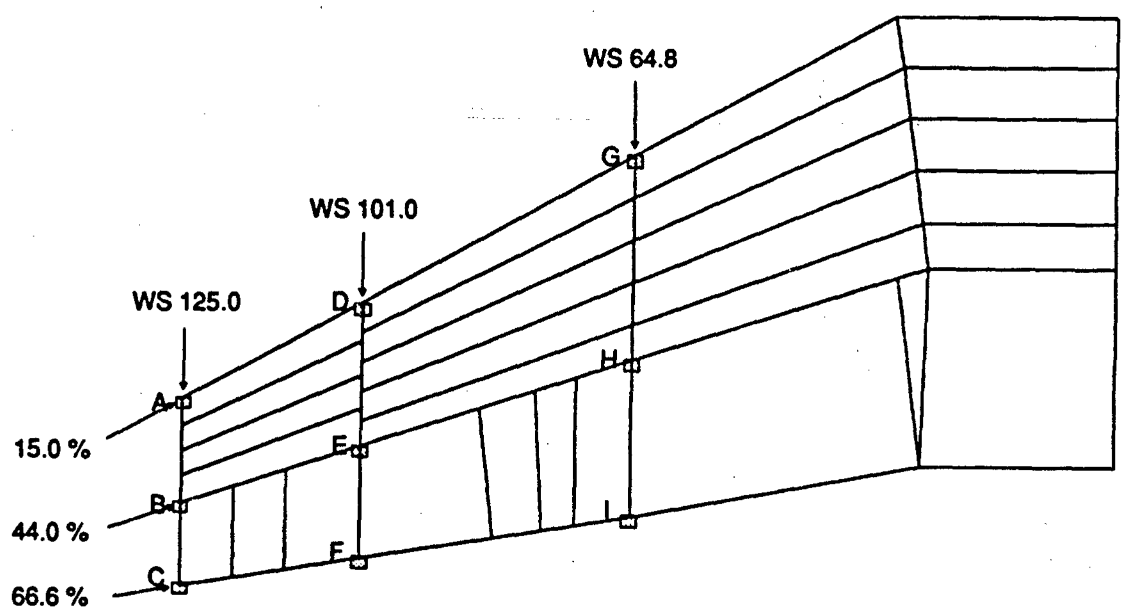

Figure 10. Position of Loading Node.

In this study, due to the software limitation of active degrees of freedom for normal modes using MSC/PAL2, the command ELIMINATE is used to reduce the number of degrees of freedom. This command(ELIMINATE) is stored in data file T38DYN.DAT(modified from data file QTSB4.DAT) for the dynamic analysis. Degree of freedom reduction is performed in order to reduce a model to a smaller size. This reduction is used primarily in the dynamic analysis, particularly to reduce the model size to one solvable in MSC/PAL2 (225 active degrees of freedom for normal modes and transient analysis). Though this reduction is not exact for the dynamic analysis, it is accurate enough that the lowest one-third of the computed resonant frequencies are accurate within 1 percent difference. The first ten natural frequencies are shown in Table 3 and the first ten mode shapes are in Figures 19a-j. The x and y translation and z rotation are constrained to calculate only the bending vibration.

Table 3. Natural Frequencies of T-38 Wing

Mode No.	Natural Frequencies (cps)
1	4.643
2	6.745
3	7.092
4	7.105
5	7.799
6	7.944
7	8.269
8	10.681
9	11.542
10	12.655

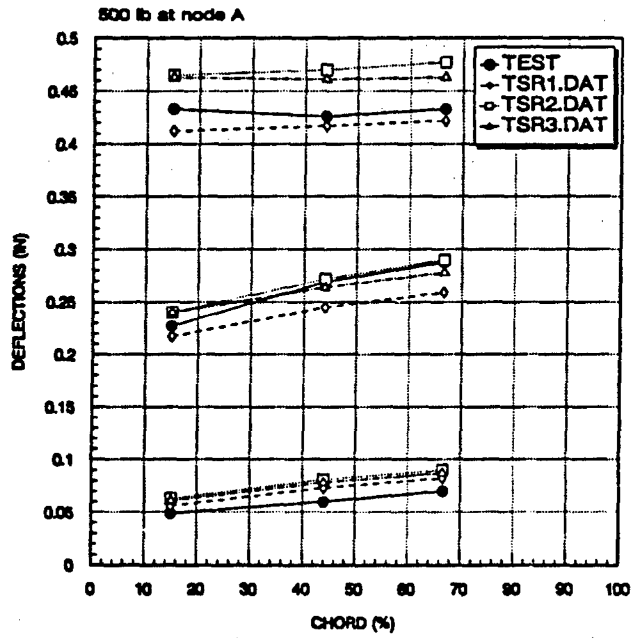

Figure 11a. Comparison of Displacements from TSRi.DAT and Test.

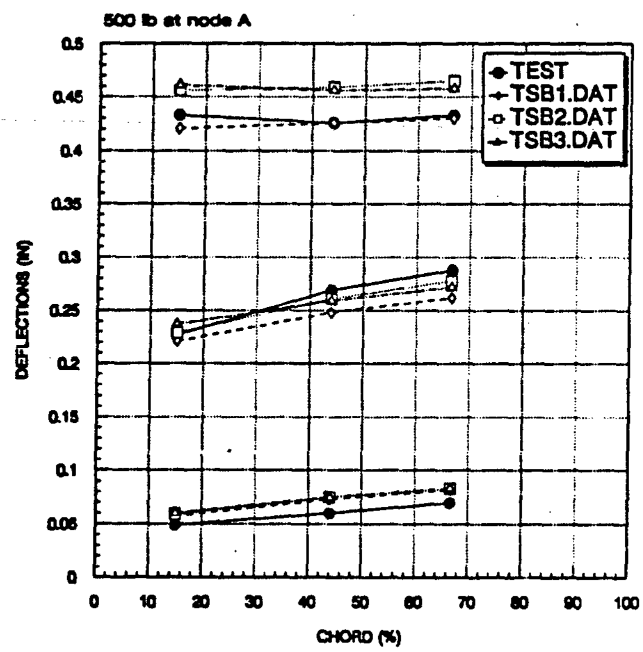

Figure 11b. Comparison of Displacements from TSBi.DAT and Test.

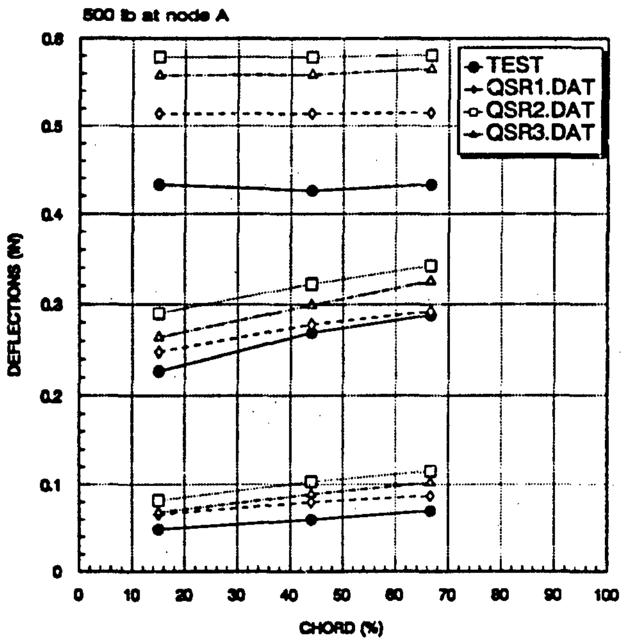

Figure 11c. Comparison of Displacements from QSRi.DAT and Test.

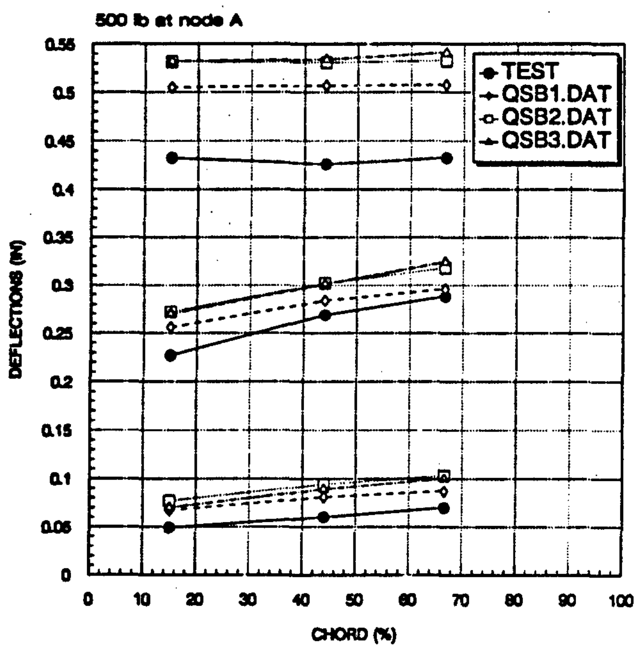

Figure 11d. Comparison of Displacements from QSBi.DAT and Test.

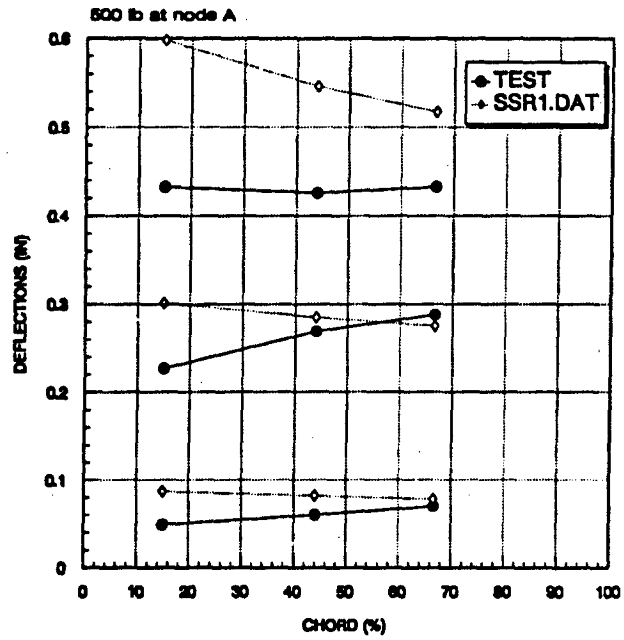

Figure 11e. Comparison of Displacements from SSR1.DAT and Test.

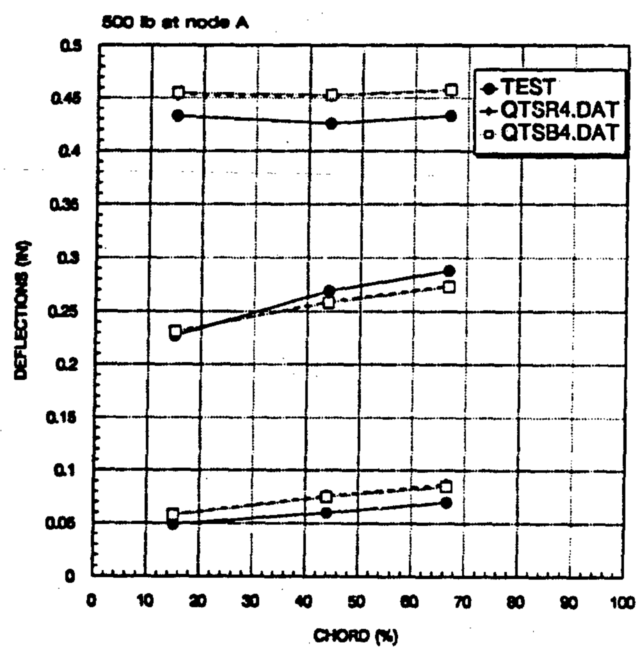

Figure 11f. Comparison of Displacements from QTSR4.DAT, QTSB4.DAT and Test.

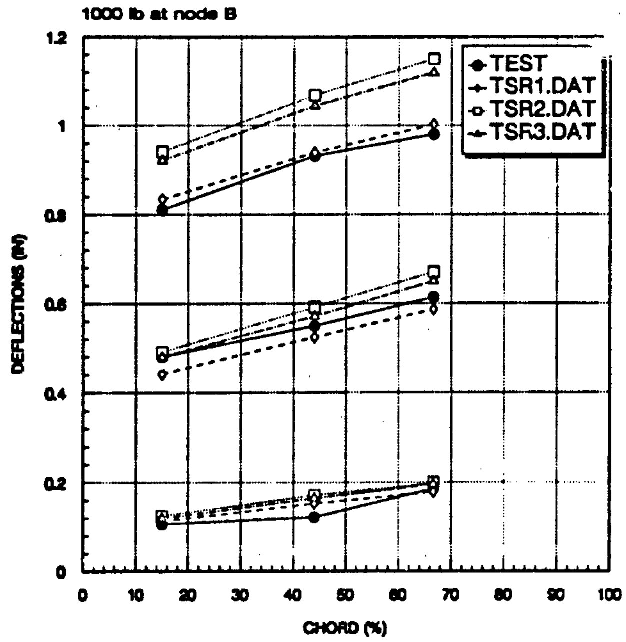

Figure 12a. Comparison of Displacements from TSRi.DAT and Test.

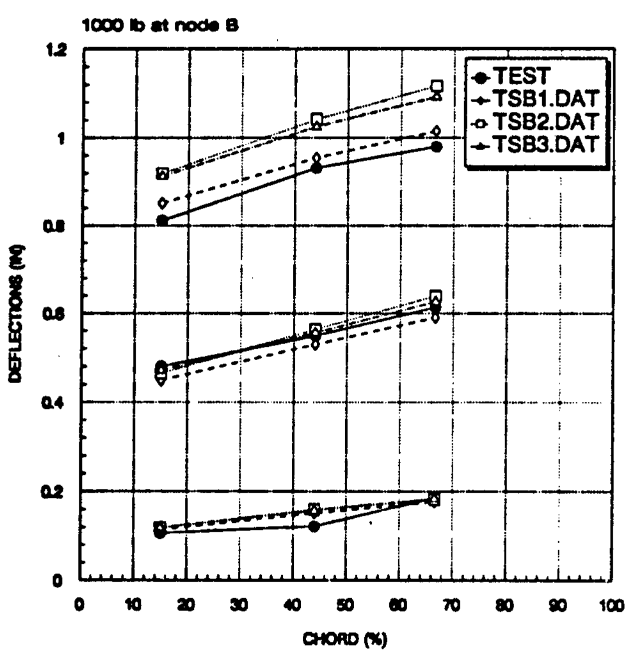

Figure 12b. Comparison of Displacements from TSBi.DAT and Test.

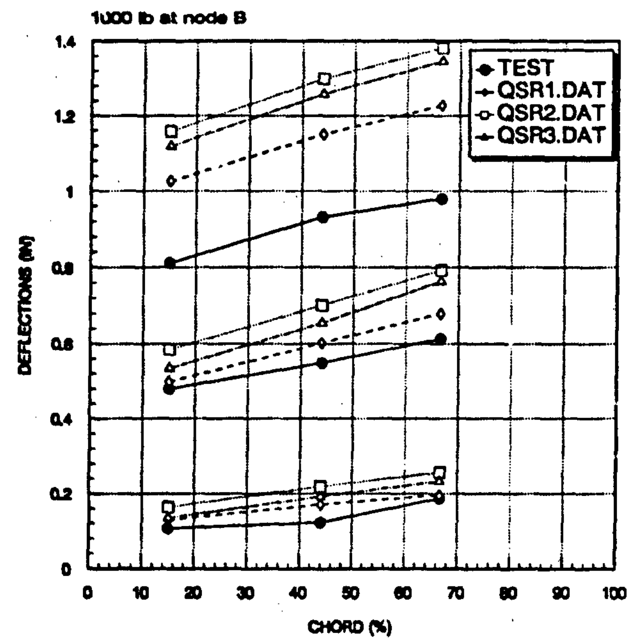

Figure 12c. Comparison of Displacements from QSRi.DAT and Test.

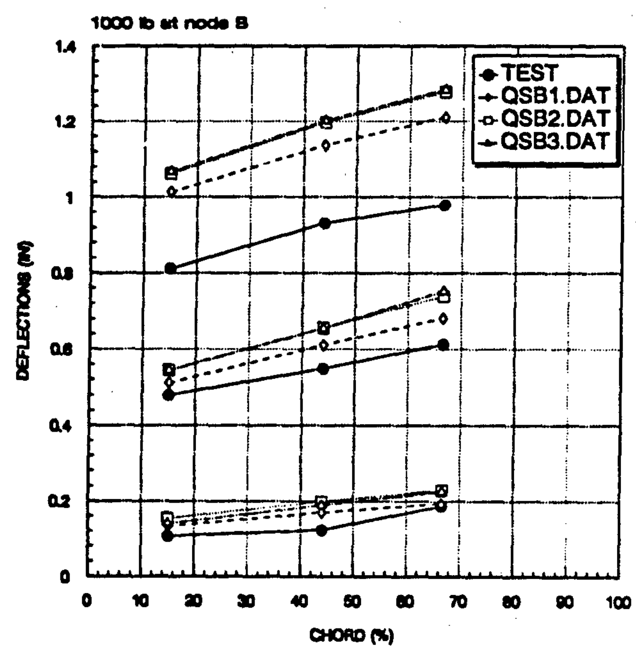

Figure 12d. Comparison of Displacements from QSBi.DAT and Test.

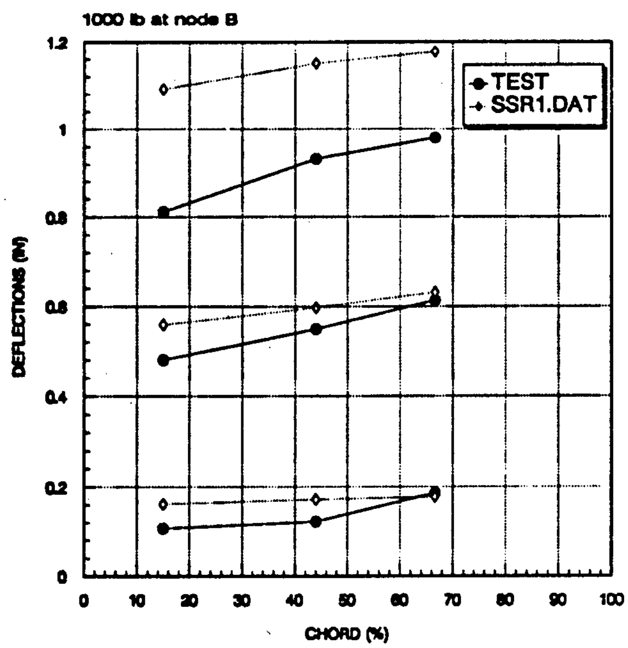

Figure 12e. Comparison of Displacements from SSR1.DAT and Test.

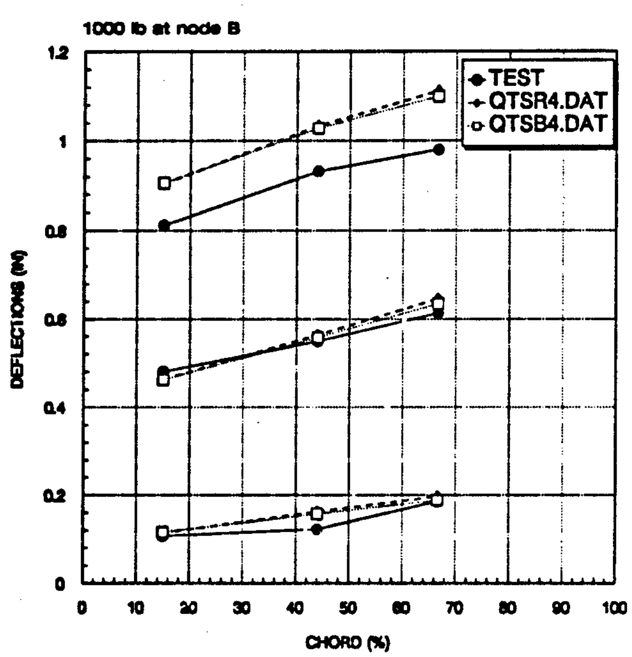

Figure 12f. Comparison of Displacements from QTSR4.DAT, QTSB4.DAT and Test.

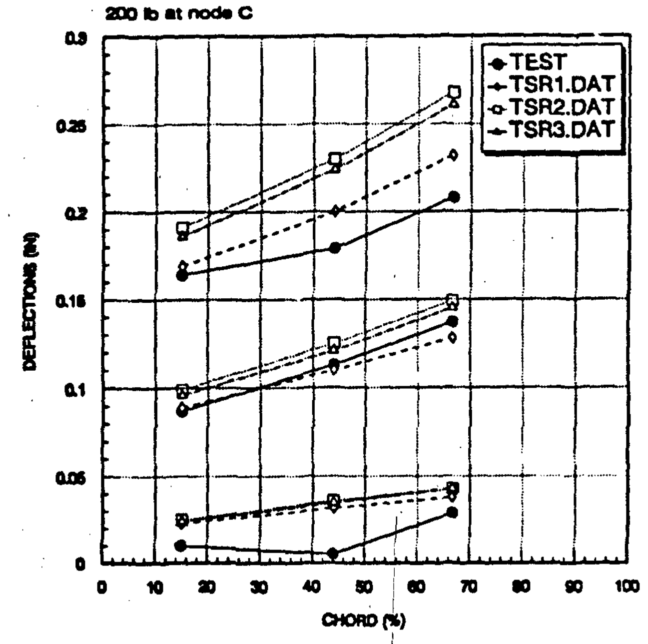

Figure 13a. Comparison of Displacements from TSRi.DAT and Test.

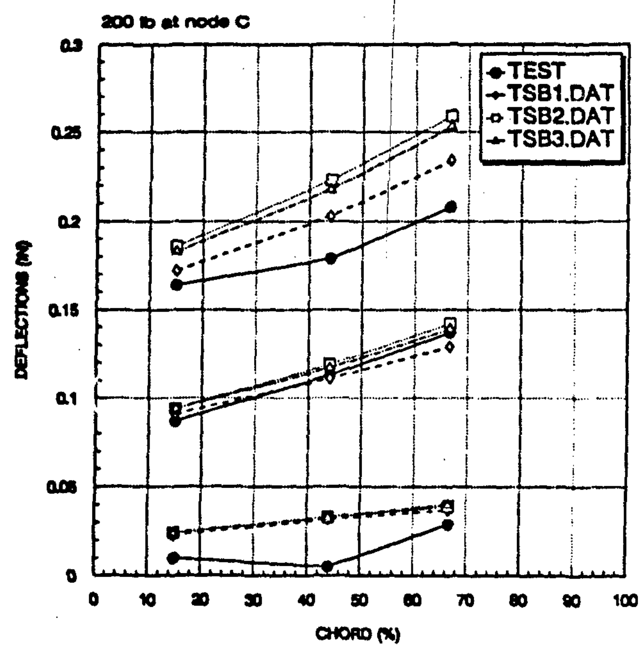

Figure 13b. Comparison of Displacements from TSBi.DAT and Test.

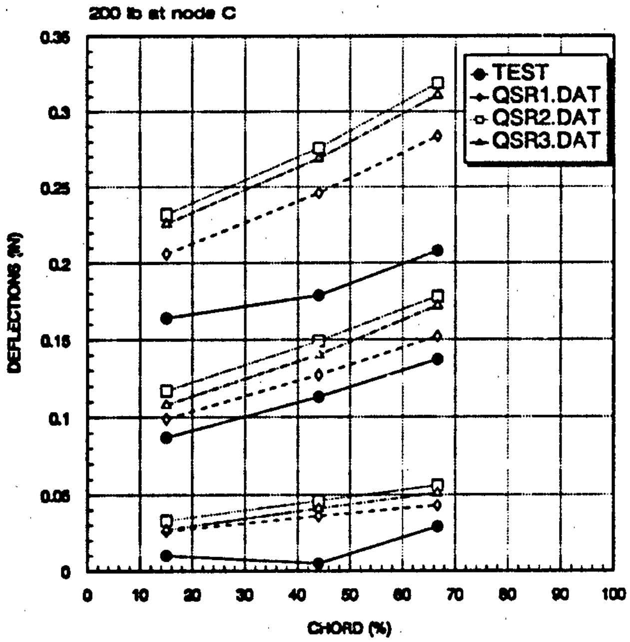

Figure 13c. Comparison of Displacements from QSRi.DAT and Test.

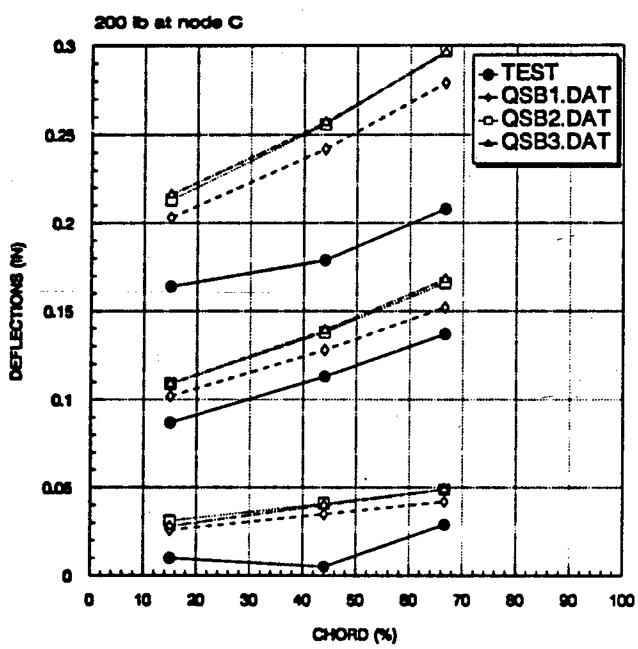

Figure 13d. Comparison of Displacements from QSBi.DAT and Test.

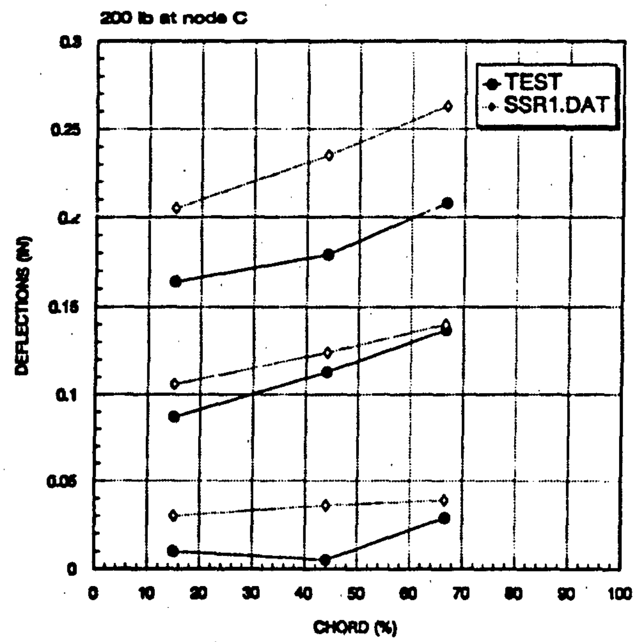

Figure 13e. Comparison of Displacements from SSR1.DAT and Test.

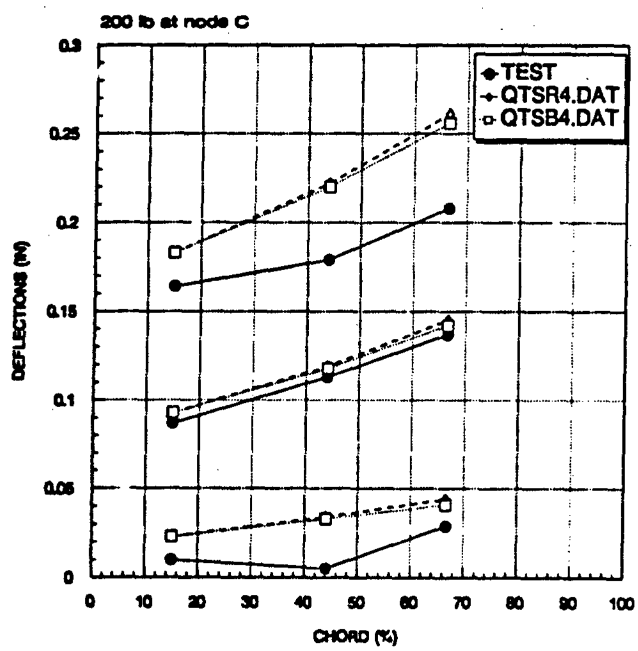

Figure 13f. Comparison of Displacements from QTSR4.DAT, QTSB4.DAT and Test.

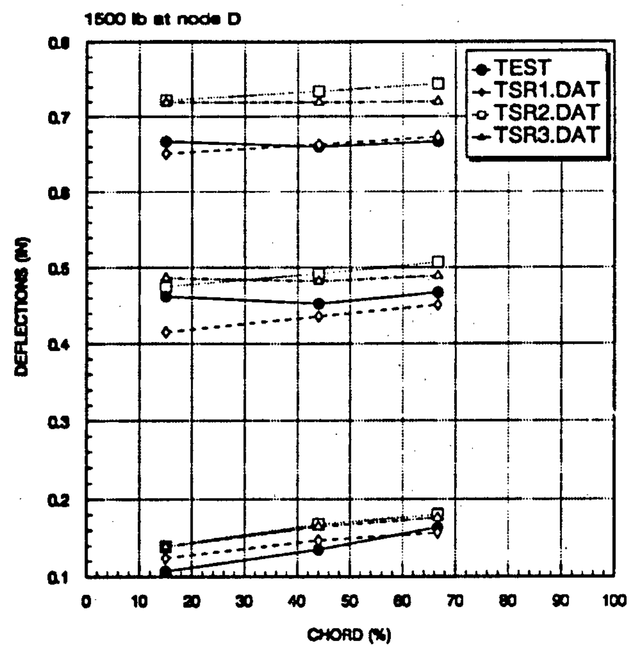

Figure 14a. Comparison of Displacements from TSRi.DAT and Test.

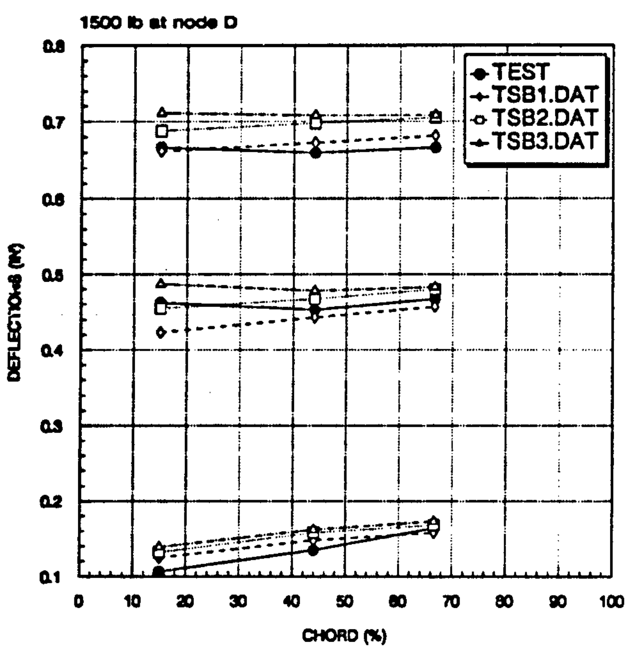

Figure 14b. Comparison of Displacements from TSBi.DAT and Test.

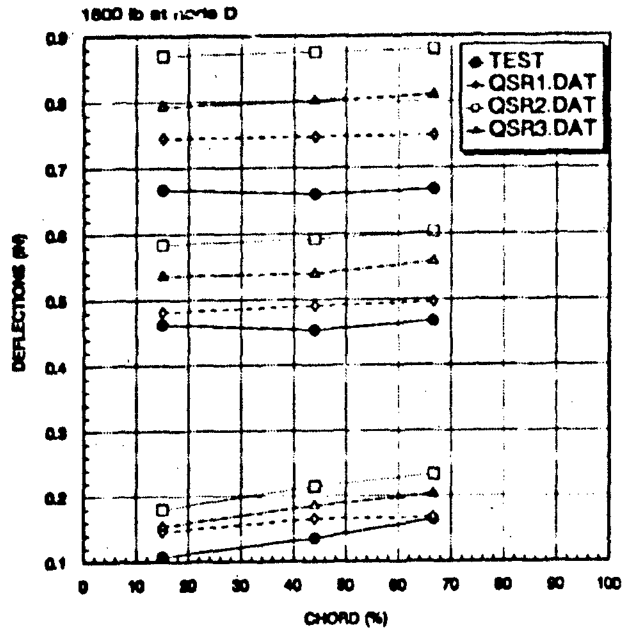

Figure 14c. Comparison of Displacements from QSRi.DAT and Test.

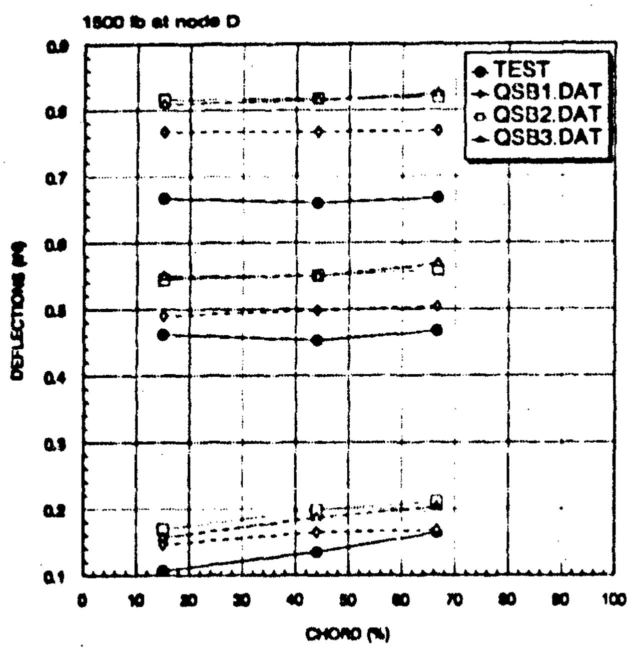

Figure 14d. Comparison of Displacements from QSBi.DAT and Test.

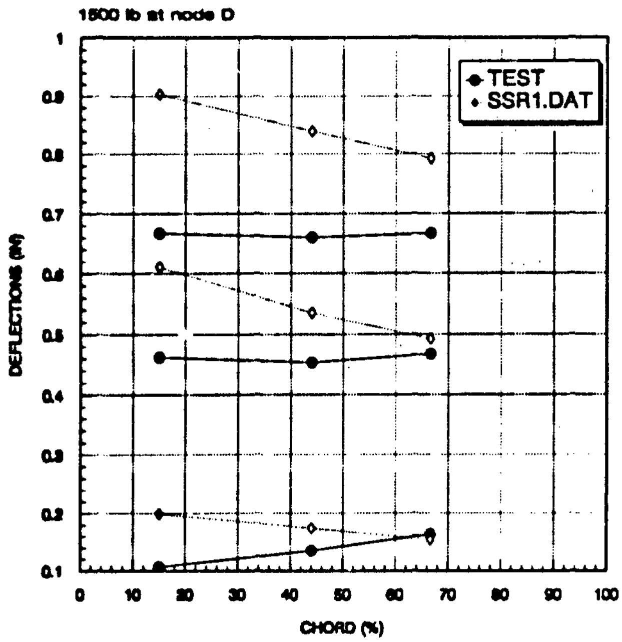

Figure 14e. Comparison of Displacements from SSR1.DAT and Test.

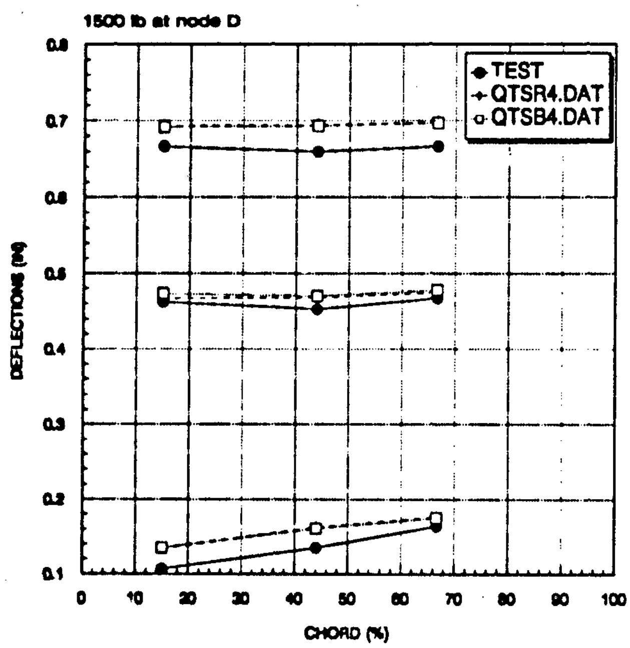

Figure 14f. Comparison of Displacements from QTSR4.DAT, QTSB4.DAT and Test.

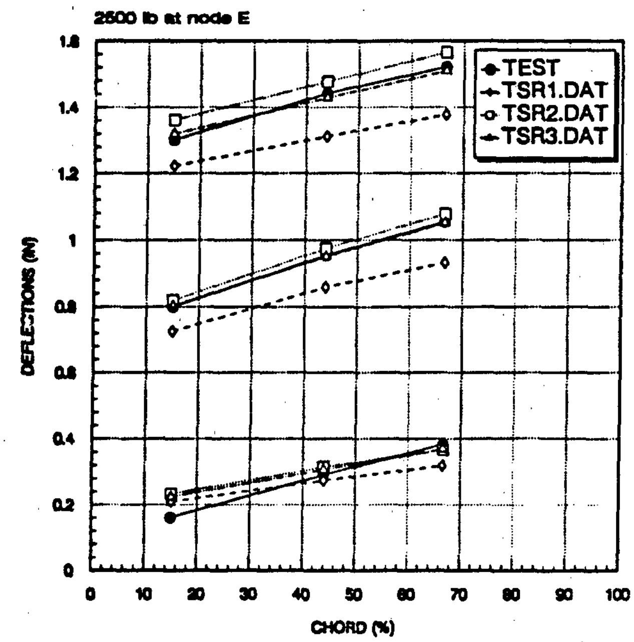

Figure 15a. Comparison of Displacements from TSRi.DAT and Test.

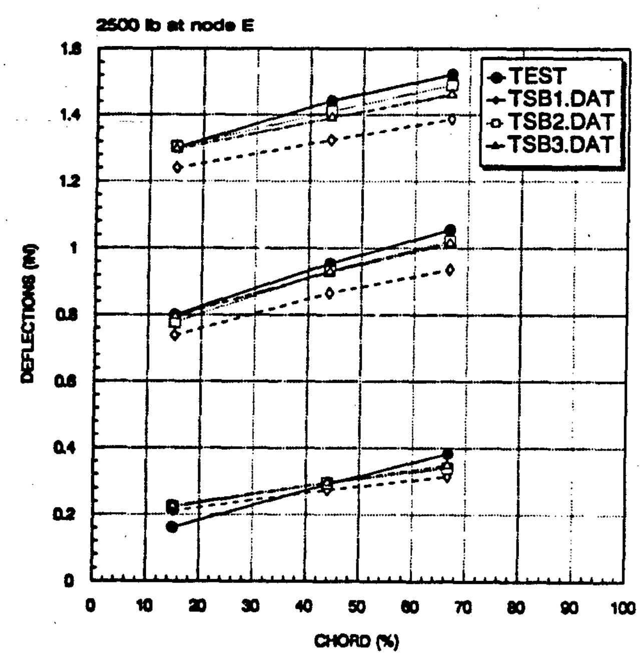

Figure 15b. Comparison of Displacements from TSBi.DAT and Test.

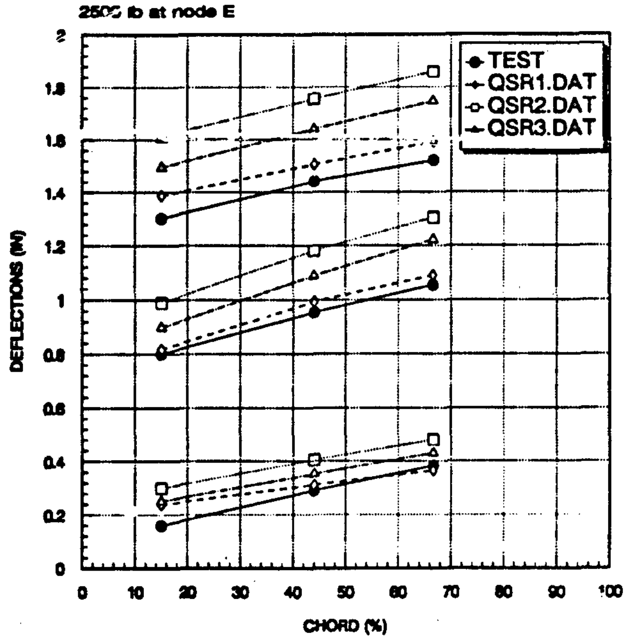

Figure 15c. Comparison of Displacements from QSRi.DAT and Test.

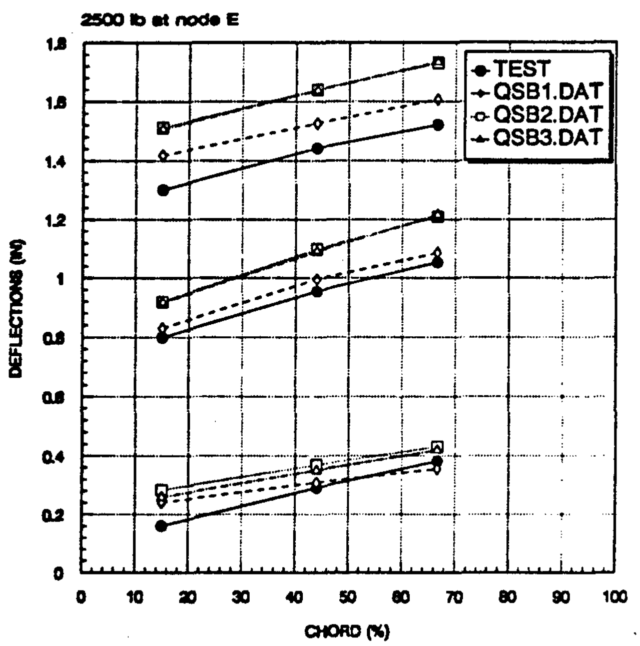

Figure 15d. Comparison of Displacements from QSBi.DAT and Test.

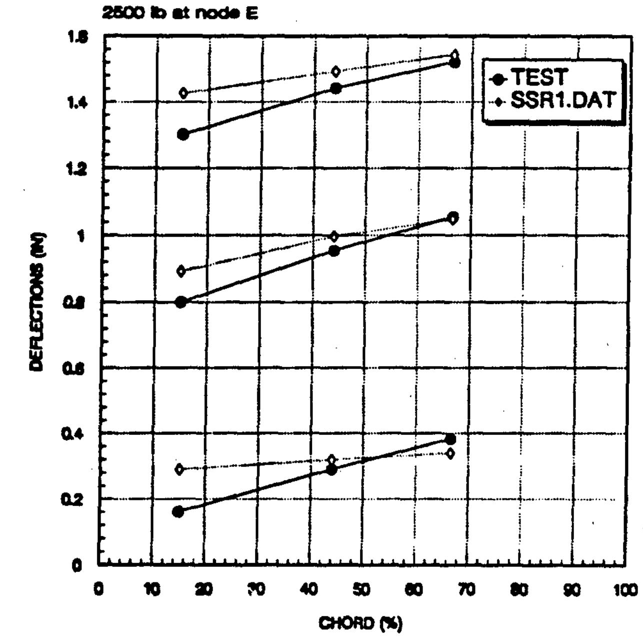

Figure 15e. Comparison of Displacements from SSR1.DAT and Test.

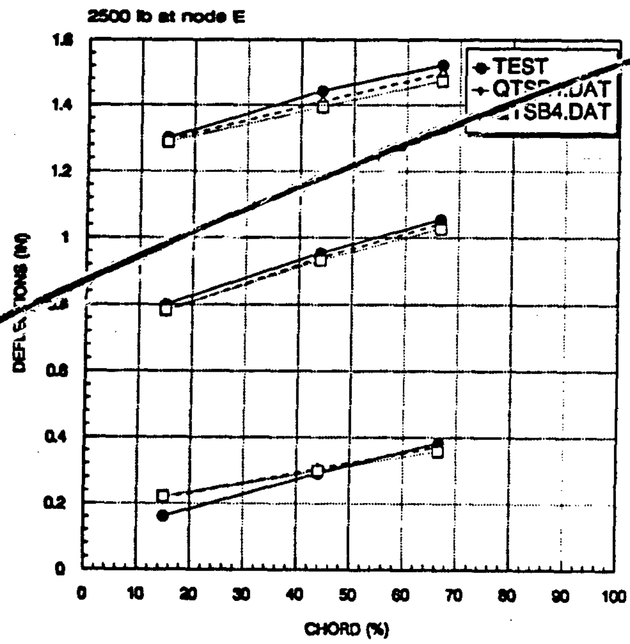

Figure 15f. Comparison of Displacements from QTSR4.DAT, QTSB4.DAT and Test.

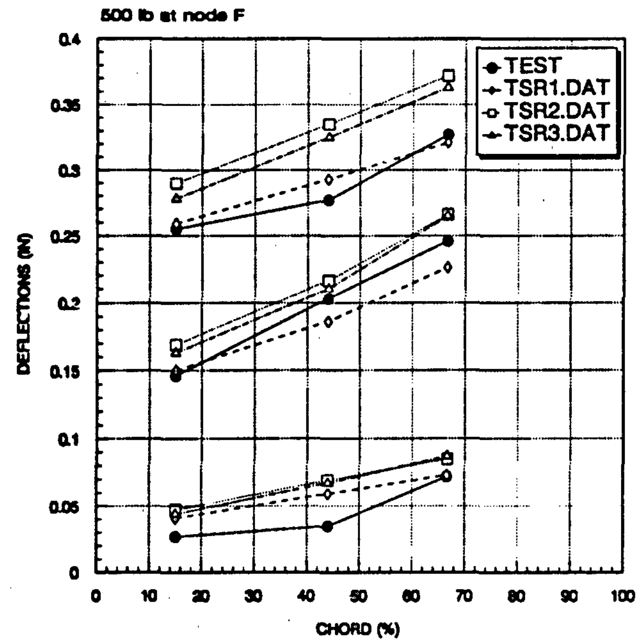

Figure 16a. Comparison of Displacements from TSRi.DAT and Test.

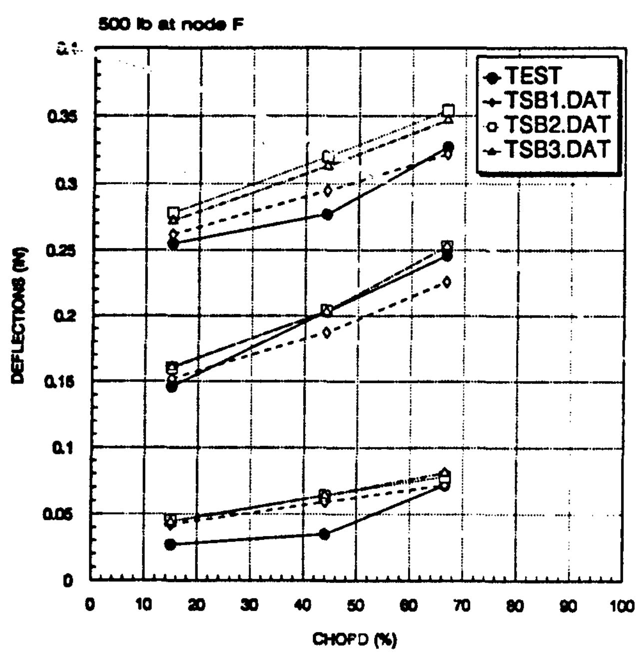

Figure 16b. Comparison of Displacements from TSBi.DAT and Test.

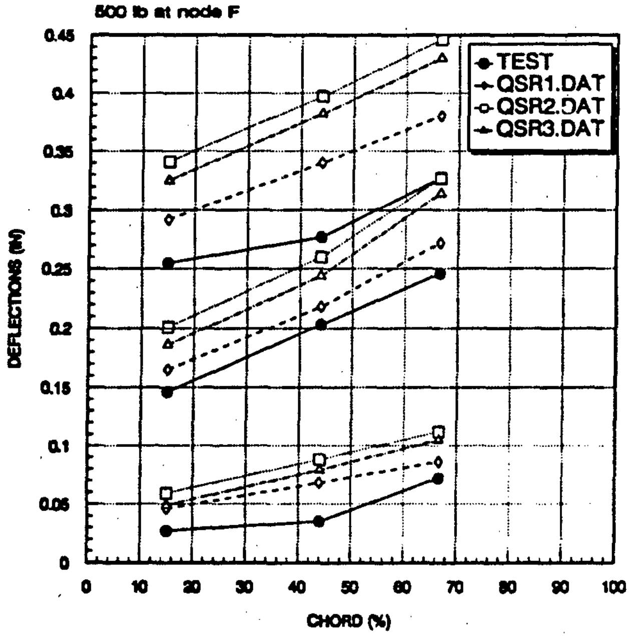

Figure 16c. Comparison of Displacements from QSRi.DAT and Test.

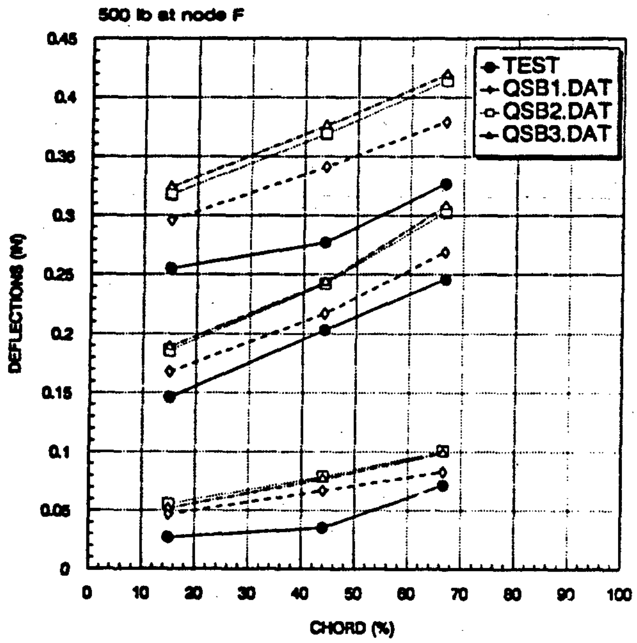

Figure 16d. Comparison of Displacements from QSBi.DAT and Test.

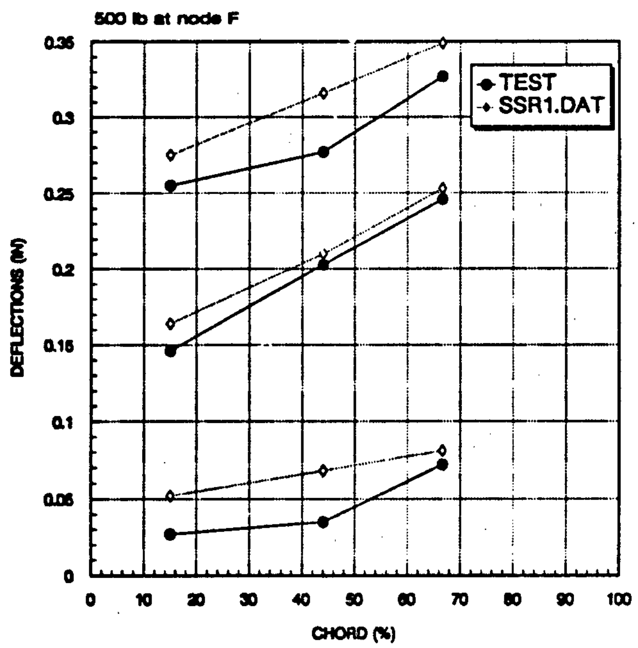

Figure 16e. Comparison of Displacements from SSR1.DAT and Test.

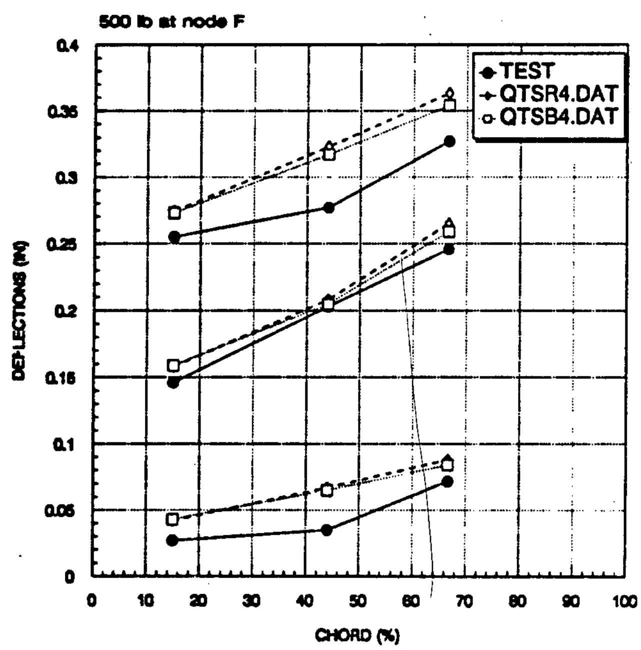

Figure 16f. Comparison of Displacements from QTSR4.DAT, QTSB4.DAT and Test.

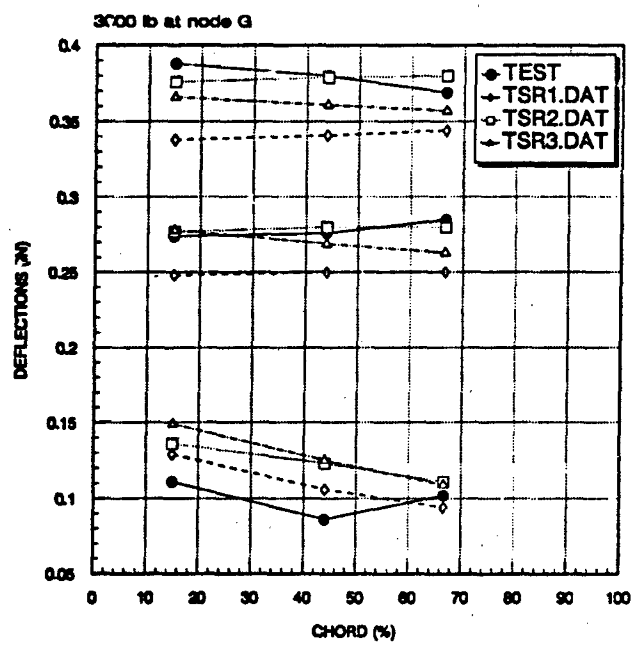

Figure 17a. Comparison of Displacements from TSRi.DAT and Test.

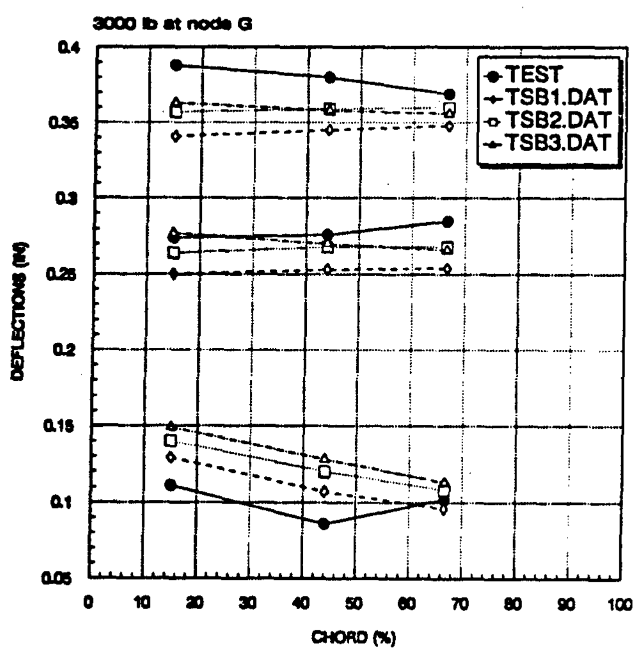

Figure 17b. Comparison of Displacements from TSBi.DAT and Test.

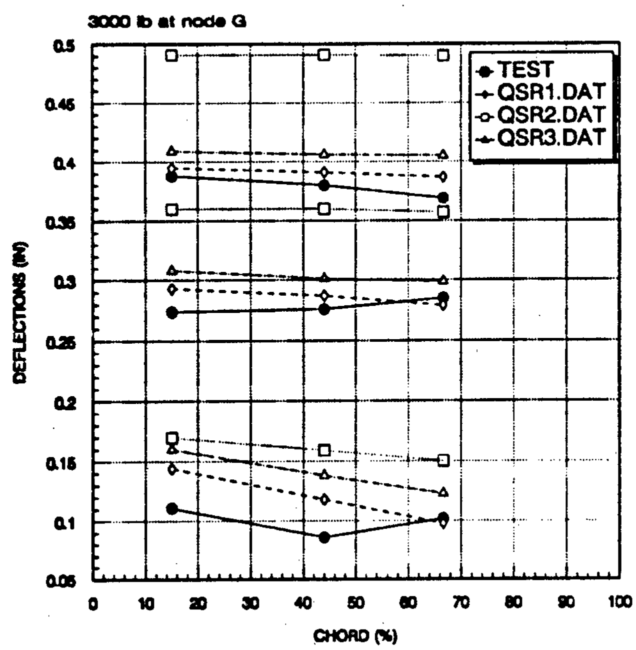

Figure 17c. Comparison of Displacements from QSRi.DAT and Test.

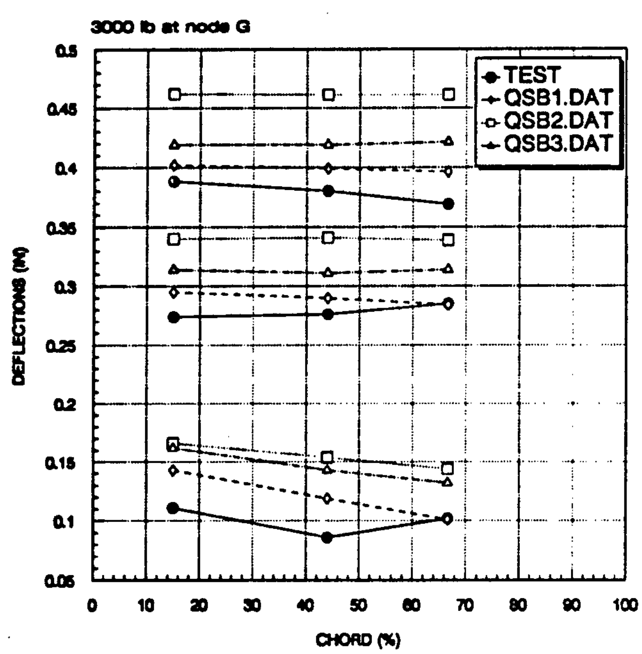

Figure 17d. Comparison of Displacements from QSBi.DAT and Test.

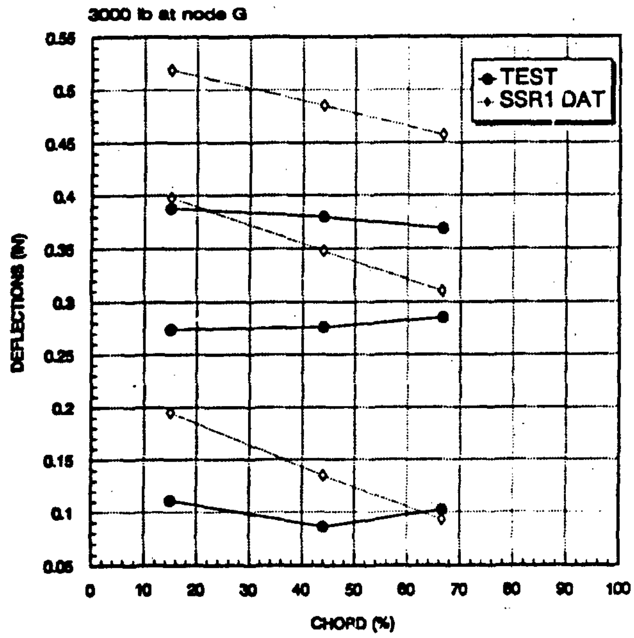

Figure 17e. Comparison of Displacements from SSR1.DAT and Test.

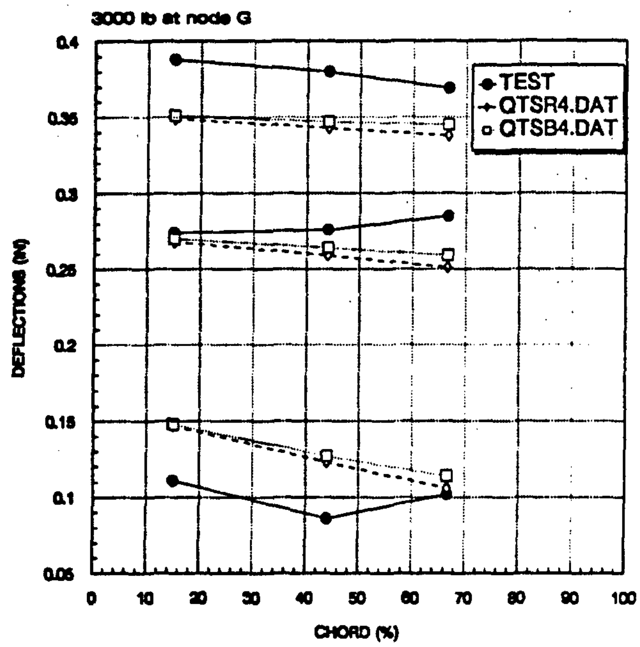

Figure 17f. Comparison of Displacements from QTSR4.DAT, QTSB4.DAT and Test.

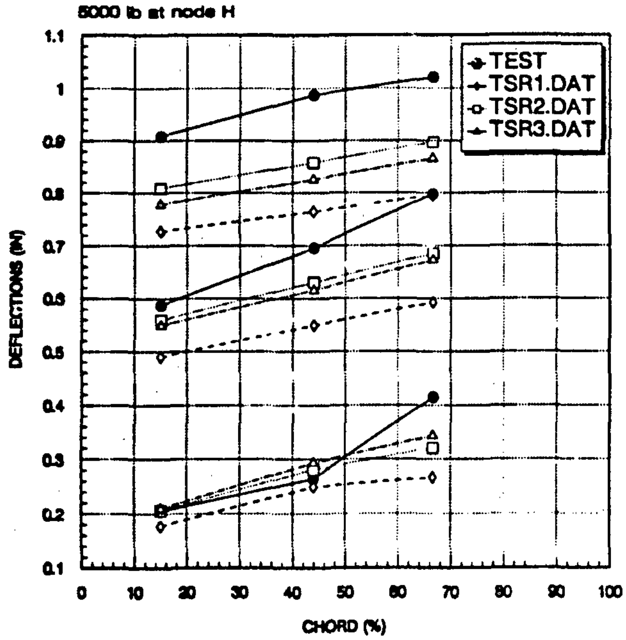

Figure 18a. Comparison of Displacements from TSRi.DAT and Test.

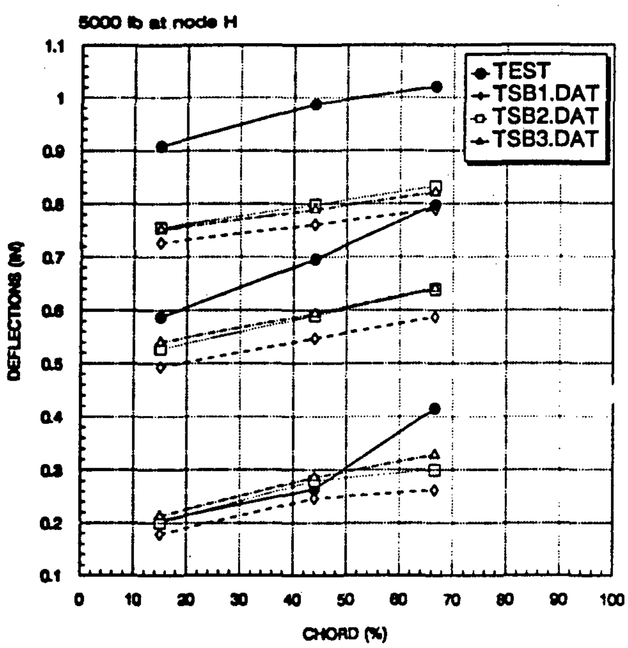

Figure 18b. Comparison of Displacements from TSBi.DAT and Test.

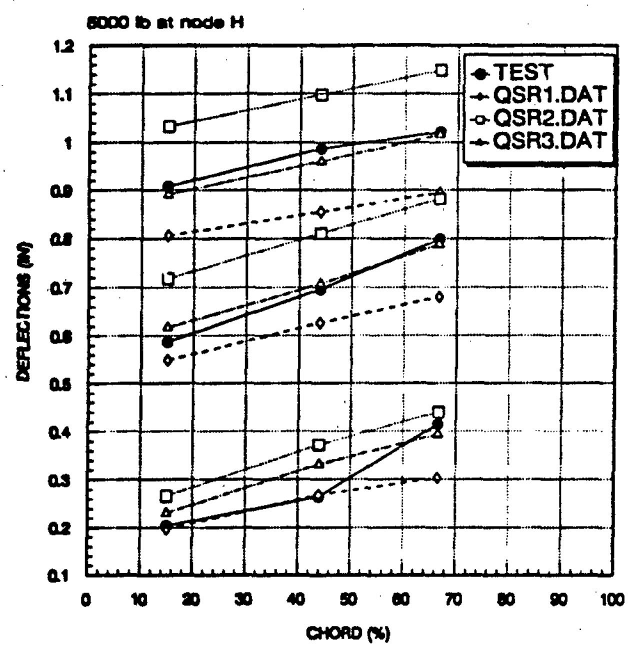

Figure 18c. Comparison of Displacements from QSRi.DAT and Test.

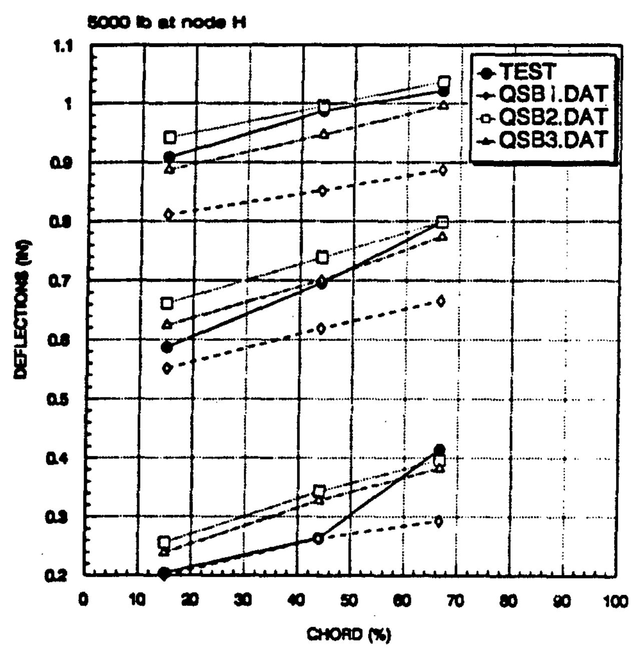

Figure 18d. Comparison of Displacements from QSBi.DAT and Test.

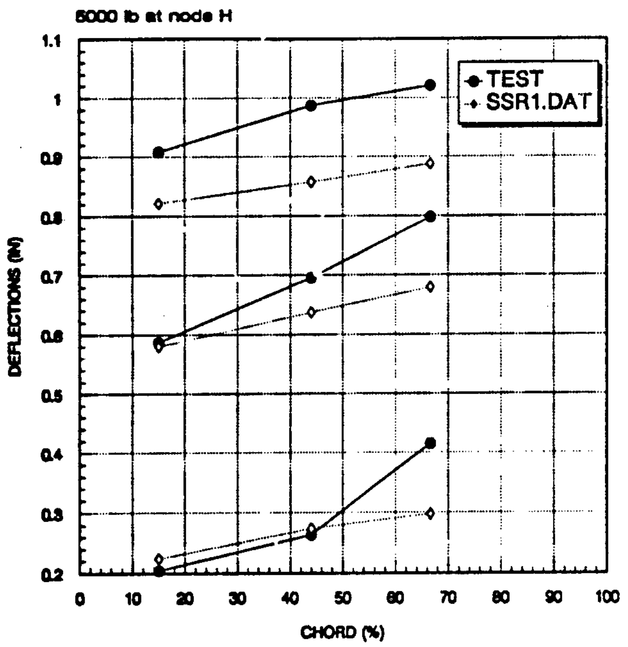

Figure 18e. Comparison of Displacements from SSR1.DAT and Test.

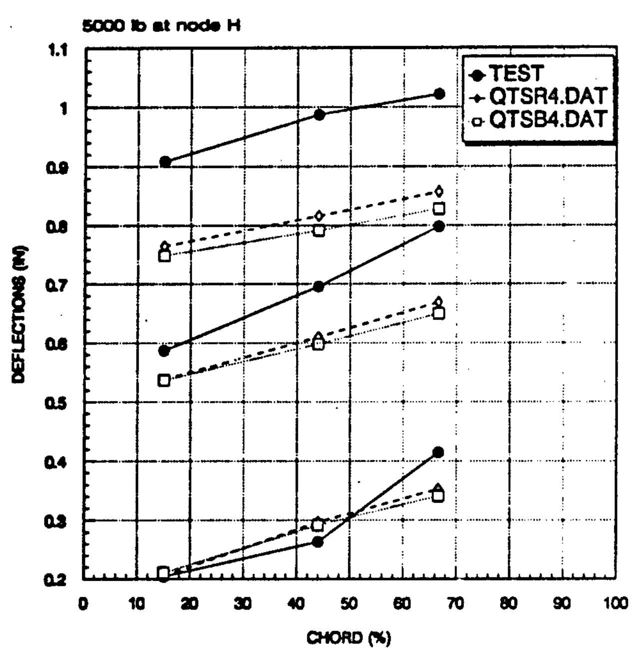

Figure 18f. Comparison of Displacements from QTSR4.DAT, QTSB4.DAT and Test.

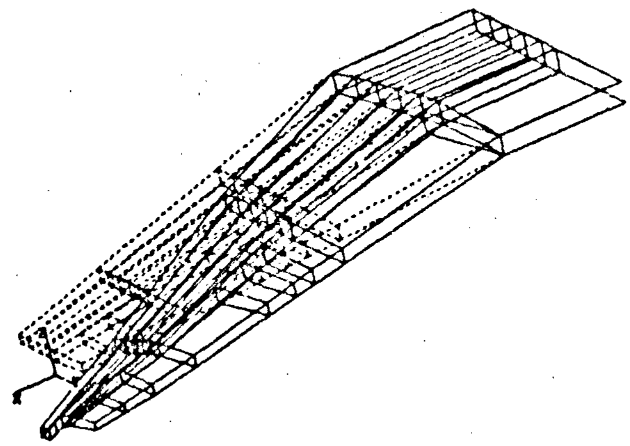

Figure 19a. Numerically Predicted Mode Shape 1, $\omega_n = 4.643$.

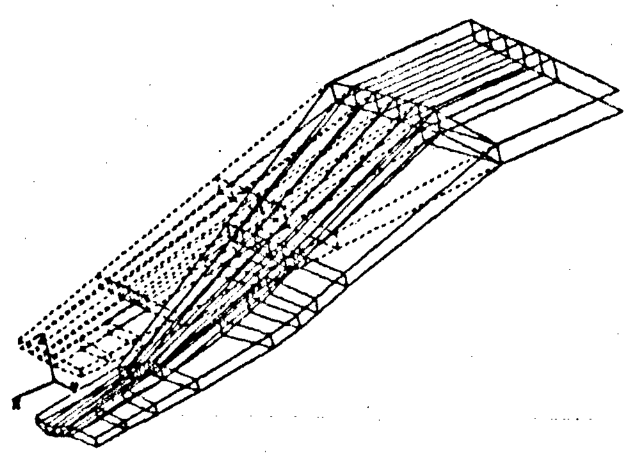

Figure 19b. Numerically Predicted Mode Shape 2, $\omega_n = 6.745$.

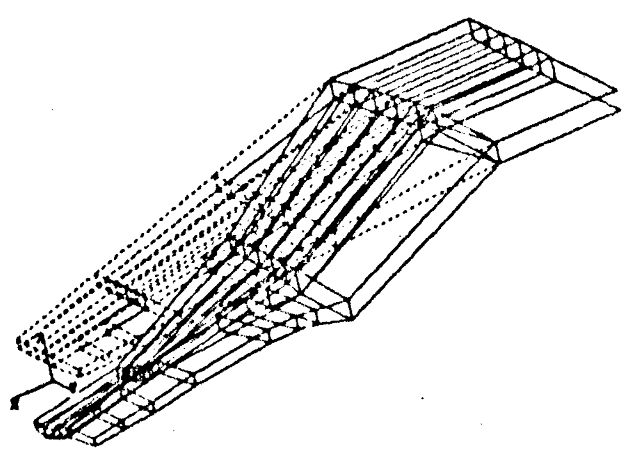

Figure 19c. Numerically Predicted Mode Shape 3, $\omega_n = 7.092$.

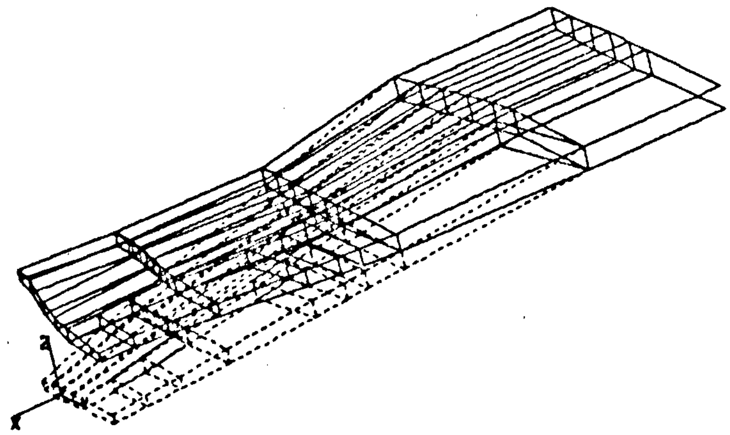

Figure 19d. Numerically Predicted Mode Shape 4. ω_n= 7.105.

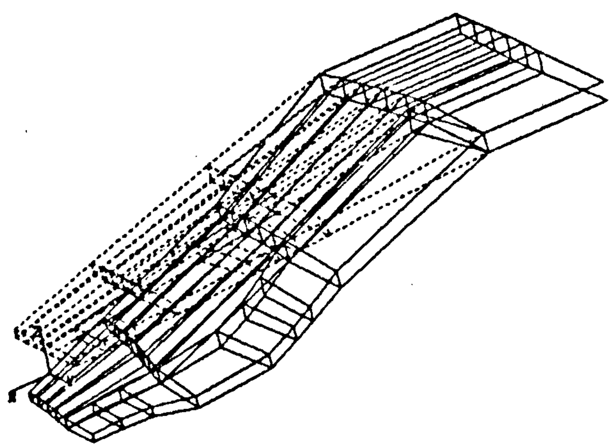

Figure 19e. Numerically Predicted Mode Shape 5. ω_n= 7.799.

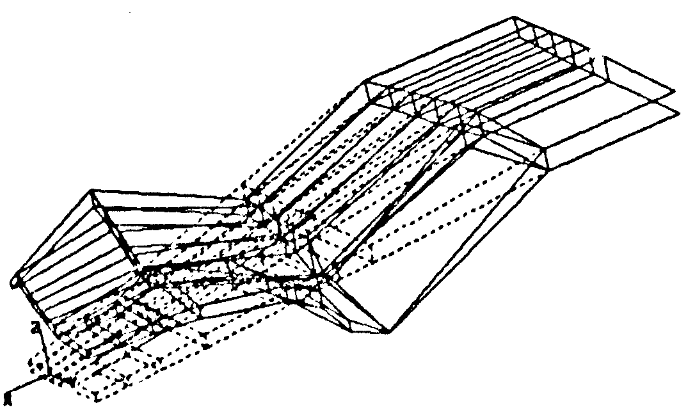

Figure 19f. Numerically Predicted Mode Shape 6. ω_n= 7.944.

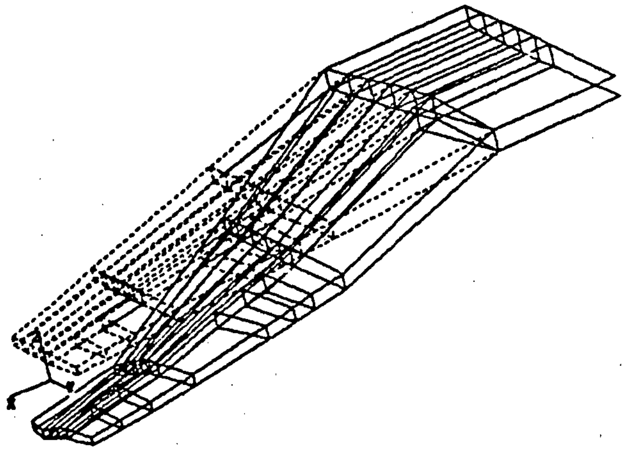

Figure 19g. Numerically Predicted Mode Shape 7. ω_n= 8.269.

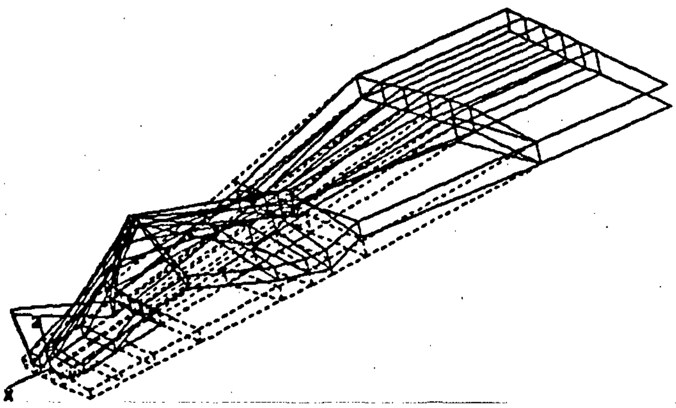

Figure 19h. Numerically Predicted Mode Shape 8. ω_n= 10.681.

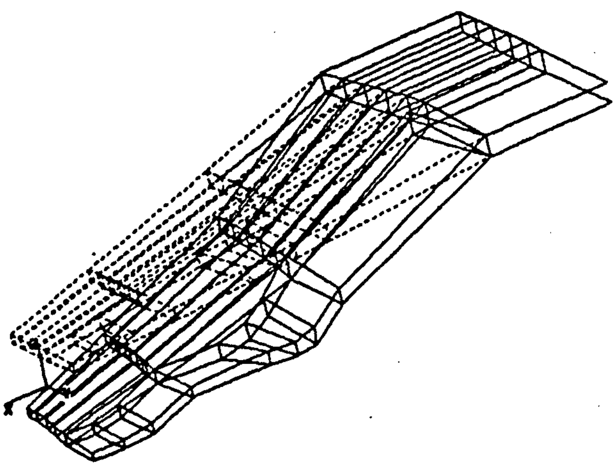

Figure 19i. Numerically Predicted Mode Shape 9. ω_n= 11.542.

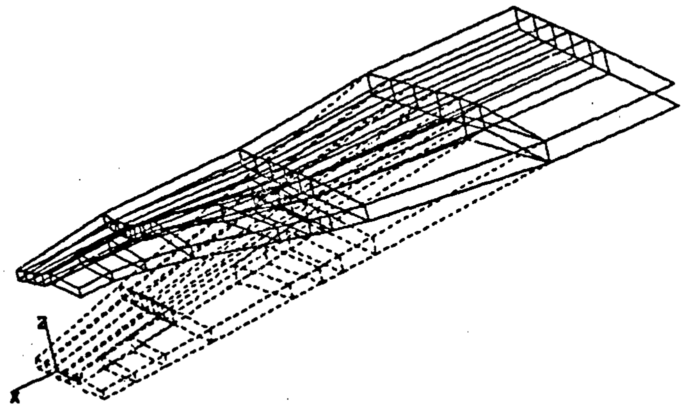

Figure 19j. Numerically Predicted Mode Shape 10, ω_n= 12.655.

NOTE: ------ Undeflected

——— Mode Shape

4. DISCUSSION OF RESULTS

All results calculated by MSC/NASTRAN and MSC/PAL2 are in very good agreement with the test results. In this report, eight different loadings are applied at each node. In a few loading cases, the finite element results are slightly different from the test results, especially for the 3,000 lb and 5,000 lb loading cases. The differences are due in part to model variations and approximations relative to the actual wing structure.

The T-38 wing skin has a slight curvature, therefore, some regions of the model skin structure require finer meshing. To achieve this, triangular elements are used instead of quadrilateral elements. Sets of data files QSRi.DAT and QSBi.DAT having quadrilateral elements are modified to the sets of data files TSRi.DAT and TSBi.DAT having triangular elements. This produces better agreement. The results from TSRi.DAT and TSBi.DAT agree very well with test results for the 500 lb, 1,000 lb, 200 lb, 1,500 lb, 2,500 lb, and 500 lb loading cases as shown in Figures 11a, 11b, 12a, 12b, 13a,13b, 14a, 14b, 15a, 15b, 16a, and 16b. The QSRi.DAT and QSBi.DAT agreement is good, but not as good as the results of TSRi.DAT and TSBi.DAT because of large aspect ratio quadrilateral plates. For example, in the case of 2,500 lb loading at node E, the results from TSR3.DAT show that the difference the between calculated and test results is 1.46 percent, and the results from QSR3.DAT has a 14.9 percent difference(In case of the deflection at node E).

In addition, the combination of quadrilateral and triangular plates is evaluated in this report. The corresponding two data files(Model 4 in Table 1) are QTSR4.DAT and QTSB4.DAT and are actually modified from QSB3.DAT and QSR3.DAT. In this case, the difference between the calculated and test results is 0.46 percent. Of particular interest, the combination of quadrilateral and triangular plate is adequate for this kind of wing skins as shown in Figures 11f-18f. In other words, use of this combination for the T-38 wing skins is significantly different as shown in Figures 15b, 15d, and 15f. Both test results and calculated results show that the loads in eight different loading cases has resulted in bending of the wing about axes parallel to the ribs and has imposed very little torsion. All results are shown in Figures 11-18.

The choice of the type of spar and rib chords depends on the wing structural model. For the current work, the spar and rib chords of the T-38 wing are modeled as beam(bar) and rod elements in separate wing models. The method of sizing the rod elements of the spar and rib of the wing is explained on pages 11-14. The results from TSBi.DAT, TSRi.DAT, QSBi.DAT, QSRi.DAT, QTSB4.DAT, and QTSR4.DAT, show the difference between the CBEAM option and the CONROD option for spar/rib chords is not significant. For example, Figures 11a and 11b show that using either option does not make any difference.

According to Reference [4], one way to treat the the effective areas of the rod element is a summation of its own area, plus the additional term comprised of the skin thickness between the two rods times one half the distance between the rods. There is assumed to be no bending and membrane stiffness in the top and bottom skins(as compared to a real wing structure and box-beam). Because of this assumption, the rod element stiffness is increased. It is the author's experience that a typical difficulty exists in the calculation of the effective area of rod. For example, from equation $\mathbf{A_{eff} = A_f + bt/2}$ (**b** is the distance between two spar or rib chords, **t** is the thickness of wing skins, and, $\mathbf{A_f}$ is the physical cross section area of spar and rib chords), and the value of **b** should be defined. In the case of the T-38 wing, it has a general quadrilateral shape, so an average value of b is taken. This procedure is used in the Model SSR1.DAT (See section 2.3). SSR1.DAT has the shear panel option for the top and bottom skins and spar and rib webs: The weakness, difficulty of the calculation of the effective area of rod, in using this procedure is shown in Figures 11e-18e.

Figures 19a-j show ten flap bending modes and the associated natural frequencies. The natural frequencies for the higher modes appear in Table 3. At this time, test data are not available for correlation with dynamic test results.

5. CONCLUSIONS

In this report, results of a static and dynamic analysis of an undamaged T-38 wing have been presented. Seven different structural models of the wing have been studied. Model 4(QTSR4.DAT and QTSB4.DAT) it featured quadrilateral and triangular plate elements for the wing skins, shear panel elements for spar/rib webs and rod or bar(beam) elements for spar/rib chords gives the best comparison with the available static data. Also, this model (used to reduce the problem size) is efficient and accurate as shown in Figures 11f-18f. Model 4 will be used as the T-38 wing model for static and dynamic aeroelasticity and flutter solutions because an accurate determination of influence coefficients is needed in such analysis.

Model SSR1.DAT that used shear panel elements for the top and bottom wing skins instead of quadrilateral or triangular plate elements is not adequate for a complex wing as discussed earlier in this report as shown in Figures 11e-18e.

The CBEAM option used for the spar and rib chords instead of the CONROD option is strongly recommended to create finite structural models for the T-38 wing or similar type wings.

6. RECOMMENDATIONS

The following recommendations are based on this research.

1) Improved results can be expected by using more nodes and elements than used in models 1, 2, 3, or 4.

2) The T-38 wing skin has variable thickness, so it is recommended that the CQUAD8 card in MSC/NASTRAN be used to define a curved quadrilateral shell element with eight grid points. For the triangular plate, CTRIA6 will be used in the follow-on effort.

3) A damaged T-38 wing structural test should be performed to allow correlation with the MSC/NASTRAN finite element code predictions.

INTENTIONALLY LEFT BLANK

7. REFERENCES

1. NOR-60-6. Static Test of Complete Airframe for the T-38A Airplane. Hawthorne, California: Northrop Aircraft, Inc., March 1960.

2. Rattinger, I., Dickenson, H., Cole, C.D., "Preliminary Report Comparison with Test of Analytically Derived Influence Coefficients for a Straight Low-Aspect Ratio Model Wing," Bell Aircraft Report No. 9001-914001, 1957.

3. An Experimental and Analytical Study of the Static Response of an Undamaged and Damaged F-84 Wing, Vols I and II. 61 JTCG/ME-76-11-1 and -2. Eglin AFB, Fla.: Joint Technical Coordinating Group for Munitions Effectiveness, Aug. 24, 1976.

4. An Experimental and Analytical Study of the Dynamic Response of an Undamaged and Damaged F-84 Wing. 61 JTCG/ME-77-2. Eglin AFB, Fla.: Joint Technical Coordinating Group for Munitions Effectiveness, Feb. 27, 1977.

5. Gockel, M. A. (Ed.), MSC/NASTRAN Dynamic Handbook, MacNeal-Schwendler Corp., Los Angeles, June 1983.

6. Analysis of Progressive Collapse of Aircraft Structures. 61 JTCG/ME-84-2. Tinker AFB, OK.:Joint Technical Coordinating Group for Munitions Effectiveness, May 30, 1986.

7. Stronge, W.J. Failure Prediction for Damaged Aircraft Wings. Proceedings of the Fifth Navy-Nastran Colloquium, NSRDC, 1974.

8. Peery, David J. Aircraft Structures. New York: McGraw-Hill, 1950

9. Bruhn, E. F. Analysis and Design of Flight Vehicle Structures. Cincinnati: Tri-State Offset Company, 1973.

10. Timoshenko, S.P. and Goodier, J.N. Theory of Elasticity. New York: McGraw-Hill Book Co., 1970.

11. NASA SP-221(03). The NASTRAN Theoretical Manual. Washington DC.: Scientific and Technical Information Division, National Aeronautics and Space Administration, March 1978.

12. Oehrli, Robert, Wing Aeroelasticity Analysis: Manuevering Aerial Target, Vol. III, US Army Ballistic Research Laboratory, Aberdeen Proving Ground, Maryland, 1988.

13. Zienkiewicz, The Finite Element Method, 3rd Ed., McGraw-Hill, London, 1977.

14. Przemieniecki, J.S., Theory of Matrix Structural Analysis, McGraw-Hill, New York, 1968.

15. Tinawi, R.A., "A Study of Various Idealizations for Wing Structures and Numerical Procedures Involved Using Matrix Methods," AIAA Paper 69-26809, 1969.

16. Granger, R.A., A Unified Method of Flutter Analysis, The Martin Company, July 1959.

APPENDIX A:

Finite Element Model Numbering Details

INTENTIONALLY LEFT BLANK

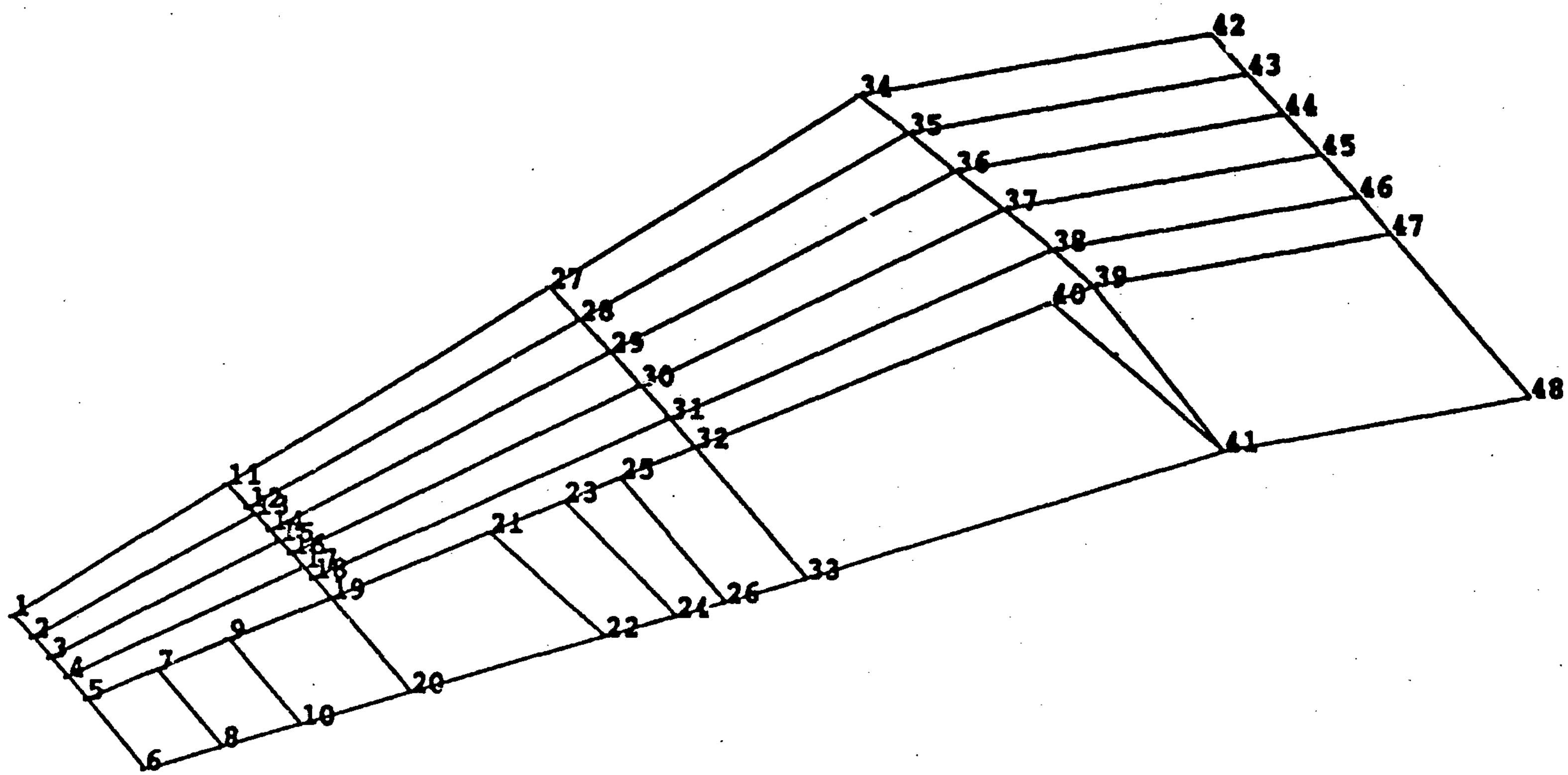

Figure A1. Node Numbers, Top Surface.

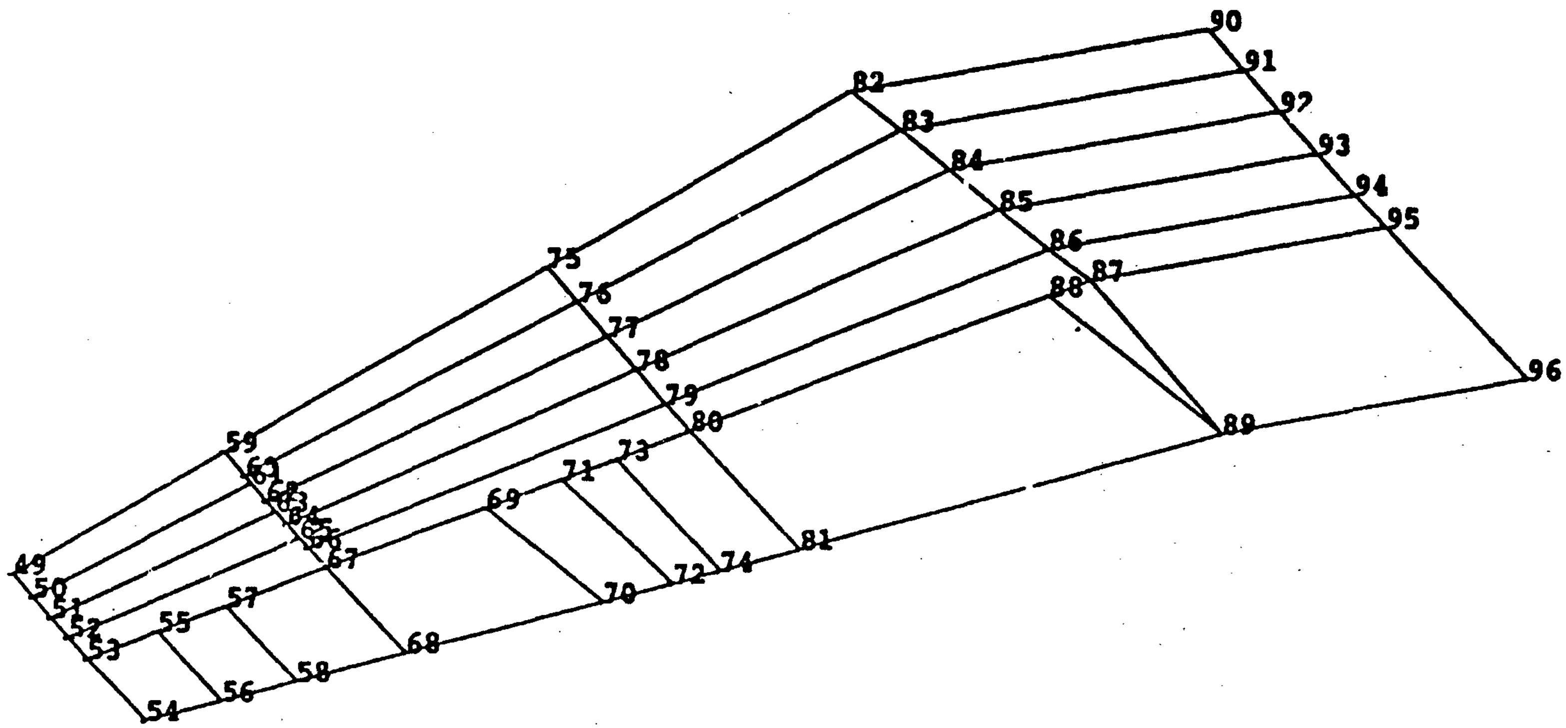

Figure A2. Node Numbers, Bottom Surface.

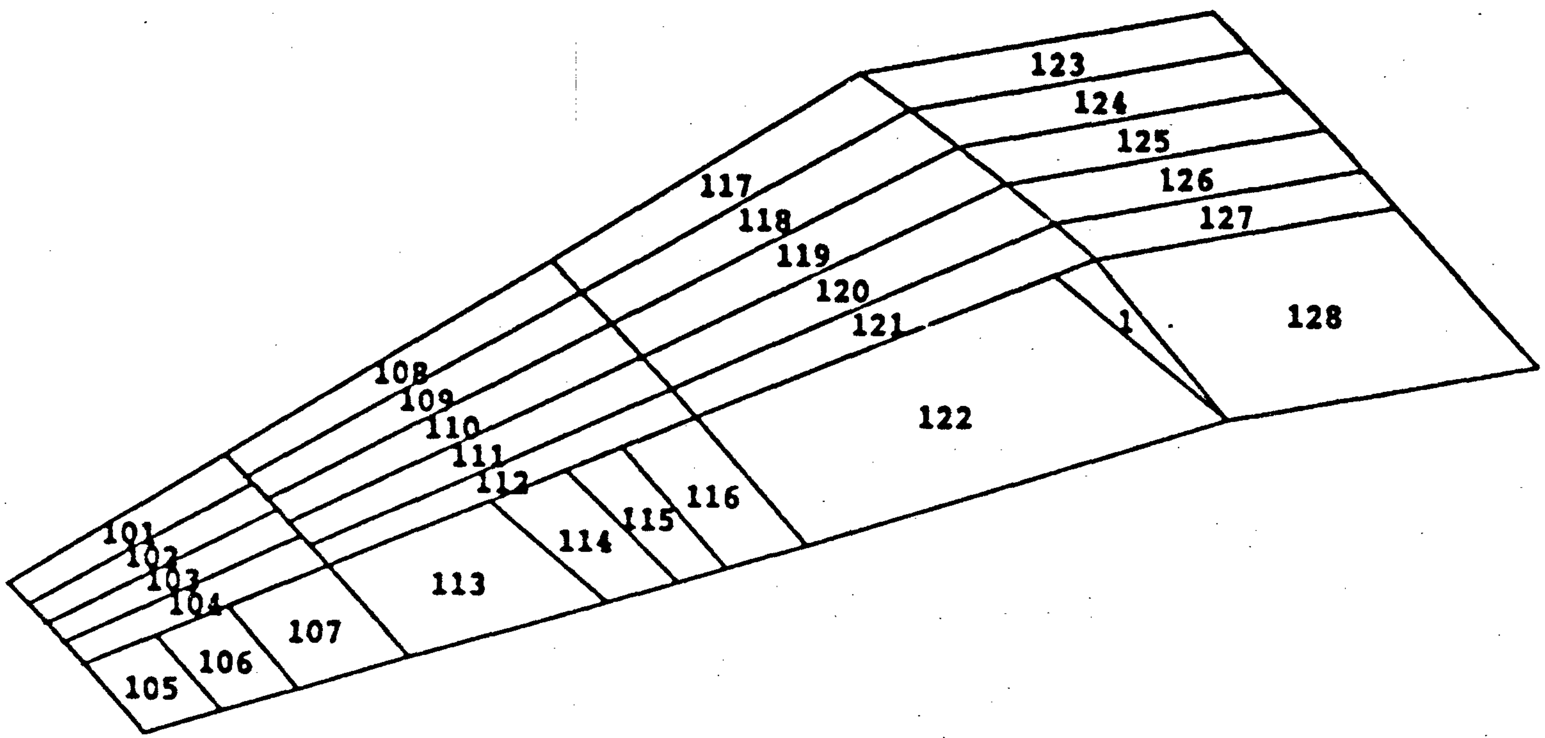

Figure A3. Skin Panel Numbers, Top Surface.

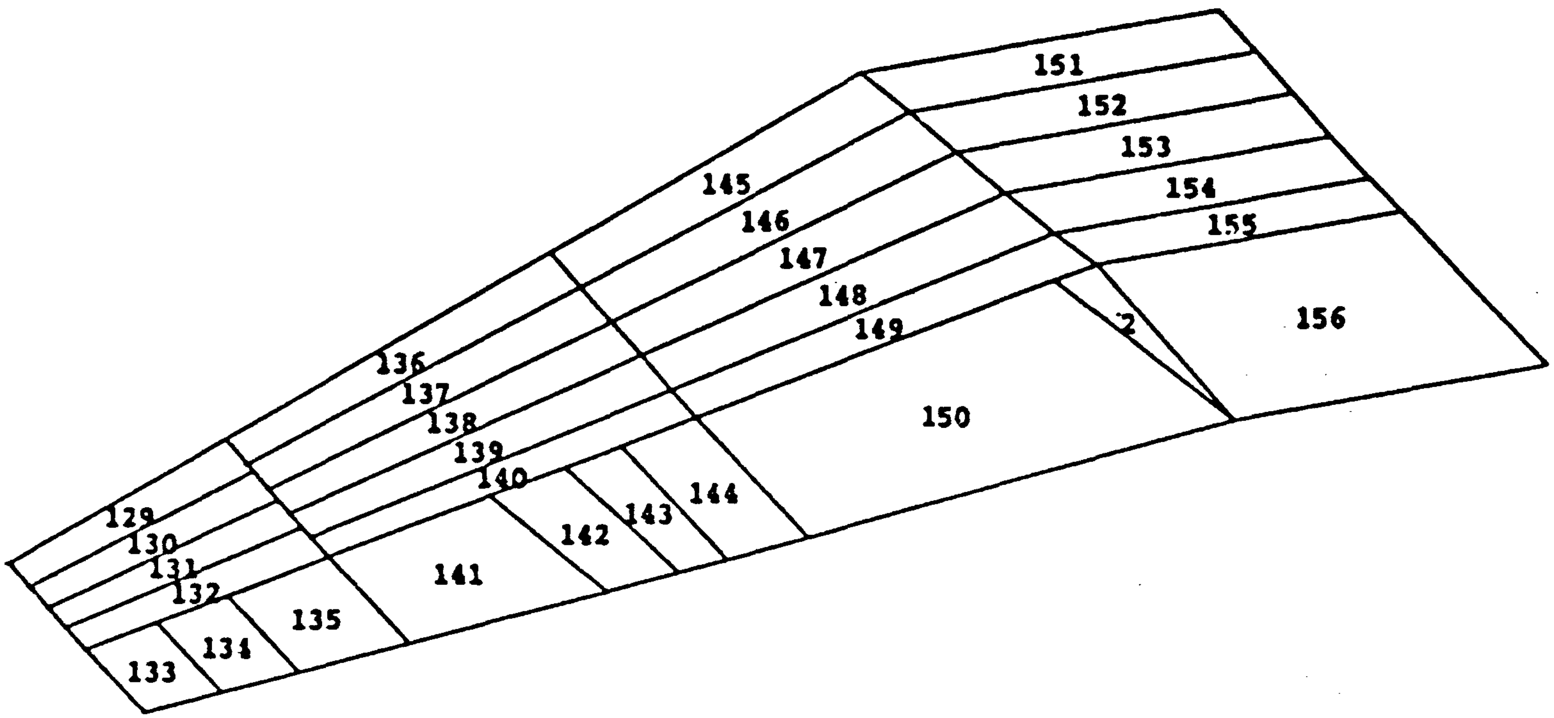

Figure A4. Skin Panel Numbers, Bottom Surface.

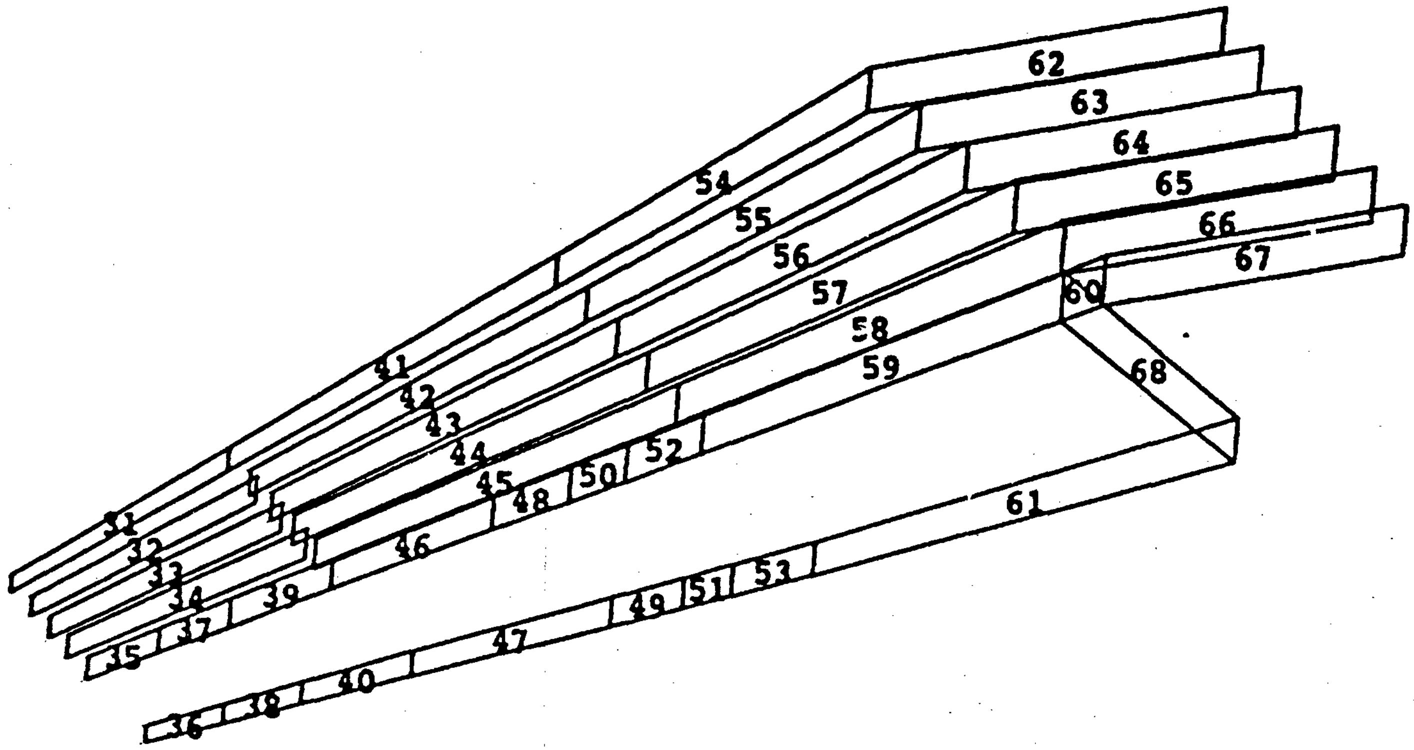

Figure A5. Spar Web Element Numbers.

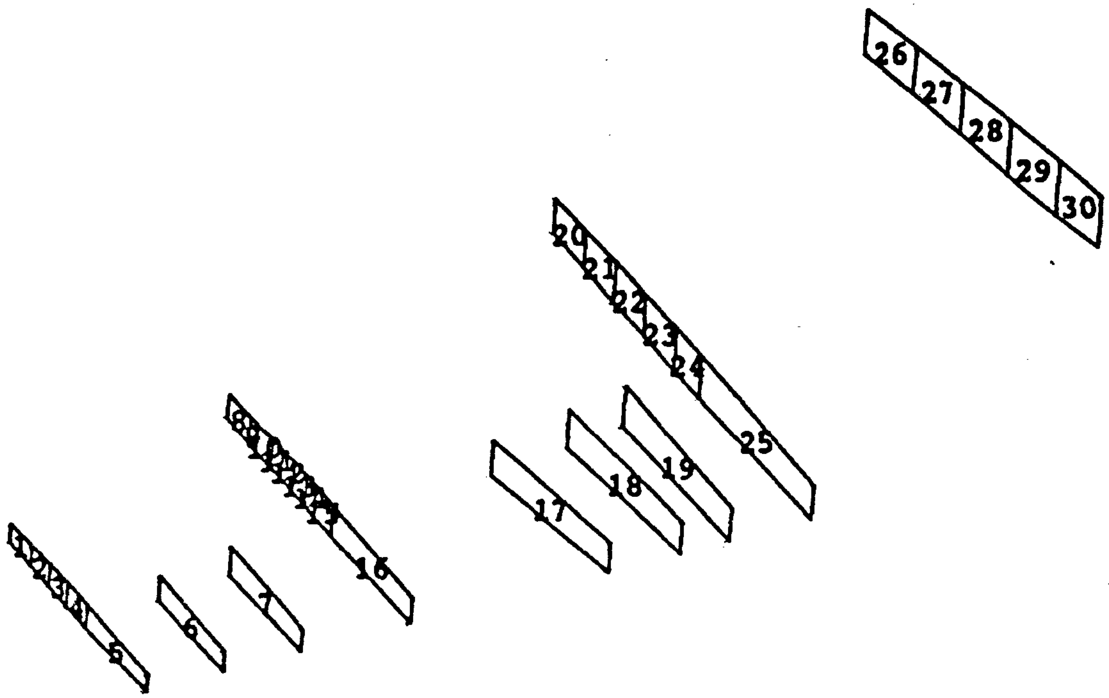

Figure A6. Rib Web Element Numbers.

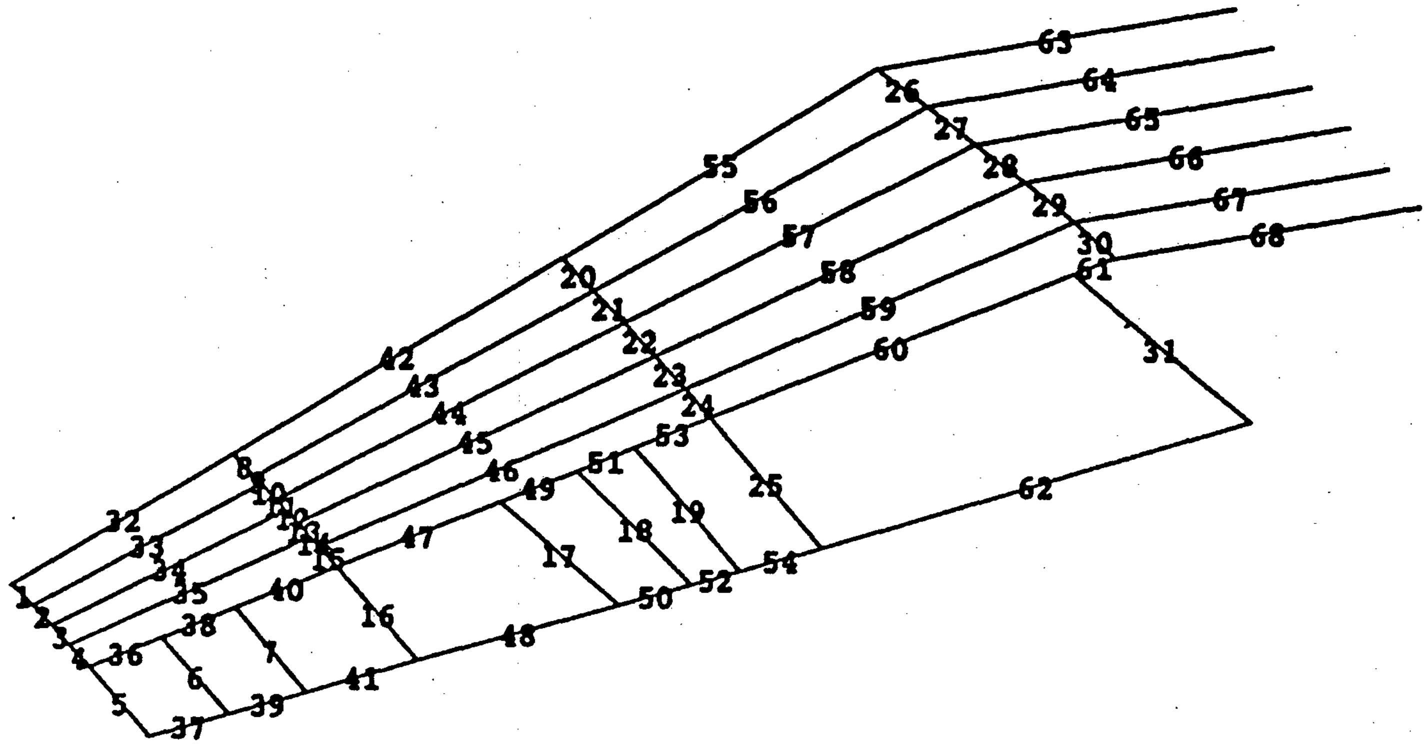

Figure A7. Spar and Rib Chord Numbers, Top Surface.

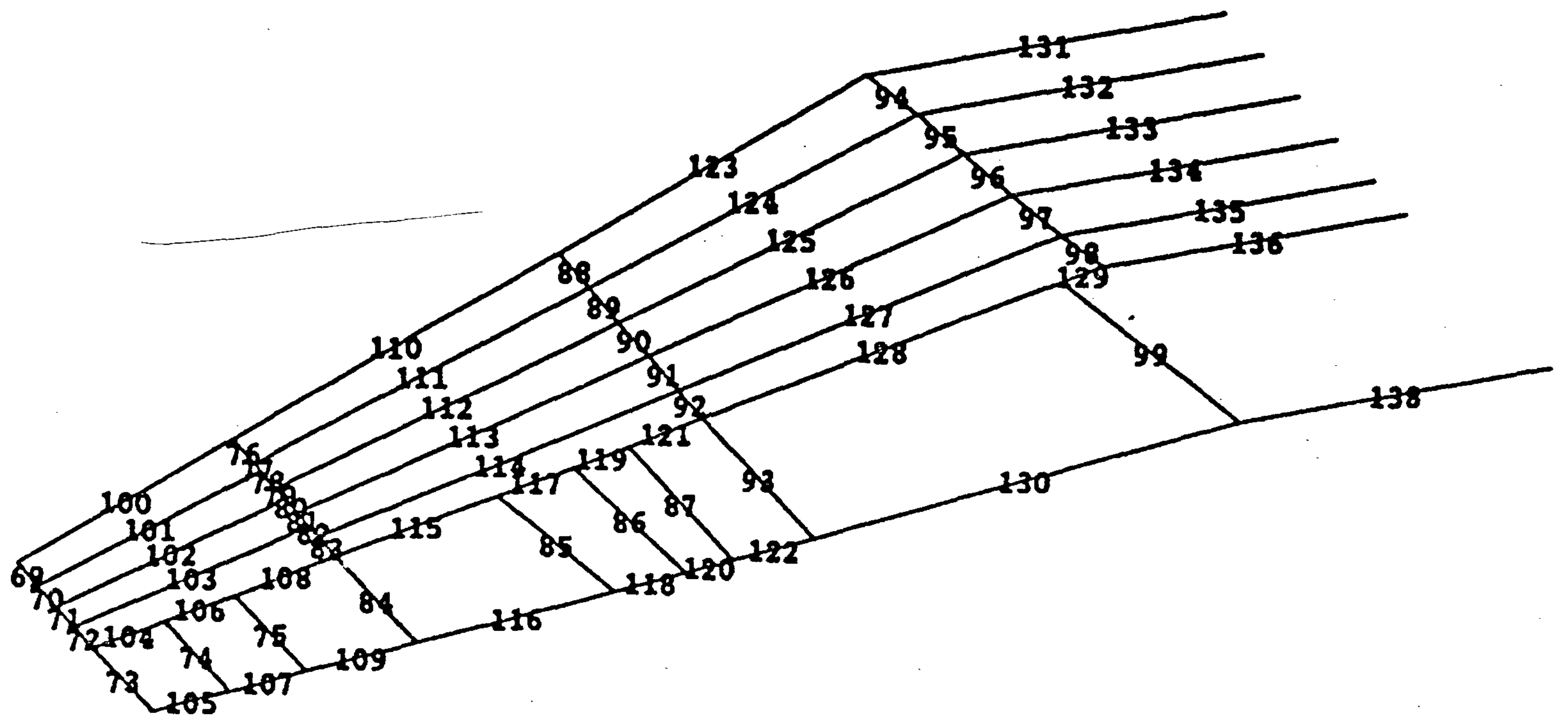

Figure A8. Spar and Rib Chord Numbers, Bottom Surface.

APPENDIX B:

Finite Element Model for Top, Middle, and Bottom

INTENTIONALLY LEFT BLANK

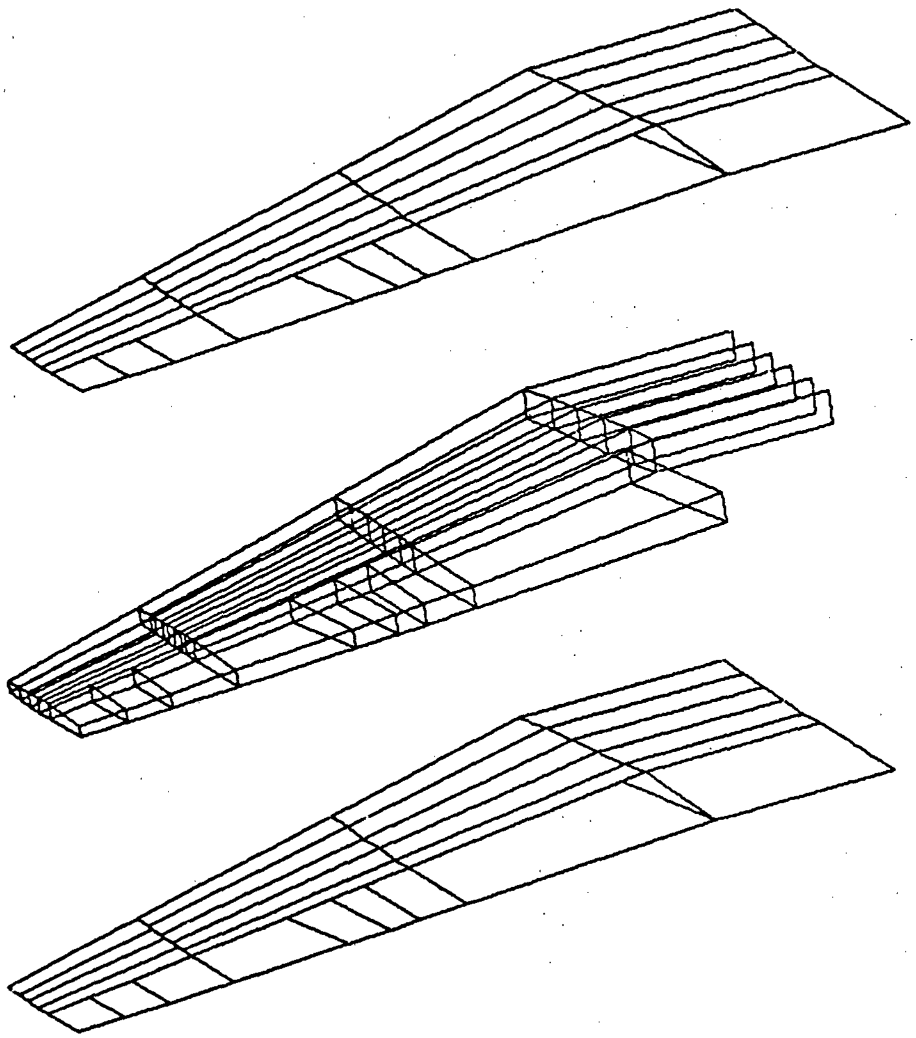

Figure B1. Finite Element Model QSB1.DAT and QSR1.DAT.

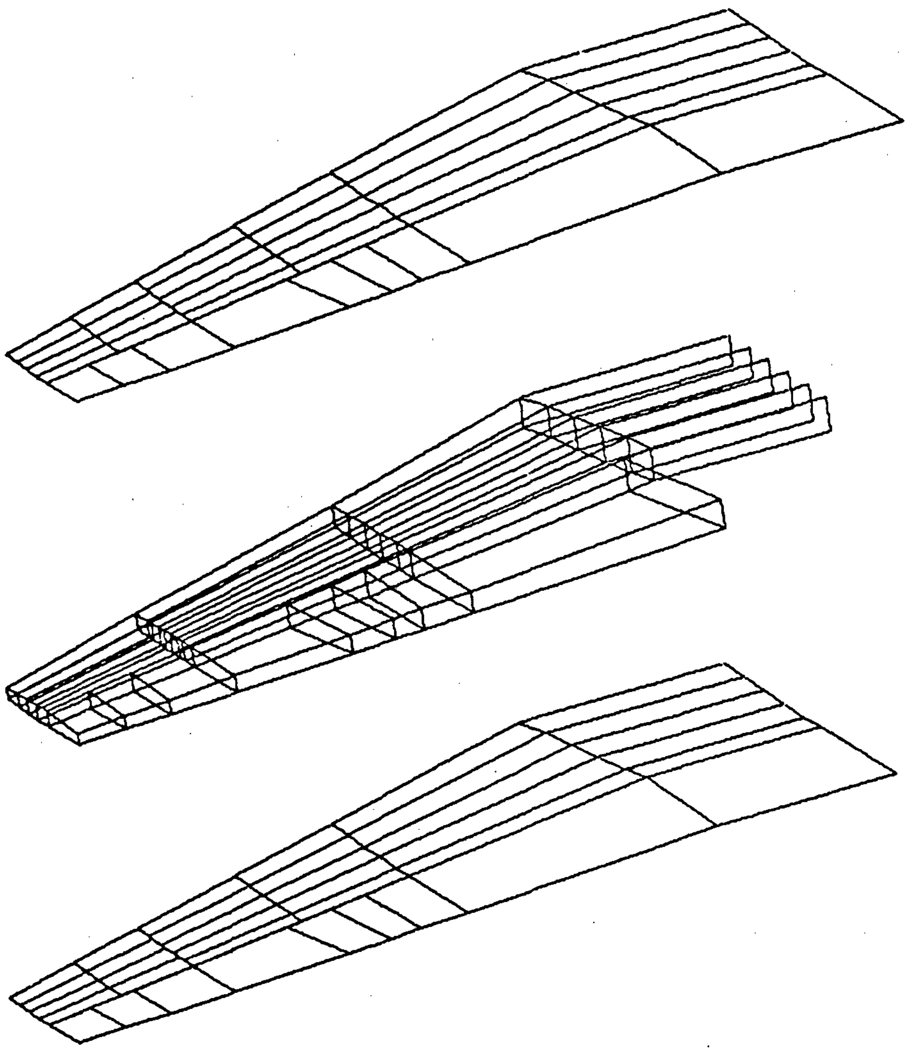

Figure B2. Finite Element Model QSB2.DAT and QSR2.DAT.

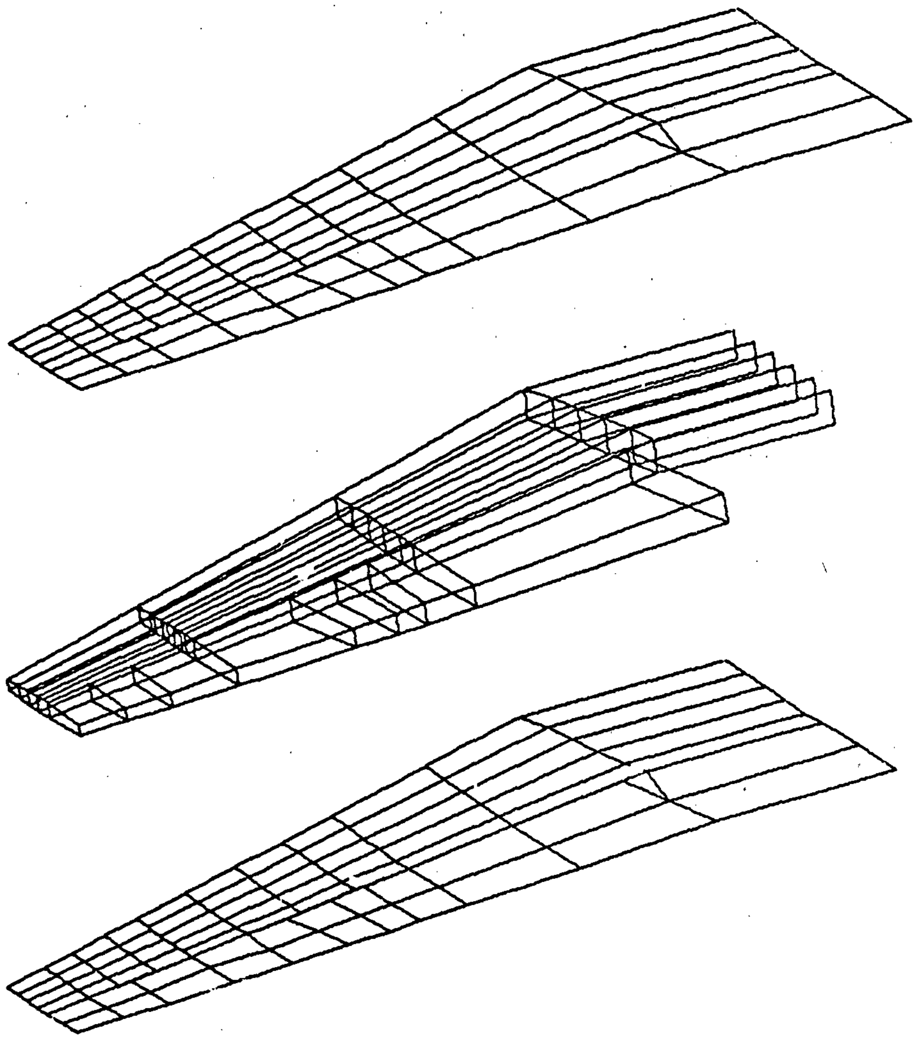

Figure B3. Finite Element Model QSB3.DAT and QSR3.DAT.

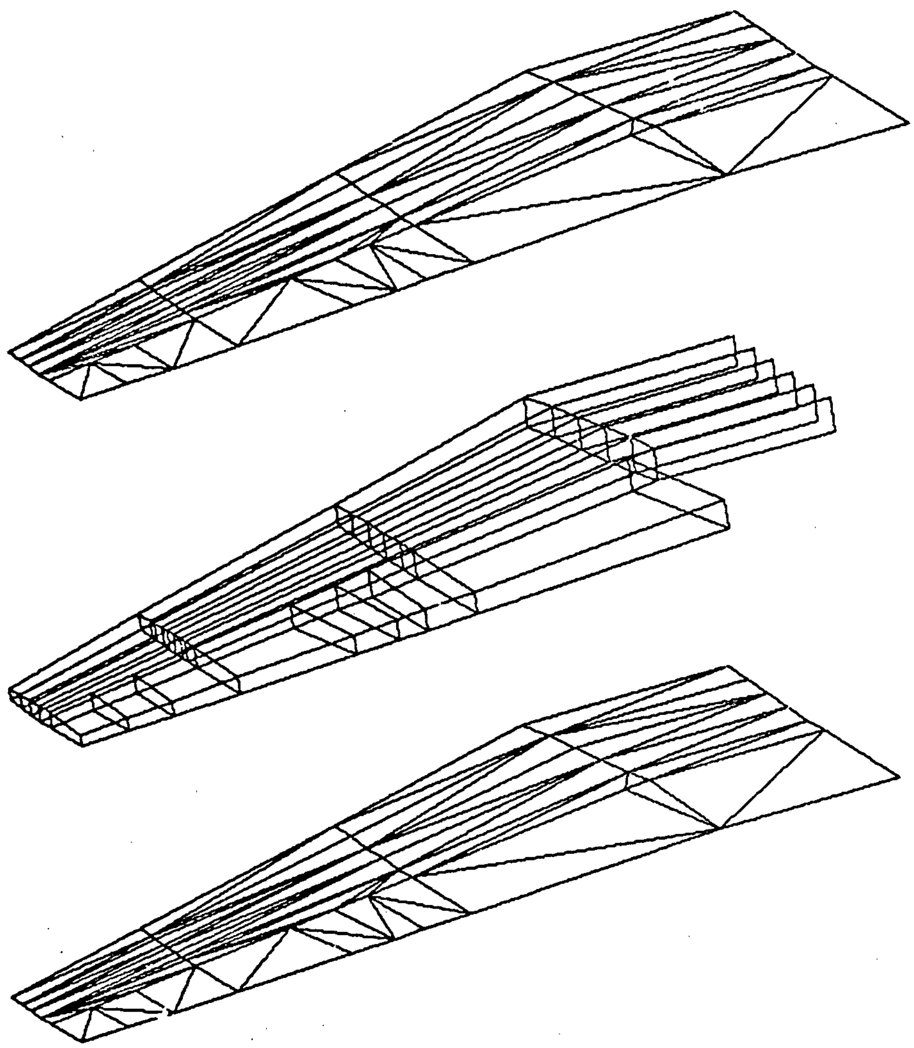

Figure B4. Finite Element Model TSB1.DAT and TSR1.DAT.

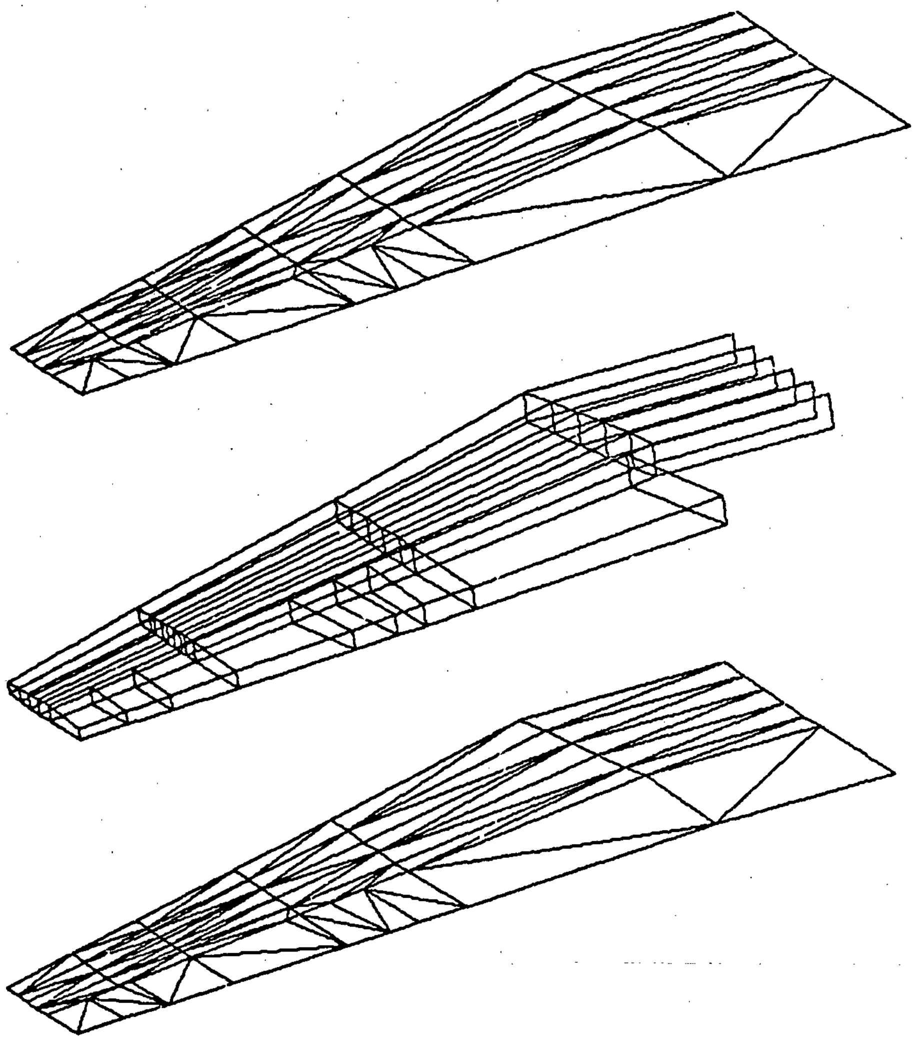

Figure B5. Finite Element Model TSB2.DAT and TSP2.DAT.

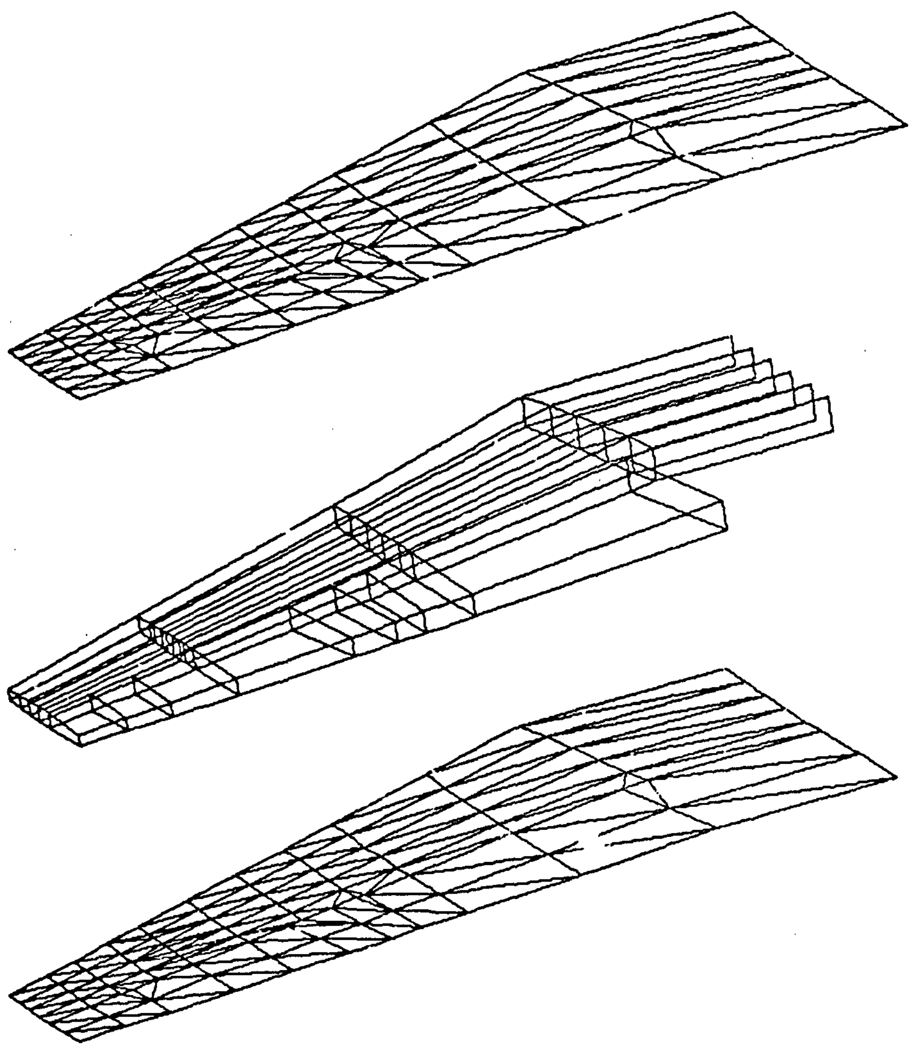

Figure B6. Finite Element Model TSB3.DAT and TSR3.DAT.

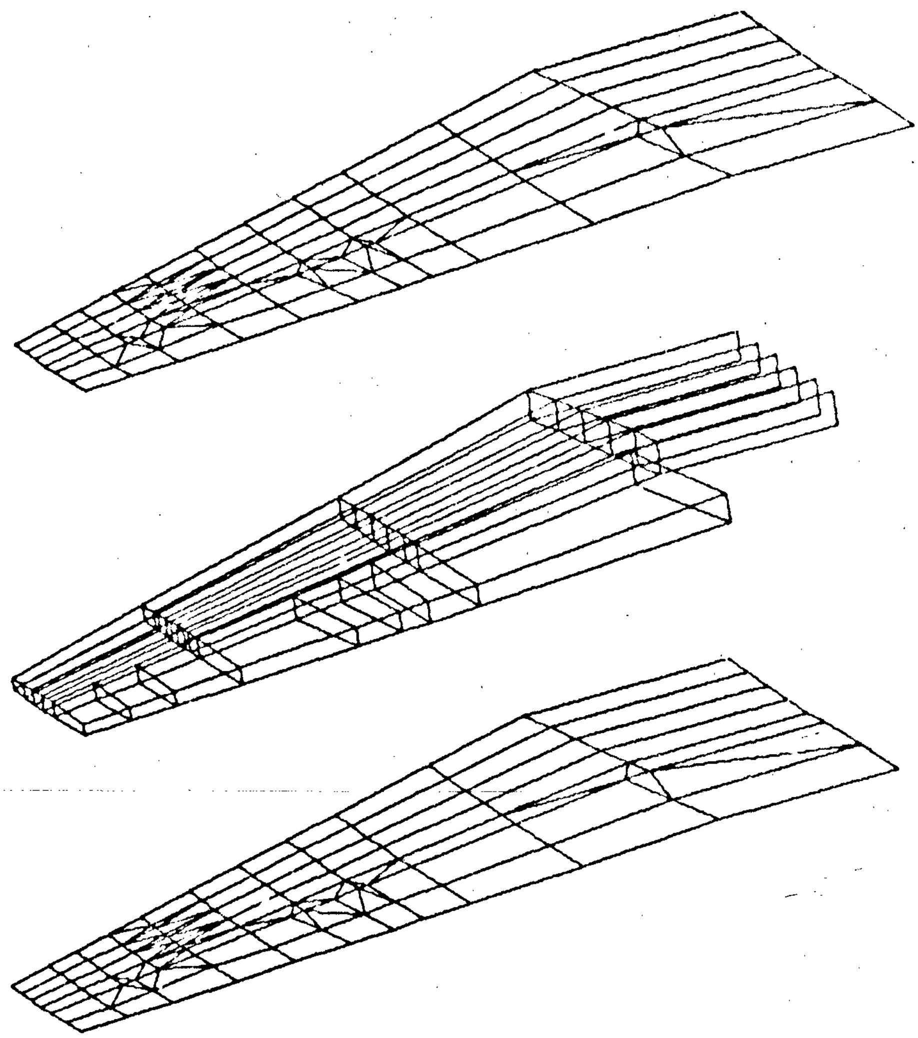

Figure B7. Finite Element Model QTSB4.DAT and QTSR4.DAT.

INTENTIONALLY LEFT BLANK

APPENDIX C:

Rattinger's Wing

INTENTIONALLY LEFT BLANK

1. Introduction

Typical static plate(box-beam) deflection analysis are sampled why different plate element are used in this report. Rattinger's wing is examined because of its structural simplicity and ease in checking out various portions of the digital program. This wing has unswept, untapered, constant-thickness, and continuous skin.

2. Boundary Conditions

This wing is considered as cantilever plate(box-beam). All fixed at wing root and all free at 15 grid points as shown in Figure C2. 100 lbs is loaded at node 3.

3. Description of Finite Element Model

Five sets of SSR.x data are used for the SHEAR panel option for the top and bottom skins as shown in Table C1. Data SSR.1 and SSR.2 are from Equation C1 and SSR.3 and SSR.4 are from Equation C2. As explained in Section 2.4, A_f is obtained and then A_{eff} is determined for the top and bottom spar/web chords.

$$A_{eff} = A_f + \frac{b_1 t_1}{2} \qquad \text{(C1)}$$

$$A_{eff} = A_f + \frac{b_1 t_1}{2} + \frac{b_2 t_2}{2} \qquad \text{(C2)}$$

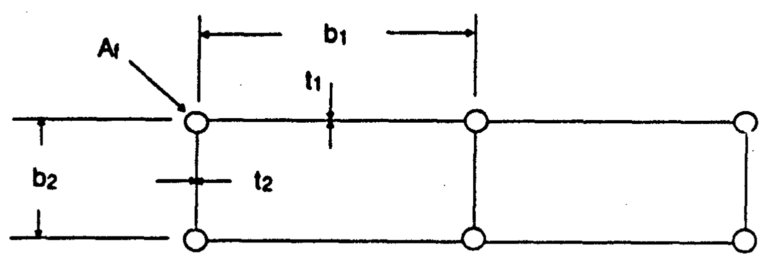

Figure C1. General Box-Beam End View.

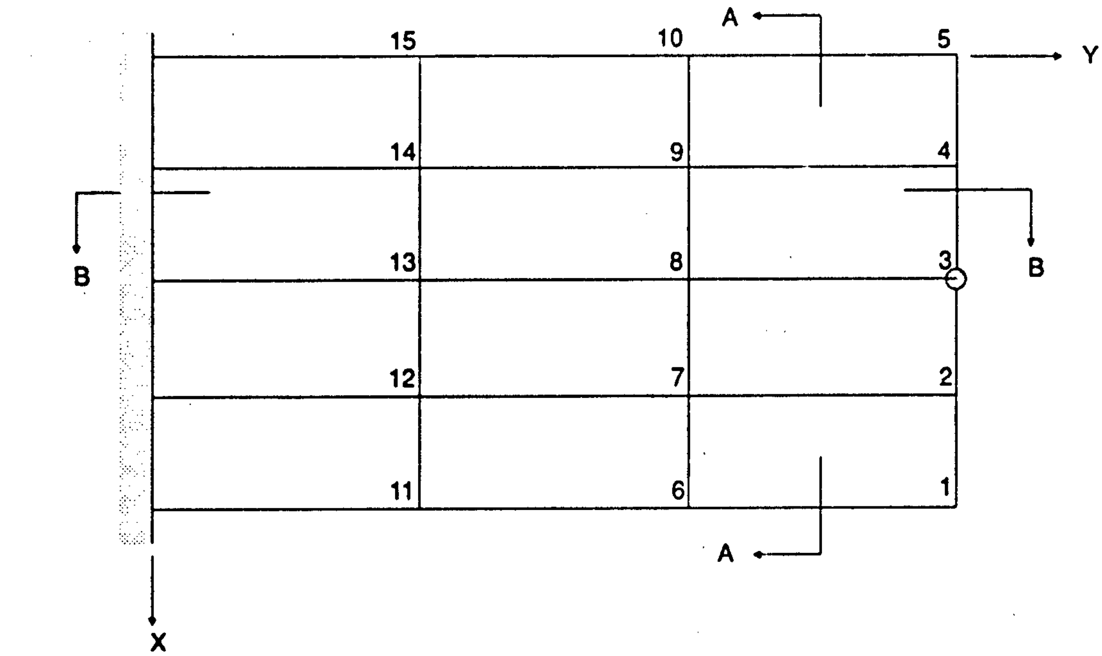

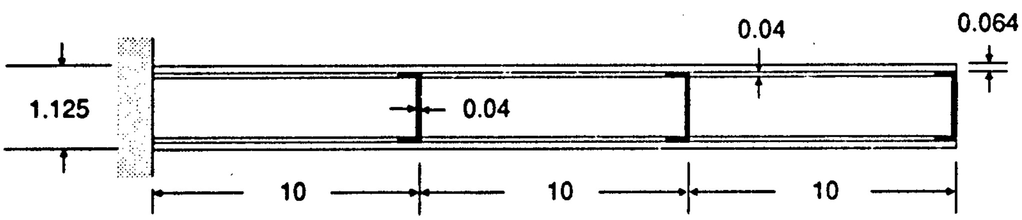

Section BB

NOTE: All Dimensions in Inches

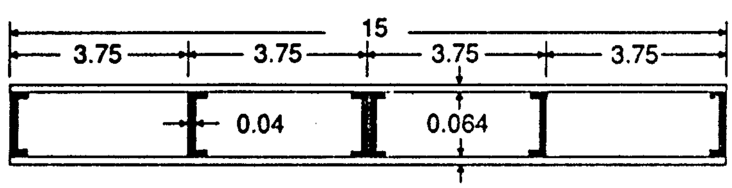

Section AA

Figure C2. Geometry of Structural Model.

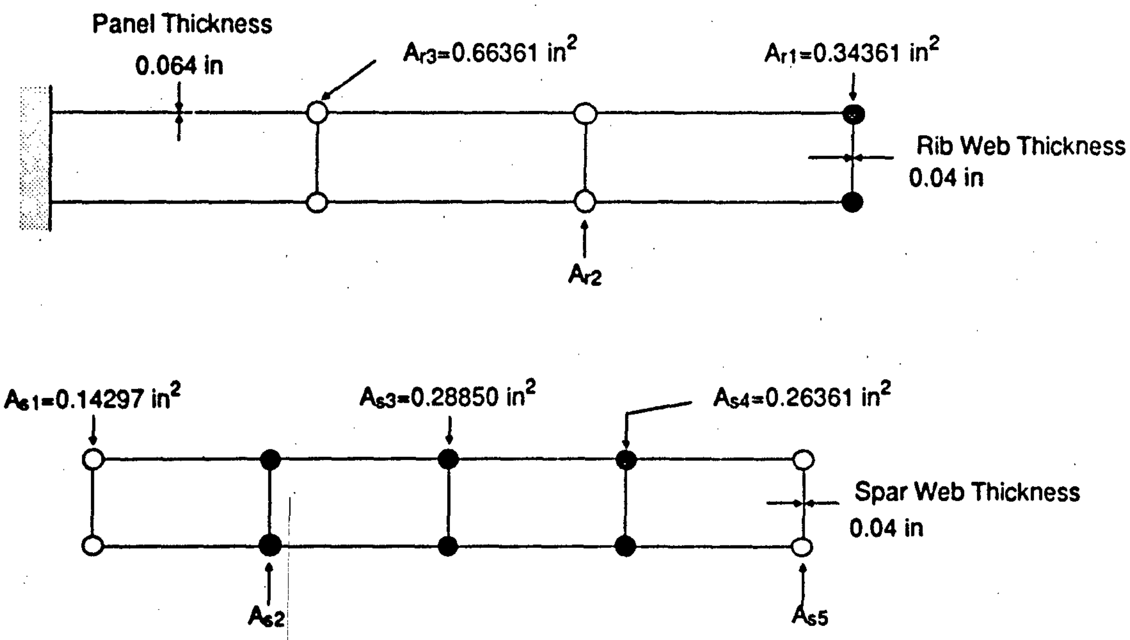

Figure C3. Finite Element Model Using Eq. C1.

Rod Element Area for SSR.3 and SSR.4

Spar Chord Area

$$A_{s1} = A_{s5} = A_f + \frac{3.75 \times 0.064}{2} = 0.14297 \text{ in}^2$$

$$A_{s2} = A_{s4} = A_f + (\frac{3.75 + 3.75}{2}) \times 0.064 = 0.26361 \text{ in}^2$$

$$A_{s3} = 2A_f + 3.75 \times 0.064 = 0.28850 \text{ in}^2$$

Rib Chord Area

$$A_{r1} = A_f + 5 \times 0.064 = 0.34361 \text{ in}^2$$

$$A_{r2} = A_{r3} = A_f + 10 \times 0.064 = 0.66361 \text{ in}^2$$

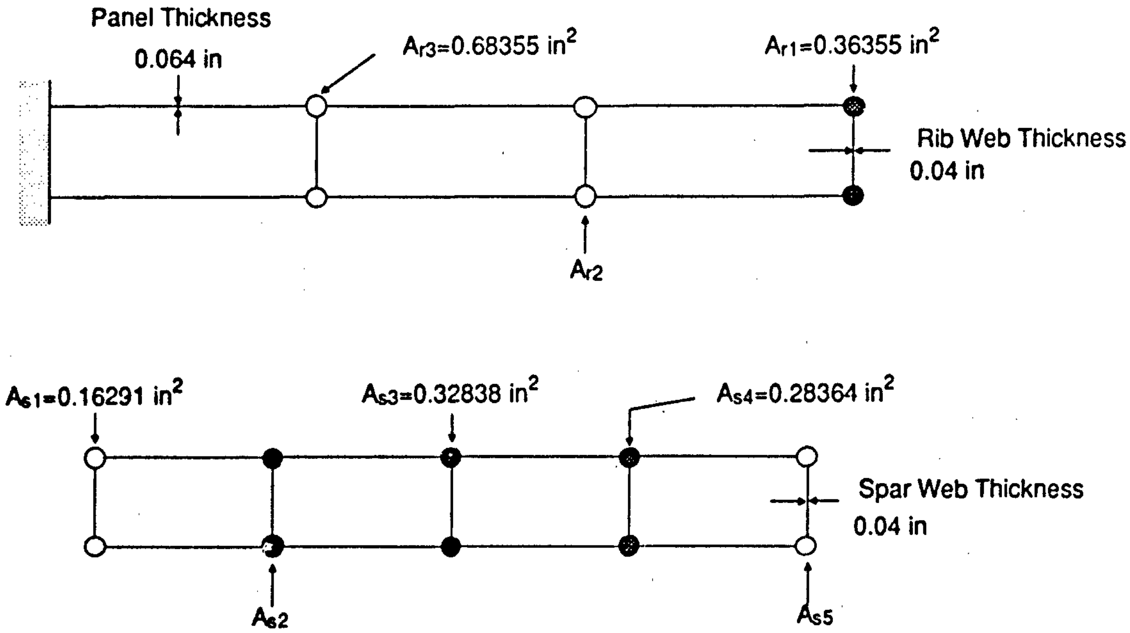

Figure C4. Finite Element Model Using Eq. C2.

Rod Element Area for SSR.1 and SSR.2

Spar Chord Area

$$A_{s1} = A_{s5} = A_f + \frac{3.75 \times 0.064}{2} + \frac{0.997 \times 0.04}{2} = 0.16291 \text{ in}^2$$

$$A_{s2} = A_{s4} = A_f + (\frac{3.75 + 3.75}{2}) \times 0.064 + \frac{0.997 \times 0.04}{2} = 0.28364 \text{ in}^2$$

$$A_{s3} = 2A_f + 3.75 \times 0.064 + \frac{0.997 \times 0.04}{2} = 0.32838 \text{ in}^2$$

Rib Chord Area

$$A_{r1} = A_f + 5 \times 0.064 + \frac{0.997 \times 0.04}{2} = 0.36355 \text{ in}^2$$

$$A_{r2} = A_{r3} = A_f + 10 \times 0.064 + \frac{0.997 \times 0.04}{2} = 0.68355 \text{ in}^2$$

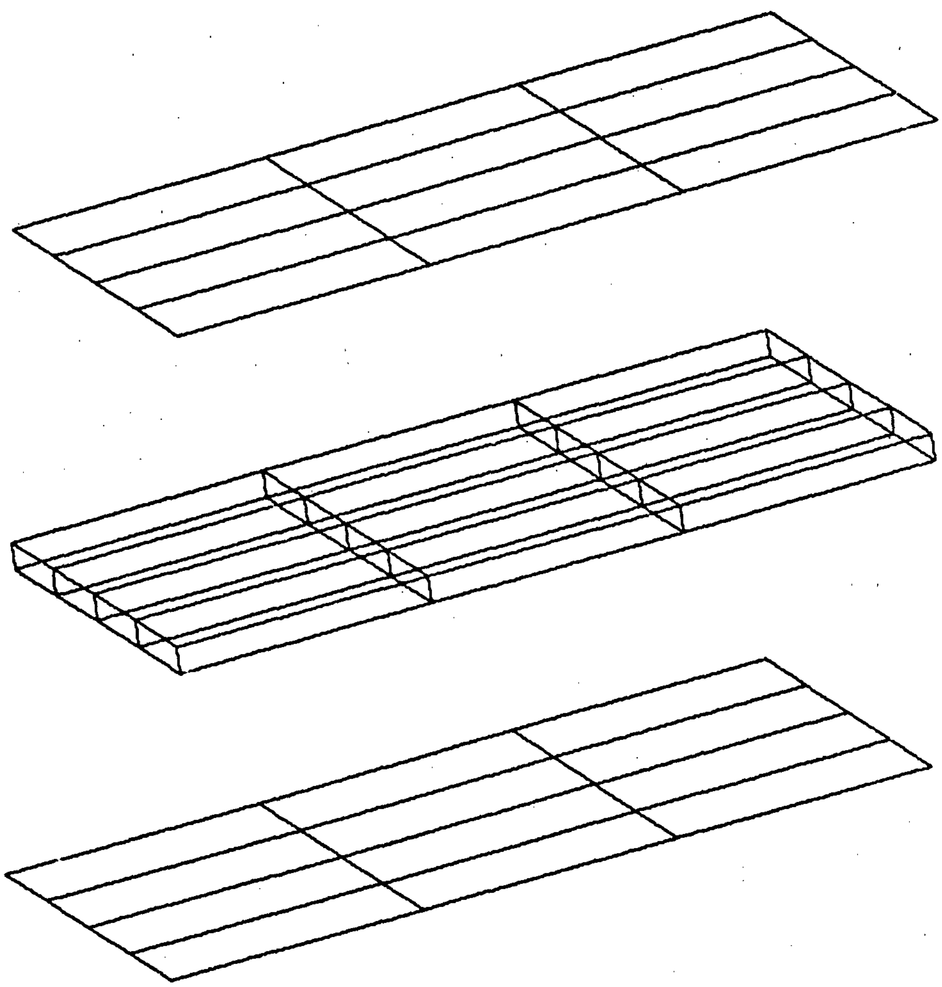

Figure C5. Finite Element Models SSR.1, SSR.2, SSR.3, SSR.4, SSR.5, QSR.1, QSR.2, QSB.1, QSB.2, QQR.1, and QQR.2 .

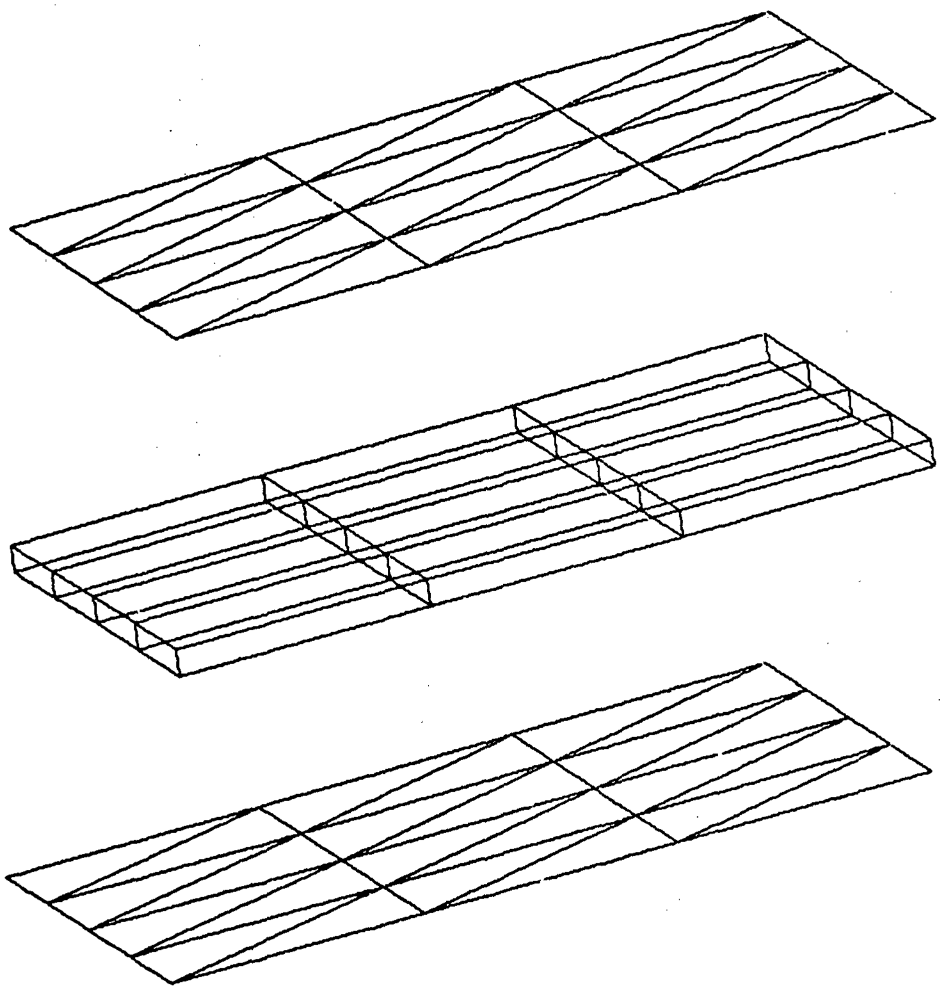

Figure C6. Finite Element Models TSR.1, TSR.2, TSB.1, TSB.2, TQR.1, and TQR.2.

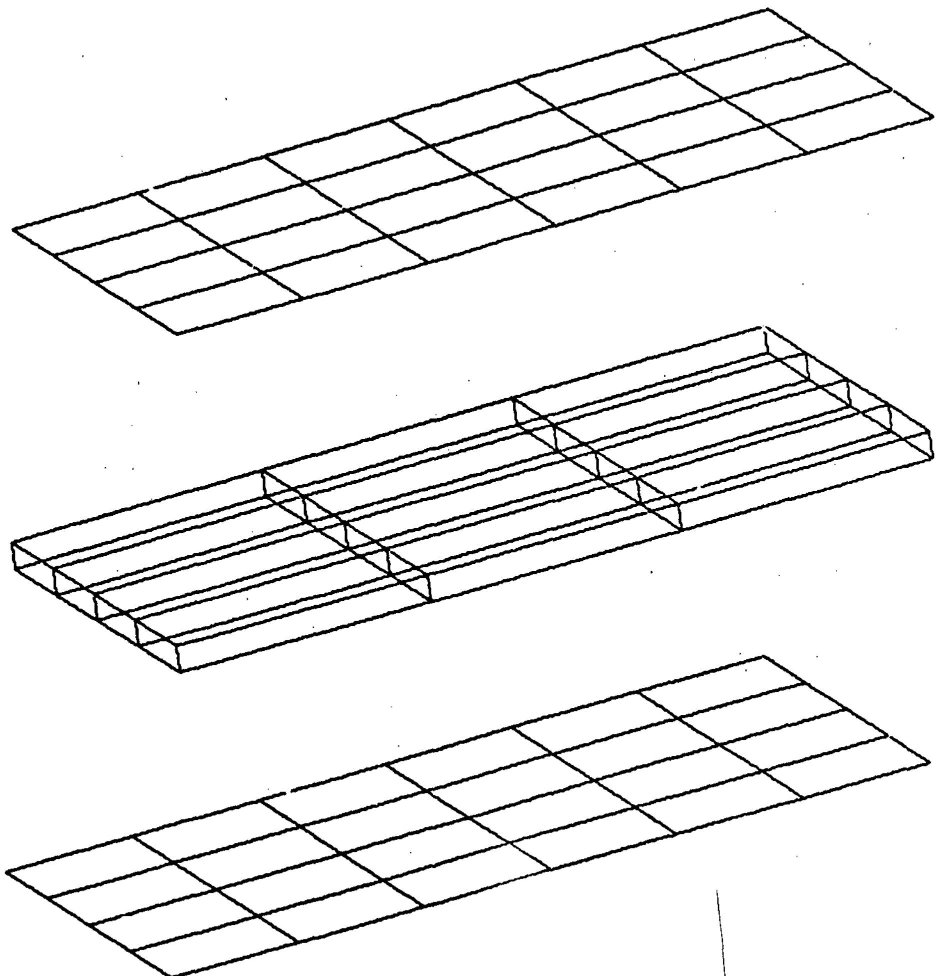

Figure C7. Finite Element Models QSR.3, QSR.4, QSB.3, and QSB.4.

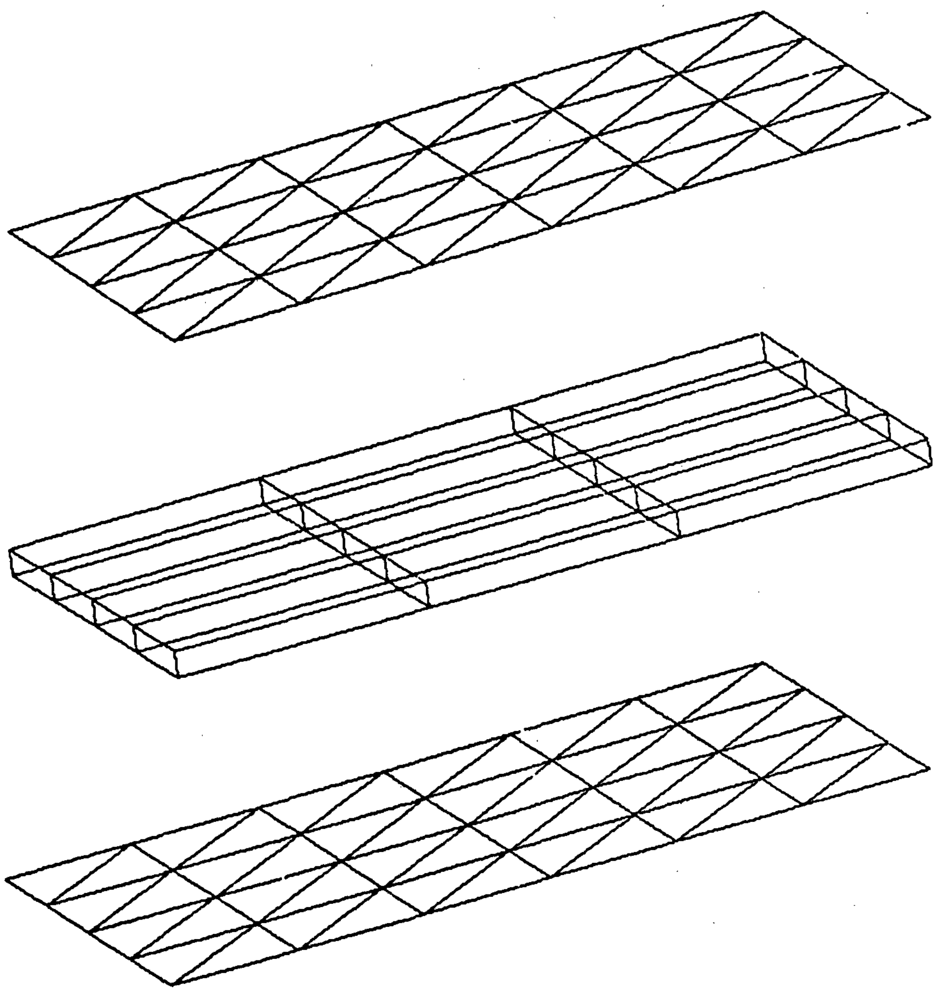

Figure C8. Finite Element Models TSR.3, TSR.4, TSB.3, and TSB.4.

Table C1. Finite Element Model Designation of Rattinger's Wing

MODEL \ ELEMENTS	SKIN ELEMENTS	STIFFNESS	WEB ELEMENTS	STIFFNESS	SPAR & RIB CHORDS
SSR.1	CSHEAR	NO	CSHEAR	NO	CROD
SSR.2	CSHEAR	YES	CSHEAR	NO	CROD
SSR.3	CSHEAR	NO	CSHEAR	NO	CROD
SSR.4	CSHEAR	YES	CSHEAR	NO	CROD
SSR.5	CSHEAR	NO	CSHEAR	YES	CROD
QSR.1	CQUAD4	YES	CSHEAR	NO	CROD
QSR.2	CQUAD4	NO	CSHEAR	NO	CROD
TSR.1	CTRIA3	YES	CSHEAR	NO	CROD
TSR.2	CTRIA3	NO	CSHEAR	NO	CROD
QSR.3	CQUAD4	YES	CSHEAR	NO	CROD
QSR.4	CQUAD4	NO	CSHEAR	NO	CROD
TSR.3	CTRIA3	NO	CSHEAR	NO	CROD
TSR.4	CTRIA3	NO	CSHEAR	NO	CROD
QSB.1	CQUAD4	YES	CSHEAR	NO	CBEAM
QSB.2	CQUAD4	NO	CSHEAR	NO	CBEAM
TSB.1	CTRIA3	YES	CSHEAR	NO	CBEAM
TSB.2	CTRIA3	NO	CSHEAR	NO	CBEAM
QSB.3	CQUAD4	YES	CSHEAR	NO	CBEAM
QSB.4	CQUAD4	NO	CSHEAR	NO	CBEAM
TSB.3	CTRIA3	YES	CSHEAR	NO	CBEAM
TSB.4	CTRIA3	NO	CSHEAR	NO	CBEAM
QQR.1	CQUAD4	YES	CQUAD4	YES	CROD
QQR.2	CQUAD4	YES	CQUAD4	NO	CROD
TQR.1	CTRIA3	YES	CQUAD4	YES	CROD
TQR.2	CTRIA3	YES	CQUAD4	NO	CROD

Table C2. Comparison of Displacements from FEM and Test

MODEL \ NODE	1	2	3	4	5	6	7
TEST	0.1520	0.1549	0.1572	0.1541	0.1511	0.0813	0.0833
SSR.1	0.1457	0.1466	0.1477	0.1466	0.1457	0.0757	0.0760
SSR.2	0.1388	0.1397	0.1408	0.1397	0.1388	0.0723	0.0725
SSR.3	0.1622	0.1632	0.1643	0.1632	0.1622	0.0843	0.0845
SSR.4	0.1537	0.1547	0.1558	0.1547	0.1537	0.0800	0.0802
SSR.5	0.1486	0.1496	0.1507	0.1496	0.1486	0.0776	0.0779
QSR.1	0.1482	0.1499	0.1513	0.1499	0.1482	0.0760	0.0773
QSR.2	0.1563	0.1581	0.1595	0.1581	0.1563	0.0799	0.0813
TSR.1	0.1453	0.1467	0.1479	0.1464	0.1446	0.0746	0.0757
TSR.2	0.1556	0.1572	0.1585	0.1570	0.1551	0.0797	0.0809
QSR.3	0.1315	0.1332	0.1347	0.1332	0.1315	0.0685	0.0697
QSR.4	0.1610	0.1630	0.1645	0.1630	0.1610	0.0830	0.0846
TSR.3	0.1303	0.1315	0.1325	0.1308	0.1288	0.0681	0.0689
TSR.4	0.1604	0.1622	0.1636	0.1620	0.1601	0.0828	0.0841
QSB.1	0.1506	0.1523	0.1537	0.1523	0.1506	0.0782	0.0785
QSB.2	0.1589	0.1607	0.1622	0.1607	0.1589	0.0813	0.0827
TSB.1	0.1475	0.1490	0.1502	0.1486	0.1468	0.0758	0.0769
TSB.2	0.1581	0.1598	0.1611	0.1596	0.1577	0.0810	0.0823
QSB.3	0.1325	0.1342	0.1357	0.1342	0.1325	0.0690	0.0702
QSB.4	0.1625	0.1645	0.1660	0.1645	0.1625	0.0838	0.0853
TSB.3	0.1312	0.1325	0.1335	0.1317	0.1297	0.0686	0.0694
TSB.4	0.1619	0.1637	0.1650	0.1635	0.1615	0.0836	0.0849
QQR.1	0.1326	0.1342	0.1335	0.1342	0.1326	0.0684	0.0695
QQR.2	0.1435	0.1451	0.1465	0.1451	0.1435	0.0736	0.0748
TQR.1	0.1302	0.1316	0.1328	0.1314	0.1298	0.0673	0.0683
TQR.2	0.1407	0.1422	0.1433	0.1418	0.1401	0.0724	0.0734

NOTE: All Dimensions in Inches

Table C2. Comparison of Displacements from FEM and Test (Con't)

8	9	10	11	12	13	14	15
0.0842	0.0826	0.0816	0.0241	0.0261	0.0254	0.0249	0.0239
0.0761	0.0760	0.0757	0.0215	0.0216	0.0216	0.0216	0.0215
0.0727	0.0725	0.0723	0.0206	0.0207	0.0207	0.0207	0.0206
0.0847	0.0845	0.0843	0.0239	0.0240	0.0240	0.0240	0.0239
0.0804	0.0802	0.0800	0.0228	0.0228	0.0228	0.0228	0.0228
0.0780	0.0779	0.0776	0.0222	0.0222	0.0222	0.0222	0.0222
0.0778	0.0773	0.0760	0.0206	0.0222	0.0225	0.0222	0.0206
0.0819	0.0813	0.0799	0.0216	0.0233	0.0236	0.0233	0.0216
0.0761	0.0754	0.0739	0.0206	0.0217	0.0219	0.0215	0.0202
0.0814	0.0807	0.0791	0.0218	0.0231	0.0233	0.0230	0.0216
0.0702	0.0697	0.0685	0.0194	0.0205	0.0208	0.0205	0.0194
0.0852	0.0846	0.0852	0.0231	0.0245	0.0249	0.0245	0.0231
0.0690	0.0682	0.0667	0.0195	0.0203	0.0204	0.0200	0.0224
0.0846	0.0839	0.0823	0.0232	0.0244	0.0247	0.0243	0.0227
0.0790	0.0785	0.0782	0.0210	0.0225	0.0228	0.0225	0.0210
0.0833	0.0827	0.0813	0.0220	0.0236	0.0240	0.0236	0.0220
0.0733	0.0765	0.0750	0.0209	0.0220	0.0222	0.0219	0.0205
0.0827	0.0820	0.0804	0.0222	0.0235	0.0237	0.0233	0.0219
0.0707	0.0702	0.0690	0.0195	0.0206	0.0209	0.0206	0.0195
0.0860	0.0853	0.0838	0.0233	0.0247	0.0251	0.0247	0.0233
0.0695	0.0687	0.0672	0.0196	0.2051	0.0206	0.0201	0.0188
0.0854	0.0847	0.0831	0.0234	0.0247	0.0249	0.0245	0.0229
0.0700	0.0695	0.0684	0.0187	0.0201	0.0203	0.0201	0.0187
0.0754	0.0748	0.0736	0.0200	0.0215	0.0218	0.0215	0.0200
0.0686	0.0681	0.0668	0.0187	0.0197	0.0199	0.0196	0.0184
0.0738	0.0731	0.0717	0.0200	0.0211	0.0212	0.0209	0.0196

NOTE: All Dimensions in Inches

INTENTIONALLY LEFT BLANK

APPENDIX D:

Input Data for QSR1.DAT

INTENTIONALLY LEFT BLANK

```
ID WING T-38 DEFLECTIONS USING QUAD4 CARDS FOR SKIN AND CSHEAR FOR WEB
SOL 24
TIME 44
DIAG 8
CEND
MAXLINES=3000
METHOD=1
SET 4 = 1 THRU 48
DISPL =4
SUBCASE 1
LOAD = 1
SUBCASE 2
LOAD = 2
SUBCASE 3
LOAD = 3
SUBCASE 4
LOAD = 4
SUBCASE 5
LOAD = 5
SUBCASE 6
LOAD = 6
SUBCASE 7
LOAD = 7
SUBCASE 8
LOAD = 8
BEGIN BULK
$       EID     CD      X       Y       Z                  CONSTRAINT
GRID    1               125.0   378.467 0.773135           456
GRID    2               125.0   381.997 0.888060           456
GRID    3               125.0   385.186 0.961194           456
GRID    4               125.0   388.261 1.002985           456
GRID    5               125.0   391.678 0.992538           456
GRID    6               125.0   401.974 0.721000           456
GRID    7               118.0   389.538 1.063861           456
GRID    8               118.0   400.936 0.852989           456
GRID    9               111.0   387.398 1.265638           456
GRID    10              111.0   399.897 0.937355           456
GRID    11              101.0   366.238 1.042225           456
GRID    12              101.0   369.983 1.149255           456
GRID    13              101.0   371.076 1.159702           456
GRID    14              101.0   373.729 1.272963           456
GRID    15              101.0   375.445 1.264180           456
GRID    16              101.0   377.474 1.328600           456
GRID    17              101.0   379.659 1.328600           456
GRID    18              101.0   381.220 1.337315           456
GRID    19              101.0   384.341 1.319072           456
GRID    20              101.0   398.386 1.093750           456
GRID    21              85.19   379.507 1.530144           456
GRID    22              83.2    395.772 1.273870           456
GRID    23              77.75   377.232 1.646627           456
GRID    24              76.7    394.808 1.331552           456
GRID    25              72.25   375.551 1.770699           456
GRID    26              72.25   394.148 1.397101           456
GRID    27              64.8    347.793 1.457463           456
GRID    28              64.8    353.065 1.572388           456
GRID    29              64.8    358.337 1.729100           456
GRID    30              64.8    363.608 1.736940           456
GRID    31              64.8    368.880 1.854480           456
```

GRID	32	64.8	373.273	1.828350	456
GRID	33	64.8	393.042	1.462650	456
GRID	34	29.92	330.021	1.922389	3456
GRID	35	28.777	336.408	2.037314	3456
GRID	36	27.867	342.867	2.162685	3456
GRID	37	26.946	349.400	2.340299	3456
GRID	38	26.015	356.008	2.371642	3456
GRID	39	25.231	361.572	2.194030	3456
GRID	40	29.3	362.731	2.156426	3456
GRID	41	26.06	386.424	1.947470	3456
GRID	42	0.0	330.021	1.922389	1456
GRID	43	0.0	336.408	2.037314	1456
GRID	44	0.0	342.867	2.162685	1456
GRID	45	0.0	349.4	2.340299	1456
GRID	46	0.0	356.008	2.371642	1456
GRID	47	0.0	361.572	2.194030	1456
GRID	48	0.0	386.424	1.947470	1456
GRID	49	125.0	378.467	-0.77313	456
GRID	50	125.0	381.997	-0.88806	456
GRID	51	125.0	385.186	-0.96119	456
GRID	52	125.0	388.261	-1.00298	456
GRID	53	125.0	391.678	-0.99253	456
GRID	54	125.0	401.974	-0.72100	456
GRID	55	118.0	389.538	-1.06386	456
GRID	56	118.0	400.936	-0.85299	456
GRID	57	111.0	387.398	-1.26564	456
GRID	58	111.0	399.897	-0.93736	456
GRID	59	101.0	366.238	-1.04223	456
GRID	60	101.0	369.983	-1.14926	456
GRID	61	101.0	371.076	-1.15970	456
GRID	62	101.0	373.729	-1.27296	456
GRID	63	101.0	375.445	-1.26418	456
GRID	64	101.0	377.474	-1.32860	456
GRID	65	101.0	379.659	-1.32860	456
GRID	66	101.0	381.220	-1.33732	456
GRID	67	101.0	384.341	-1.31907	456
GRID	68	101.0	398.386	-1.09375	456
GRID	69	85.19	379.507	-1.53014	456
GRID	70	83.2	395.772	-1.27387	456
GRID	71	77.75	377.232	-1.64663	456
GRID	72	76.7	394.808	-1.33155	456
GRID	73	72.25	375.551	-1.77069	456
GRID	74	72.25	394.148	-1.39710	456
GRID	75	64.8	347.793	-1.45746	456
GRID	76	64.8	353.065	-1.57239	456
GRID	77	64.8	358.337	-1.72910	456
GRID	78	64.8	363.608	-1.73694	456
GRID	79	64.8	368.880	-1.85448	456
GRID	80	64.8	373.273	-1.82835	456
GRID	81	64.8	393.042	-1.46265	456
GRID	82	29.92	330.021	-1.92239	3456
GRID	83	28.777	336.408	-2.03731	3456
GRID	84	27.867	342.867	-2.16269	3456
GRID	85	26.946	349.400	-2.34029	3456
GRID	86	26.015	356.008	-2.37164	3456
GRID	87	25.231	361.572	-2.19403	3456
GRID	88	29.3	362.731	-2.15643	3456
GRID	89	26.06	386.424	-1.94747	3456

GRID	90	0.0	330.021	-1.92239	1456
GRID	91	0.0	336.408	-2.03731	1456
GRID	92	0.0	342.867	-2.16269	1456
GRID	93	0.0	349.4	-2.34029	1456
GRID	94	0.0	356.008	-2.37164	1456
GRID	95	0.0	361.572	-2.19403	1456
GRID	96	0.0	386.424	-1.94747	1456

$	EID	G1	G2	MID	CSA
CONROD	1	1	2	1	0.106742
CONROD	2	2	3	1	0.110107
CONROD	3	3	4	1	0.112086
CONROD	4	4	5	1	0.112622
CONROD	5	5	6	1	0.119206
CONROD	6	7	8	1	0.255194
CONROD	7	9	10	1	0.246097
CONROD	8	11	12	1	0.159778
CONROD	9	12	13	1	0.159778
CONROD	10	13	14	1	0.164029
CONROD	11	14	15	1	0.164029
CONROD	12	15	16	1	0.166860
CONROD	13	16	17	1	0.166860
CONROD	14	17	18	1	0.167765
CONROD	15	18	19	1	0.167765
CONROD	16	19	20	1	0.163841
CONROD	17	21	22	1	0.154423
CONROD	18	23	24	1	0.139074
CONROD	19	25	26	1	0.139074
CONROD	20	27	28	2	0.667360
CONROD	21	28	29	2	0.681896
CONROD	22	29	30	2	0.689985
CONROD	23	30	31	2	0.695839
CONROD	24	31	32	2	0.699954
CONROD	25	32	33	2	0.681363
CONROD	26	34	35	1	0.213887
CONROD	27	35	36	1	0.223157
CONROD	28	36	37	1	0.237261
CONROD	29	37	38	1	0.256984
CONROD	30	38	39	1	0.274676
CONROD	31	40	41	1	0.192684
CONROD	32	1	11	1	0.362960
CONROD	33	2	13	1	0.094927
CONROD	34	3	15	1	0.095374
CONROD	35	4	17	1	0.097067
CONROD	36	5	7	1	0.128680
CONROD	37	6	8	1	0.148729
CONROD	38	7	9	1	0.128680
CONROD	39	8	10	1	0.148729
CONROD	40	9	19	1	0.128680
CONROD	41	10	20	1	0.148729
CONROD	42	11	27	1	0.400786
CONROD	43	12	28	1	0.084990
CONROD	44	14	29	1	0.091382
CONROD	45	16	30	1	0.128673
CONROD	46	18	31	1	0.126535
CONROD	47	19	21	1	0.147487
CONROD	48	20	22	1	0.145914

```
CONROD  49   21  23  1  0.147487
CONROD  50   22  24  1  0.145914
CONROD  51   23  25  1  0.163193
CONROD  52   24  26  1  0.145914
CONROD  53   25  32  1  0.163193
CONROD  54   26  33  1  0.145914
CONROD  55   27  34  1  0.623202
CONROD  56   28  35  1  0.136110
CONROD  57   29  36  1  0.158313
CONROD  58   30  37  1  0.196573
CONROD  59   31  38  1  0.198040
CONROD  60   32  40  1  0.390376
CONROD  61   40  39  1  0.390376
CONROD  62   33  41  1  0.104919
CONROD  63   34  42  1  0.172374
CONROD  64   35  43  1  0.145401
CONROD  65   36  44  1  0.167005
CONROD  66   37  45  1  0.184835
CONROD  67   38  46  1  0.216165
CONROD  68   39  47  1  0.243853
$lower skin chords
CONROD  69   49  50  1  0.106742
CONROD  70   50  51  1  0.110107
CONROD  71   51  52  1  0.112086
CONROD  72   52  53  1  0.112622
CONROD  73   53  54  1  0.119206
CONROD  74   55  56  1  0.255194
CONROD  75   57  58  1  0.246097
CONROD  76   59  60  1  0.159778
CONROD  77   60  61  1  0.159778
CONROD  78   61  62  1  0.164029
CONROD  79   62  63  1  0.164029
CONROD  80   63  64  1  0.166860
CONROD  81   64  65  1  0.166860
CONROD  82   65  66  1  0.167765
CONROD  83   66  67  1  0.167765
CONROD  84   67  68  1  0.163841
CONROD  85   69  70  1  0.154423
CONROD  86   71  72  1  0.139074
CONROD  87   73  74  1  0.139074
CONROD  88   75  76  2  0.667360
CONROD  89   76  77  2  0.681896
CONROD  90   77  78  2  0.689985
CONROD  91   78  79  2  0.695839
CONROD  92   79  80  2  0.699954
CONROD  93   80  81  2  0.681363
CONROD  94   82  83  1  0.213887
CONROD  95   83  84  1  0.223157
CONROD  96   84  85  1  0.237261
CONROD  97   85  86  1  0.256984
CONROD  98   86  87  1  0.274676
CONROD  99   88  89  1  0.192684
CONROD  100  49  59  1  0.362960
CONROD  101  50  61  1  0.094927
CONROD  102  51  63  1  0.095374
CONROD  103  52  65  1  0.097067
CONROD  104  53  55  1  0.128680
CONROD  105  54  56  1  0.148729
```

CONROD	106	55	57	1	0.128680
CONROD	107	56	58	1	0.148729
CONROD	108	57	67	1	0.128680
CONROD	109	58	68	1	0.148729
CONROD	110	59	75	1	0.400786
CONROD	111	60	76	1	0.084990
CONROD	112	62	77	1	0.091382
CONROD	113	64	78	1	0.128673
CONROD	114	66	79	1	0.126535
CONROD	115	67	69	1	0.147487
CONROD	116	68	70	1	0.145914
CONROD	117	69	71	1	0.147487
CONROD	118	70	72	1	0.145914
CONROD	119	71	73	1	0.163193
CONROD	120	72	74	1	0.145914
CONROD	121	73	80	1	0.163193
CONROD	122	74	81	1	0.145914
CONROD	123	75	82	1	0.623202
CONROD	124	76	83	1	0.136110
CONROD	125	77	84	1	0.158313
CONROD	126	78	85	1	0.196573
CONROD	127	79	86	1	0.198040
CONROD	128	80	88	1	0.390376
CONROD	129	88	87	1	0.390376
CONROD	130	81	89	1	0.104919
CONROD	131	82	90	1	0.172374
CONROD	132	83	91	1	0.145401
CONROD	133	84	92	1	0.167005
CONROD	134	85	93	1	0.184835
CONROD	135	86	94	1	0.216165
CONROD	136	87	95	1	0.243853
$CONROD	137	41	48	1	0.24
$CONROD	138	89	96	1	0.24

$	EID	G1	G2	MID	CSA
CONROD	201	1	49	1	0.24
CONROD	202	2	50	1	0.24
CONROD	203	3	51	1	0.24
CONROD	204	4	52	1	0.24
CONROD	205	5	53	1	0.24
CONROD	206	6	54	1	0.24
CONROD	207	7	55	1	0.24
CONROD	208	8	56	1	0.24
CONROD	209	9	57	1	0.24
CONROD	210	10	58	1	0.24
CONROD	211	11	59	1	0.24
CONROD	212	12	60	1	0.24
CONROD	213	13	61	1	0.24
CONROD	214	14	62	1	0.24
CONROD	215	15	63	1	0.24
CONROD	216	16	64	1	0.24
CONROD	217	17	65	1	0.24
CONROD	218	18	66	1	0.24
CONROD	219	19	67	1	0.24
CONROD	220	20	68	2	0.24
CONROD	221	21	69	2	0.24
CONROD	222	22	70	2	0.24
CONROD	223	23	71	2	0.24

CONROD	224	24	72	2	0.24
CONROD	225	25	73	2	0.24
CONROD	226	26	74	1	0.24
CONROD	227	27	75	1	0.24
CONROD	228	28	76	1	0.24
CONROD	229	29	77	1	0.24
CONROD	230	30	78	1	0.24
CONROD	231	31	79	1	0.24
CONROD	232	32	80	1	0.24
CONROD	233	33	81	1	0.24
CONROD	234	34	82	1	0.24
CONROD	235	35	83	1	0.24
CONROD	236	36	84	1	0.24
CONROD	237	37	85	1	0.24
CONROD	238	38	86	1	0.24
CONROD	239	39	87	1	0.24
CONROD	240	40	88	1	0.24
CONROD	241	41	89	1	0.24
$CONROD	242	42	90	1	0.24
$CONROD	243	43	91	1	0.24
$CONROD	244	44	92	1	0.24
$CONROD	245	45	93	1	0.24
$CONROD	246	46	94	1	0.24
$CONROD	247	47	95	1	0.24
$CONROD	248	48	96	1	0.24

$	EID	PID	G1	G2	G3	G4
CQUAD4	101	101	2	13	11	1
CQUAD4	102	102	3	15	13	2
CQUAD4	103	103	4	17	15	3
CQUAD4	104	104	5	19	17	4
CQUAD4	105	105	6	8	7	5
CQUAD4	106	106	8	10	9	7
CQUAD4	107	107	10	20	19	9
CQUAD4	108	108	12	28	27	11
CQUAD4	109	109	14	29	28	12
CQUAD4	110	110	16	30	29	14
CQUAD4	111	111	18	31	30	16
CQUAD4	112	112	19	32	31	18
CQUAD4	113	113	20	22	21	19
CQUAD4	114	114	22	24	23	21
CQUAD4	115	115	24	26	25	23
CQUAD4	116	116	26	33	32	25
CQUAD4	117	117	28	35	34	27
CQUAD4	118	118	29	36	35	28
CQUAD4	119	119	30	37	36	29
CQUAD4	120	120	31	38	37	30
CQUAD4	121	121	32	39	38	31
CQUAD4	122	122	33	41	40	32
CQUAD4	123	123	35	43	42	34
CQUAD4	124	124	36	44	43	35
CQUAD4	125	125	37	45	44	36
CQUAD4	126	126	38	46	45	37
CQUAD4	127	127	39	47	46	38
CQUAD4	128	128	50	61	59	49
CQUAD4	129	129	51	63	61	50
CQUAD4	130	130	52	65	63	51
CQUAD4	131	131	53	67	65	52

CQUAD4	132	132	54	56	55	53
CQUAD4	133	133	56	58	57	55
CQUAD4	134	134	58	68	67	57
CQUAD4	135	135	60	76	75	59
CQUAD4	136	136	62	77	76	60
CQUAD4	137	137	64	78	77	62
CQUAD4	138	138	66	79	78	64
CQUAD4	139	139	67	80	79	66
CQUAD4	140	140	68	70	69	67
CQUAD4	141	141	70	72	71	69
CQUAD4	142	142	72	74	73	71
CQUAD4	143	143	74	81	80	73
CQUAD4	144	144	76	83	82	75
CQUAD4	145	145	77	84	83	76
CQUAD4	146	146	78	85	84	77
CQUAD4	147	147	79	86	85	78
CQUAD4	148	148	80	87	86	79
CQUAD4	149	149	81	89	88	80
CQUAD4	150	150	83	91	90	82
CQUAD4	151	151	84	92	91	83
CQUAD4	152	152	85	93	92	84
CQUAD4	153	153	86	94	93	85
CQUAD4	154	154	87	95	94	86
CQUAD4	155	155	41	48	47	39
CQUAD4	156	156	89	96	95	87

$	PID	MID1	TH	MID2	12I/T3
PSHELL	101	4	0.09	4	
PSHELL	102	4	0.0625	4	
PSHELL	103	4	0.0645	4	
PSHELL	104	4	0.067	4	
PSHELL	105	4	0.06	4	
PSHELL	106	4	0.065	4	
PSHELL	107	4	0.07	4	
PSHELL	108	4	0.1415	4	
PSHELL	109	4	0.116	4	
PSHELL	110	4	0.1255	4	
PSHELL	111	4	0.13	4	
PSHELL	112	4	0.133	4	
PSHELL	113	4	0.04	4	
PSHELL	114	4	0.11	4	
PSHELL	115	4	0.095	4	
PSHELL	116	4	0.095	4	
PSHELL	117	4	0.175	4	
PSHELL	118	4	0.195	4	
PSHELL	119	4	0.2055	4	
PSHELL	120	4	0.216	4	
PSHELL	121	4	0.2395	4	
PSHELL	122	4	0.025	4	
PSHELL	123	4	0.207	4	
PSHELL	124	4	0.230	4	
PSHELL	125	4	0.244	4	
PSHELL	126	4	0.258	4	
PSHELL	127	4	0.290	4	
PSHELL	128	4	0.065	4	
PSHELL	129	4	0.055	4	
PSHELL	130	4	0.055	4	
PSHELL	131	4	0.055	4	

PSHELL	132	4	0.058	4
PSHELL	133		0.038	4
PSHELL	134		0.038	4
PSHELL	135		0.1115	4
PSHELL	136	4	0.1065	4
PSHELL	137	4	0.115	4
PSHELL	138	4	0.1215	4
PSHELL	139	4	0.1215	4
PSHELL	140	4	0.038	4
PSHELL	141	4	0.038	4
PSHELL	142	4	0.08	4
PSHELL	143	4	0.08	4
PSHELL	144	4	0.1725	4
PSHELL	145	4	0.132	4
PSHELL	146	4	0.1965	4
PSHELL	147	4	0.2215	4
PSHELL	148	4	0.239	4
PSHELL	149	4	0.04	4
PSHELL	150	4	0.21	4
PSHELL	151	4	0.22	4
PSHELL	152	4	0.24	4
PSHELL	153	4	0.27	4
PSHELL	154	4	0.298	4
PSHELL	155	4	0.3	4
PSHELL	156	4	0.3	4

$	EID	PID	G1	G2	G3	G4
CSHEAR	1	1	49	50	2	1
CSHEAR	2	2	50	51	3	2
CSHEAR	3	3	51	52	4	3
CSHEAR	4	4	52	53	5	4
CSHEAR	5	5	53	54	6	5
CSHEAR	6	6	55	56	8	7
CSHEAR	7	7	57	58	10	9
CSHEAR	8	8	59	60	12	11
CSHEAR	9	9	60	61	13	12
CSHEAR	10	10	61	62	14	13
CSHEAR	11	11	62	63	15	14
CSHEAR	12	12	63	64	16	15
CSHEAR	13	13	64	65	17	16
CSHEAR	14	14	65	66	18	17
CSHEAR	15	15	66	67	19	18
CSHEAR	16	16	67	68	20	19
CSHEAR	17	17	69	70	22	21
CSHEAR	18	18	71	72	24	23
CSHEAR	19	19	73	74	26	25
CSHEAR	20	20	75	76	28	27
CSHEAR	21	21	76	77	29	28
CSHEAR	22	22	77	78	30	29
CSHEAR	23	23	78	79	31	30
CSHEAR	24	24	79	80	32	31
CSHEAR	25	25	80	81	33	32
CSHEAR	26	26	82	83	35	34
CSHEAR	27	27	83	84	36	35
CSHEAR	28	28	84	85	37	36
CSHEAR	29	29	85	86	38	37
CSHEAR	30	30	86	87	39	38
CSHEAR	31	31	49	59	11	1

CSHEAR	32	32	50	61	13	2
CSHEAR	33	33	51	63	15	3
CSHEAR	34	34	52	65	17	4
CSHEAR	35	35	53	55	7	5
CSHEAR	36	36	54	56	8	6
CSHEAR	37	37	55	57	9	7
CSHEAR	38	38	56	58	10	8
CSHEAR	39	39	57	67	19	9
CSHEAR	40	40	58	68	20	10
CSHEAR	41	41	59	75	27	11
CSHEAR	42	42	60	76	28	12
CSHEAR	43	43	62	77	29	14
CSHEAR	44	44	64	78	30	16
CSHEAR	45	45	66	79	31	18
CSHEAR	46	46	67	69	21	19
CSHEAR	47	47	68	70	22	20
CSHEAR	48	48	69	71	23	21
CSHEAR	49	49	70	72	24	22
CSHEAR	50	50	71	73	25	23
CSHEAR	51	51	72	74	26	24
CSHEAR	52	52	73	80	32	25
CSHEAR	53	53	74	81	33	26
CSHEAR	54	54	75	82	34	27
CSHEAR	55	55	76	83	35	28
CSHEAR	56	56	77	84	36	29
CSHEAR	57	57	78	85	37	30
CSHEAR	58	58	79	86	38	31
CSHEAR	59	59	80	88	40	32
CSHEAR	60	60	88	87	39	40
CSHEAR	61	61	81	89	41	33
CSHEAR	62	62	82	90	42	34
CSHEAR	63	63	83	91	43	35
CSHEAR	64	64	84	92	44	36
CSHEAR	65	65	85	93	45	37
CSHEAR	66	66	86	94	46	38
CSHEAR	67	67	87	95	47	39
CSHEAR	68	68	88	89	41	40

$	PID	MID1	TH
PSHEAR	1	7	0.08
PSHEAR	2	7	0.08
PSHEAR	3	7	0.08
PSHEAR	4	7	0.08
PSHEAR	5	7	0.09
PSHEAR	6	7	0.13
PSHEAR	7	7	0.13
PSHEAR	8	7	0.09
PSHEAR	9	7	0.09
PSHEAR	10	7	0.09
PSHEAR	11	7	0.09
PSHEAR	12	7	0.09
PSHEAR	13	7	0.09
PSHEAR	14	7	0.09
PSHEAR	15	7	0.09
PSHEAR	16	7	0.09
PSHEAR	17	7	0.08
PSHEAR	18	7	0.08
PSHEAR	19	7	0.08

PSHEAR	20	2	0.365			
PSHEAR	21	2	0.365			
PSHEAR	22	2	0.365			
PSHEAR	23	2	0.365			
PSHEAR	24	2	0.365			
PSHEAR	25	2	0.365			
PSHEAR	26	7	0.10			
PSHEAR	27	7	0.10			
PSHEAR	28	7	0.10			
PSHEAR	29	7	0.10			
PSHEAR	30	7	0.10			
PSHEAR	31	7	0.16			
PSHEAR	32	7	0.09			
PSHEAR	33	7	0.09			
PSHEAR	34	7	0.09			
PSHEAR	35	7	0.12			
PSHEAR	36	7	0.12			
PSHEAR	37	7	0.12			
PSHEAR	38	7	0.12			
PSHEAR	39	7	0.12			
PSHEAR	40	7	0.12			
PSHEAR	41	7	0.16			
PSHEAR	42	7	0.09			
PSHEAR	43	7	0.09			
PSHEAR	44	7	0.09			
PSHEAR	45	7	0.09			
PSHEAR	46	7	0.12			
PSHEAR	47	7	0.14			
PSHEAR	48	7	0.12			
PSHEAR	49	7	0.14			
PSHEAR	50	7	0.12			
PSHEAR	51	7	0.14			
PSHEAR	52	7	0.12			
PSHEAR	53	7	0.14			
PSHEAR	54	7	0.16			
PSHEAR	55	7	0.1			
PSHEAR	56	7	0.105			
PSHEAR	57	7	0.11			
PSHEAR	58	7	0.11			
PSHEAR	59	7	0.11			
PSHEAR	60	7	0.11			
PSHEAR	61	7	0.11			
PSHEAR	62	7	0.08			
PSHEAR	63	7	0.08			
PSHEAR	64	7	0.10			
PSHEAR	65	7	0.09			
PSHEAR	66	7	0.1			
PSHEAR	67	7	0.105			
PSHEAR	68	7	0.1			
CTRIA3	1	1	40	41	39	
CTRIA3	2	1	88	89	87	
PSHELL	1	4	0.3	4		
$	MID	E	G	NU	RHO	A
MAT1	4	10.3E6		0.3	1.0	
MAT1	2	30.0E6		0.3	1.0	

```
MAT1     1        10.3E6               0.3      1.0
MAT1     7        10.3E6               0.3      1.0

FORCE    1        1                    -500.0  0.0       0.0       1.0
FORCE    2        5                    -1000.0 0.0       0.0       1.0
FORCE    3        6                    -200.0  0.0       0.0       1.0
FORCE    4        11                   -1500.0 0.0       0.0       1.0
FORCE    5        19                   -2500.0 0.0       0.0       1.0
FORCE    6        20                   -500.0  0.0       0.0       1.0
FORCE    7        27                   -3000.0 0.0       0.0       1.0
FORCE    8        32                   -5000.0 0.0       0.0       1.0

$LOAD    SID      S       S1       L1       S2       L2
$LOAD     3        1.0     1.0      4        1.0      1

$        SID      CID     G        N1       N2       N3
$RAV     4        0       32.2     0.0      0.0      -1.0

EIGR     1        MGIV    0.0      1000.0            20
130
+30      MAX
ENDDATA
//
```

INTENTIONALLY LEFT BLANK

No. of Copies	Organization
2	Administrator Defense Technical Info Center ATTN: DTIC-DDA Cameron Station Alexandria, VA 22304-6145
1	Commander U.S. Army Materiel Command ATTN: AMCAM 5001 Eisenhower Ave. Alexandria, VA 22333-0001
1	Director U.S. Army Research Laboratory ATTN: AMSRL-D 2800 Powder Mill Rd. Adelphi, MD 20783-1145
1	Director U.S. Army Research Laboratory ATTN: AMSRL-OP-CI-AD, Tech Publishing 2800 Powder Mill Rd. Adelphi, MD 20783-1145
2	Commander U.S. Army Armament Research, Development, and Engineering Center ATTN: SMCAR-IMI-I Picatinny Arsenal, NJ 07806-5000
2	Commander U.S. Army Armament Research, Development, and Engineering Center ATTN: SMCAR-TDC Picatinny Arsenal, NJ 07806-5000
1	Director Benet Weapons Laboratory U.S. Army Armament Research, Development, and Engineering Center ATTN: SMCAR-CCB-TL Watervliet, NY 12189-4050
(Unclass. only) 1	Commander U.S. Army Rock Island Arsenal ATTN: SMCRI-IMC-RT/Technical Library Rock Island, IL 61299-5000
1	Director U.S. Army Aviation Research and Technology Activity ATTN: SAVRT-R (Library) M/S 219-3 Ames Research Center Moffett Field, CA 94035-1000

No. of Copies	Organization
1	Commander U.S. Army Missile Command ATTN: AMSMI-RD-CS-R (DOC) Redstone Arsenal, AL 35898-5010
1	Commander U.S. Army Tank-Automotive Command ATTN: ASQNC-TAC-DIT (Technical Information Center) Warren, MI 48397-5000
1	Director U.S. Army TRADOC Analysis Command ATTN: ATRC-WSR White Sands Missile Range, NM 88002-5502
1	Commandant U.S. Army Field Artillery School ATTN: ATSF-CSI Ft. Sill, OK 73503-5000
(Class. only) 1	Commandant U.S. Army Infantry School ATTN: ATSH-CD (Security Mgr.) Fort Benning, GA 31905-5660
(Unclass. only) 1	Commandant U.S. Army Infantry School ATTN: ATSH-CD-CSO-OR Fort Benning, GA 31905-5660
1	WL/MNOI Eglin AFB, FL 32542-5000
	<u>Aberdeen Proving Ground</u>
2	Dir, USAMSAA ATTN: AMXSY-D AMXSY-MP, H. Cohen
1	Cdr, USATECOM ATTN: AMSTE-TC
1	Dir, ERDEC ATTN: SCBRD-RT
1	Cdr, CBDA ATTN: AMSCB-CI
1	Dir, USARL ATTN: AMSRL-SL-I
10	Dir, USARL ATTN: AMSRL-OP-CI-B (Tech Lib)

No. of Copies	Organization
1	Department of the Army U.S. Army Natick Research, Development, and Engineering Center Aero-Mechanical Engineering Directorate ATTN: STRNC-UE, Andrea M. Blanas Natick, MA 01760-5017
1	Syracuse University Department of Civil Engineering ATTN: Professor James A. Mandel Syracuse, NY 13244
1	Syracuse University Department of Aerospace Engineering ATTN: Professor V. R. Murthy Syracuse, NY 13244

USER EVALUATION SHEET/CHANGE OF ADDRESS

This Laboratory undertakes a continuing effort to improve the quality of the reports it publishes. Your comments/answers to the items/questions below will aid us in our efforts.

1. ARL Report Number ARL-TR-99 Date of Report March 1993

2. Date Report Received ______

3. Does this report satisfy a need? (Comment on purpose, related project, or other area of interest for which the report will be used.) ______

4. Specifically, how is the report being used? (Information source, design data, procedure, source of ideas, etc.) ______

5. Has the information in this report led to any quantitative savings as far as man-hours or dollars saved, operating costs avoided, or efficiencies achieved, etc? If so, please elaborate. ______

6. General Comments. What do you think should be changed to improve future reports? (Indicate changes to organization, technical content, format, etc.) ______

CURRENT ADDRESS

Organization

Name

Street or P.O. Box No.

City, State, Zip Code

7. If indicating a Change of Address or Address Correction, please provide the Current or Correct address above and the Old or Incorrect address below.

OLD ADDRESS

Organization

Name

Street or P.O. Box No.

City, State, Zip Code

(Remove this sheet, fold as indicated, staple or tape closed, and mail.)

DEPARTMENT OF THE ARMY

OFFICIAL BUSINESS

BUSINESS REPLY MAIL
FIRST CLASS PERMIT No 0001, APG, MD

Postage will be paid by addressee

NO POSTAGE NECESSARY IF MAILED IN THE UNITED STATES

Director
U.S. Army Research Laboratory
ATTN: AMSRL-OP-CI-B (Tech Lib)
Aberdeen Proving Ground, MD 21005-5066